2008

# Identification of Polycyclic Aromatic Hydrocarbons in the Supercritical Pyrolysis Products of Synthetic Jet Fuel S-8 and Methylcyclohexane

Jorge Oswaldo Ona Ruales
*Louisiana State University and Agricultural and Mechanical College*, jona1@lsu.edu

# IDENTIFICATION OF POLYCYCLIC AROMATIC HYDROCARBONS IN THE SUPERCRITICAL PYROLYSIS PRODUCTS OF SYNTHETIC JET FUEL S-8 AND METHYLCYCLOHEXANE

**A Dissertation**
**Submitted to the Graduate Faculty of the**
**Louisiana State University and**
**Agricultural and Mechanical College**
**in partial fulfillment of the**
**requirements for the degree of**
**Doctor of Philosophy**

**in**

**The Department of Chemical Engineering**

**by**
**Jorge Oswaldo Oña Ruales**
**Ingeniero Quimico, Universidad Central del Ecuador – Quito, 2000**
**May, 2008**

## ACKNOWLEDGEMENTS

I would like to thank the following:

My advisor, **Prof. Mary Julia Wornat**, for her wise guidance during the last six years, for introduce me to the world of polycyclic aromatic hydrocarbons, and for showing me how to transform my observations into words and the words into scientific papers. **Dr. Elmer Ledesma**, for his patience teaching me the fundamentals of chromatography and for his friendship. My colleagues **Shiju Thomas**, **Jerome Robles**, **Michelle Somers**, **Franz Ehrenhauser**, **Sean Bagley**, **Nimesh Poddar**, and **Joy Alcanzare** for their friendship and support during these years. **Dr. John Fetzer**, for his professional suggestions and comments about my research. **Dr. Jennifer McClaine** and **Dr. Xia Zhang**, two former post-docs, for their technical assistance. My committee members, **Dr. Karsten Thompson**, **Dr. Isiah Warner**, **Dr. Armando Corripio**, and **Dr. David Young**, for their help during the general exam and the dissertation defense.

Finally, I am forever grateful to the following:

My wife, **Diana**, for her constant love and company; my mother, **Yolanda**; my father, **Jorge**; my sisters, **Lucy** and **Very**; and my nieces, **Andreita**, **Ana Paula**, and **Emily**, for years and years of inspiration and encouragement.

## TABLE OF CONTENTS

## LIST OF TABLES

## LIST OF FIGURES

## ABSTRACT

Inside the pre-combustor fuel lines of future high-speed aircraft, at supercritical conditions, hydrocarbon fuels react to form polycyclic aromatic hydrocarbons (PAH) and eventually solid deposits. These deposits can block fuel lines and lead to undesirable effects for the aircraft operation. To elucidate the pathways that lead to the formation of PAH (and ultimately, solids formation), the identification of the PAH products generated by the reactions is critical. In this context, two fuels have been analyzed: synthetic jet fuel S-8 and methylcyclohexane. Synthetic jet fuel S-8 is important due to its non-petroleum origin. Methylcyclohexane is important due to its endothermic behavior. Therefore, the goal of this study is the identification of the PAH products from the supercritical pyrolysis of synthetic jet fuel S-8 and from the pyrolysis of methylcyclohexane. With the purpose of identifying the unknown PAH, each pyrolysis product mixture has been analyzed by gas chromatography with mass spectrometric detection, and by high-pressure liquid chromatography with ultraviolet-visible diode-array and mass spectrometric detection (HPLC/UV/MS). The HPLC/UV information has allowed the identification of sixty-one and thirty-nine different products from the supercritical pyrolysis of synthetic jet fuel S-8 and from the supercritical pyrolysis of methylcyclohexane, respectively, at the most drastic conditions. Further interpretation of the UV spectra by means of the alkyl substitution effect, the UV solvent based adjustment, and the Annellation Theory, and confirmation of product identities using the MS spectra have provided irrefutable clues for the identification of twenty-four PAH from the synthetic jet fuel pyrolysis and sixteen PAH from the methylcyclohexane pyrolysis, respectively. Out of the eighty-five total PAH products reported from the supercritical pyrolysis of synthetic jet fuel S-8, twenty-nine unsubstituted PAH with six or more rings have never before been identified in the pyrolysis of a

long-chain alkane fuel. In addition, out of the fifty-five total PAH products reported from the supercritical pyrolysis of methylcyclohexane, fifteen unsubstituted PAH with six or more rings have never before been identified as products of methylcyclohexane. Finally, it has been observed that the increases of temperature, pressure, and residence time, favor the formation of heavier PAH—the precursors to the solid deposits.

# CHAPTER 1. INTRODUCTION

This study is about the identification of polycyclic aromatic hydrocarbons (PAH) in the supercritical pyrolysis products of synthetic jet fuel S-8 and in the supercritical pyrolysis products of methylcyclohexane. The main purpose of this research is help to achieve a clear understanding of the mechanisms of formation of carbonaceous solids inside the pre-combustor fuel lines of modern aircraft. In this environment, the fuel is subjected to pressures and temperatures that exceed the critical values of most hydrocarbon fuels promoting reactions of solid formation that decrease the aircraft performance [Edwards]. Therefore, the identification of PAH, intermediate products of these reactions, is critical so as to develop reaction pathways to better elucidate the formation of these unwanted solids and find out means to avoid them. In addition to this particular application, the identification of PAH will also allow the development of better removal techniques to target specific PAH contained in polluted environments. Furthermore, due to the electronic properties of aromatic compounds, the discovery of new PAH will promote their use in novel organic conductors [Gamma et al.], solar cells [Hiramoto et al.], photo- and electroluminescent devices [Schlichting et al., Holtrup et al., Debad et al.], optically active polymers [Fiesel et al.], and non-linear optical materials [Burland et al., Marks and Ratner, Bahl et al.]. From a health perspective, the results of this study will allow the identification of new carcinogenic and mutagenic metabolites formed by representative PAH [Freudenthal and Jones].

## 1.1. Synthetic Jet Fuel S-8

The synthetic jet fuel S-8 (critical temperature = 373 $^{o}$C, critical pressure = 21.8 atm) [Edwards] is a fuel mixture made from natural gas [Air Force Research Laboratory] composed mainly (~100%) of large paraffinic fractions ($C_7$-$C_{18}$) [Syntroleum]. Figure 1.1. shows the gas

chromatography flame ionization (GC/FID) chromatogram of a sample of synthetic jet fuel S-8 analyzed in our laboratory.

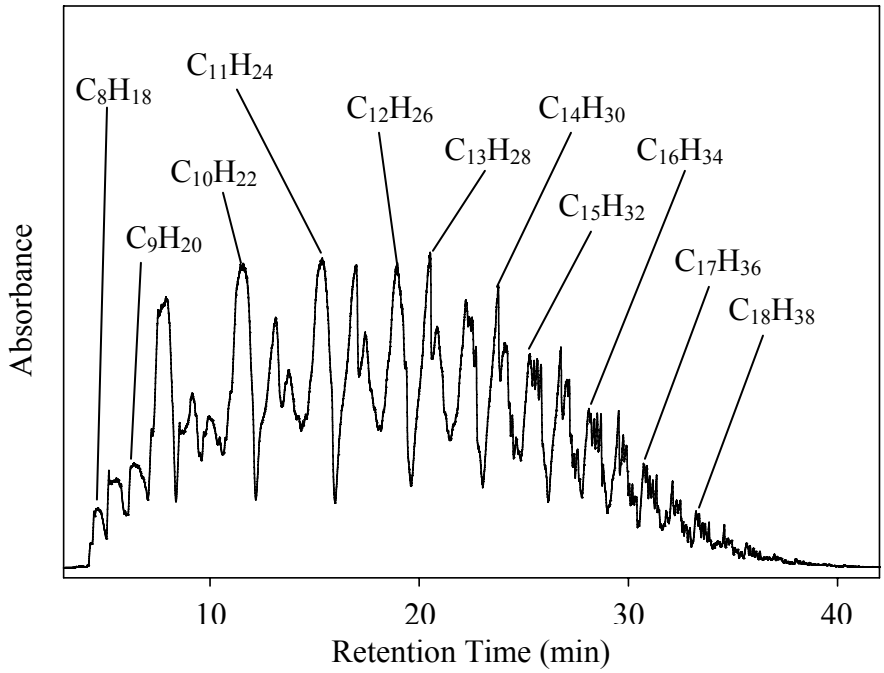


Figure 1.1. GC/FID Chromatogram of the Synthetic Jet Fuel S-8.

The synthetic fuels are fuels produced from non-traditional petroleum sources. These fuels are playing an increasingly important role to satisfy the future energy demands. Due to their uncommon properties, the synthetic fuels can result in significantly different energy generation performance than that obtained with conventional fuels [Edelman et al.].

The synthetic jet fuels are manufactured from a hydrocarbon feedstock using a Fischer-Tropsch process [Dagget et al. 2007]. The Fisher-Tropsch process starts with the gasification of the source, e.g., coal, natural gas, oil shale, tar sand, or biomatter, to produce a mixture of gases carbon monoxide and hydrogen, which is called the synthesis gas. The synthesis gas is subjected to a reaction at elevated pressures, at moderate temperatures, and in the presence of catalysts, e.g., cobalt or iron, to generate different types of alkanes and water [Freerks and Muzzell]. The

nature and properties of the synthetic fuel produced will depend on the amount and type of alkanes generated.

Synthetic jet fuels show significant promise as fuels that could be easily integrated into present and future aircraft with little or no modification to current aircraft designs [Dagget et al. 2006]. The positive features of synthetic jet fuels include: a cleaner fuel with no sulfur and no aromatics, higher thermal stability, possible lower particulate engine emissions, and lower deposits formation. In contrast, the negative attributes include: poorer lubricating properties, lower volumetric heat content, possible contributions to fuel system elastomer leakage, and increased $CO_2$ emissions during its manufacture [Dagget et al. 2006].

**1.2. Methylcyclohexane**

Methylcyclohexane (critical temperature = 299 $^{o}$C, critical pressure = 34 atm) is a naphthenic (cycloparaffinic) hydrocarbon with a potential applicability as an endothermic fuel, i.e., a fuel that can undergo a controlled heat absorbing reaction prior to combustion [Sobel and Spadaccini, Stewart]. Giving up its latent and sensible heat through endothermic reactions, e.g., the dehydrogenation depicted in Figure 1.3., methylcyclohexane can provide a heat sink of up to 2190 kJ kg$^{-1}$ [Orme et al.].

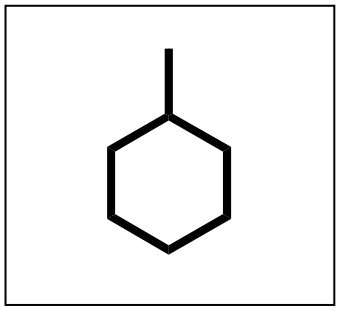

Figure 1.2. Methylcyclohexane

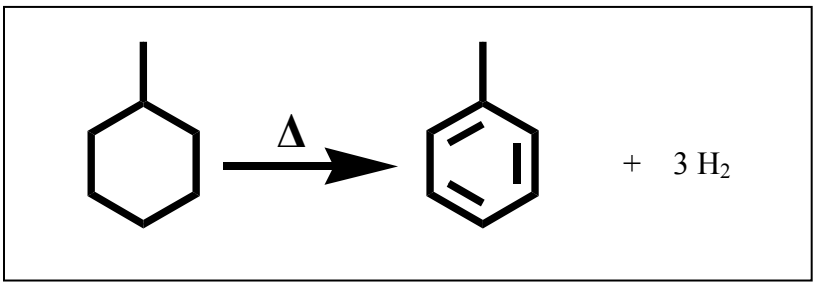


Figure 1.3. Reaction of Dehydrogenation of Methylcyclohexane

This heat sink capacity makes it an attractive candidate fuel for modern supersonic aircraft applications, where the enormous cooling demands exceed the heat sink capacities of traditional non-endothermic fuels [Edwards]. In fact, methylcyclohexane is present as one of the naphthenic fractions of some multi-component fuels [Stewart], e.g., about 10% v/v of the fuel JP-9 represents methylcyclohexane [Oh et al.].

When methylcyclohexane is subjected to conditions of temperature above 400 $^{o}$C it decomposes following pyrolytic reaction pathways [Gül et al.]. Previous studies of methylcyclohexane at pyrolytic conditions reported the formation of ethylene, methane, propylene, 1,3-butadiene, isopropene, cyclohexene, alkylcyclopentanes, benzene and toluene as the major products. Propane, 1-butene, 3-methylbutene, 1-methylcyclohexenes, pentadienes, 2-heptene, cyclohexane, methylcyclo-pentadienes, cyclohexadienes and $C_8$ aromatics were also detected and constitute minor products [Stewart, Pant and Kunzru, Lai and Song].

In comparison with cyclohexane, another naphthenic fuel with similar endothermic behavior, methylcyclohexane has better physical characteristics─lower melting and higher boiling points; thus, it is a more practical fuel [Lander and Nixon]. Despite of these advantages, it has been demonstrated that the pyrolytic products of methylcyclohexane lead to the formation of polycyclic aromatic hydrocarbons (PAH) [Stewart]. The PAH are considered precursors of

carbonaceous solid deposits [Glassman] that can seriously affect the performance of modern aircrafts [Edwards].

### 1.3. Synopsis

First, this study presents an overview of the theory of supercritical fluids with some introductory notes about the supercritical pyrolysis of methylcylohexane and the supercritical pyrolysis of toluene. The next part refers to the analytical techniques applied for the identification of PAH products. Then, the chapter about experimental methods describes the supercritical pyrolysis reactor and the full experimental procedure. Subsequently, the results and discussion part shows the necessary evidence to certify the presence of PAH in the supercritical pyrolysis products of synthetic jet fuel S-8 and in the supercritical pyrolysis products of methylcyclohexane. Later, the summary and conclusions chapter recapitulates the research carried out in this study and define the conclusions obtained. At the end, to close this study, the recommendations and appendices are presented.

# CHAPTER 2. SUPERCRITICAL FLUIDS

This chapter is devoted to the explanation of the main characteristics of a supercritical fluid and its pressure-dependent reactions. In addition, details about the kinetic parameters associated with the effect of pressure at supercritical conditions are presented. To complement this explanation, background information about the main products obtained from the supercritical pyrolysis of methylcyclohexane and from the supercritical pyrolysis of toluene is shown.

## 2.1. Generalities

Almost any chemical substance can be transferred into the four conditions of matter (gas, liquid, solid, or supercritical fluid) by the variation of pressure (p) and temperature (T). The equilibrium point of the p-T diagram in which the gas, the liquid, and the supercritical fluid coexist is called the critical point. Supercritical fluids are compressed and heated substances beyond the critical point that is characteristic of each substance [Dinjus et al.].

Within the supercritical region there is continuity in physical properties of the fluid between the gas and the liquid states. The consequence is that supercritical fluids have properties, which are a curious hybrid of those normally associated with liquids and gases. Thus, under most conditions, the viscosities and diffusivities are similar to those of gases while the density is closer to that of a liquid [Dinjus et al. and Metzger et al.].

A supercritical fluid, essentially a gas with a liquid-like density, is a unique environment for chemical kinetic studies. Since the solvent properties of a supercritical fluid vary strongly with pressure (unlike liquids or gases), the elementary reactions in a supercritical environment have strong pressure dependence [Stewart]. A unique property of supercritical fluids is their pressure dependent density. If the temperature is constant, density can be adjusted from that of a gas to that of a liquid without any discontinuity. It is common to focus on the region where the

reduced temperature ($T_r = T / T_c$, where *Tr* and *Tc* are the reduced temperature and critical temperature, respectively) and the reduced pressure ($p_r = p / p_c$, where *pr* and *pc* are the reduced pressure and critical pressure, respectively) are of the order of unity. In this region, considerable changes in fluid density and related properties, such as solubility of the material, are observed with small changes in pressure [Dinjus et al.].

## 2.2. Supercritical Fluid Phase Pyrolysis

### 2.2.1. Chemical Reactions under High Pressure

A study of reaction kinetics in a supercritical environment takes some elements of kinetic theory from the gas-phase, some from liquid-phase, and adds some properties unique to the supercritical environment [Stewart].

Metzger et al. found that a supercritical environment promoted specific hydrocarbon reaction mechanisms, which were strongly favored under supercritical conditions. They suggested that the very high densities of the supercritical state were promoting addition reactions not commonly seen in gas-phase pyrolysis studies and at much higher rates than the lower temperature liquid-phase studies. What makes supercritical fluids unique is that all of the solute/solvent interactions that influence reaction rates in the liquid-phase, but are pressure-invariant in the liquid, are pressure-dependent in a supercritical fluid because the density and the solvent properties vary strongly with pressure [Stewart]. These solute/solvent interactions are absent from the gas-phase due to the low density of that environment.

According to Stewart, as the pressure increases isothermally, the intermolecular spacing and the mean free path quickly contract. For a certain compound, in contrast to gas-phase pyrolysis where a given unimolecular or bimolecular reaction is not typically influenced by the presence of molecular neighbors, pyrolysis in a supercritical fluid may be significantly

influenced by the concentration of the medium. The high-density supercritical environment creates a shell of solvent molecules around a given molecule of interest. This solvent shell, as said by Laidler, results in many rapid collisions with a diminished variety of collisional partners. The high density environment can also result in changes in elementary reaction rate constants as solvent molecules hinder or assist the formation of transition states [Stewart].

The problem of interpreting and predicting the effects of high pressures on reaction rates is linked to the understanding of the volume changes that occur in the activation processes [Tiltscher and Hofmann].

**2.2.2. Transition-State Theory**

The Transition-State Theory is a convenient and powerful formalism for explaining and interpreting the kinetics of elementary reactions. This theory views a chemical reaction as occurring via a transition-state species (or an activated complex) [Savage et al.].

The concept of the Transition-State Theory is summarized by the following reaction:

$$A + B \rightleftharpoons X^{\neq} \longrightarrow P \qquad \text{Equation 2.1.}$$

For a bimolecular reaction a chemical equilibrium is assumed between the reactants A and B, and the transition state $X^{\neq}$. The reaction proceeds via a gradual rearrangement of atomic positions between those of reactants and those of products, P. The energy of the system however, increases initially to a maximum, the transition state, before falling to that of the products. The transition state, although being only metastable, is ascribed all the thermodynamic properties of a normal species, i.e. energy, entropy, volume, etc. [Tiltscher and Hofmann].

### 2.2.3. Pressure Effects – Activation Volume

From the Transition-State Theory rate and classical thermodynamics [Tiltscher and Hofmann], one can show that:

$$\left(\frac{\partial \ln k}{\partial p}\right)_T = \frac{1}{R_g T}\left(\frac{\partial \Delta G^{\neq}}{\partial p}\right)_T = -\frac{\Delta V^{\neq}}{R_g T} \qquad \text{Equation 2.2.}$$

where, $k$ is the rate constant, $p$ is the pressure, $\Delta G^{\neq}$ is the free energy of activation, $\Delta V^{\neq}$ is the activation volume, $R_g$ is the gas constant, and $T$ is the temperature. With the above assumptions $\Delta V^{\neq}$ is the difference between the sum of the partial molar volumes ($V_A^m$, $V_B^m$) of the reactants and the partial molar volume of the transition state ($V_x^{\neq}$), which can be immediately seen from the volume profile along the reaction coordinate.

$$\Delta V^{\neq} = (V_A^m + V_B^m) - V_x^{\neq} \qquad \text{Equation 2.3.}$$

Equation 2.3. predicts an increase or decrease in rate with pressure if the transition state occupies a smaller or larger volume than the total volume of the reactants, respectively.

Wu et al. noted that the properties of a supercritical fluid near its critical point, unlike the properties of a liquid, can change markedly with pressure and that these changes can also influence kinetics.

## 2.3. Products of the Supercritical Pyrolysis of Methylcyclohexane

The products of the supercritical pyrolysis of methylcyclohexane have been collected and analyzed in the gas and in the liquid phases by Stewart. Dimethylcyclopentanes isomers were among the most abundant products collected in the liquid phase [Stewart]. In the gas phase on the other hand, methane, propene, and ethane were among the most abundant products collected [Stewart]. The following paragraphs present a summarized description of four major products from the supercritical pyrolysis of methylcyclohexane.

### 2.3.1. Methylcyclohexene

Methylcyclohexene isomers are found to be major intermediates in the supercritical pyrolysis of methylcyclohexane [Stewart]. As indicated by Stewart, methylcyclohexene isomers are formed via H-atom abstraction from methylcyclohexane followed by β-scission of a C-H bond or an H-donation reaction.

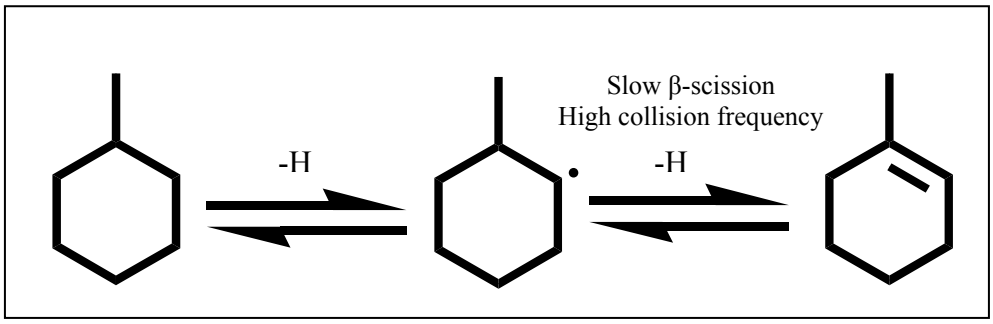


Figure 2.1. Methylcyclohexene Formation

### 2.3.2. Alkanes

The presence of alkanes (ethane, propane, cyclohexane, and others) is explained by Stewart based on two factors: 1) slower β-scission resulting from lower temperatures and 2) a reduced characteristic time of collision and reaction with H-donor molecules resulting from the high density. These factors result in the formation of alkanes instead of 1-olefins which are common of β-scission.

### 2.3.3. Alkylcyclopentanes

Figure 2.2., extracted from Lai and Song, illustrates the formation of methylcyclopentane from methylcyclohexane. This mechanism has been explained by Stewart using an argument proposed previously by Davis. Davis suggested that the high concentration of the supercritical environment created a cage of solvent molecules around a solute molecule of interest. A cage could then have prevented a cyclical hexeneyl intermediate, a structure with significant bond

strain, from opening up to form the large straight hexeneyl. Instead the molecule was forced via the space limitations of the cage to form the more compact product, methylcyclopentane. Because methylcyclopentane had not been observed in prior gas phase methylcyclohexane pyrolysis studies, the formation of cyclical $C_5$ species appeared to be a consequence of the high concentration environment.

According to Stewart, the abundance of cyclical $C_5$ compounds may significantly promote PAH and solid formation. Continuing the analogy of these observations to the studies of soot formation, Glassman reported that under diffusion flame conditions, cyclopentene had a greater tendency to soot than did cyclohexene. In general, methyl-substituted cyclical $C_5$ species can relatively easily pyrolyze to methylcyclopentadiene, which through subsequent isomerization reactions leads to benzene. Benzene is one of the major precursors to the formation of PAH molecules.

Stewart emphasizes that assuming similar pyrolysis mechanisms apply under the supercritical conditions as are observed in typical diffusion flame conditions, methylcyclohexane may therefore be more prone to solid formation than other fuels which are not inclined to cyclical $C_5$ formation.

Finally, Stewart mentions that the absence of products of ring contraction in gas-phase studies, i.e., alkylcycloalkanes, supported Davis' hypothesis that formation of alkylcyclopentanes, in supercritical environments, may involve a solute/solvent caging interaction.

Figure 2.3. illustrates the formation of identical methyl-hexeneyl intermediates in the gas-phase and the supercritical phase. In both phases, products of further unimolecular decomposition, ethene and propene, were observed. β-scission is thought to be very important in

both these environments. However, the products of the ring contraction process, alkyl-cyclopentanes, were observed only in the supercritical phase, supporting the Davis' hypothesis.

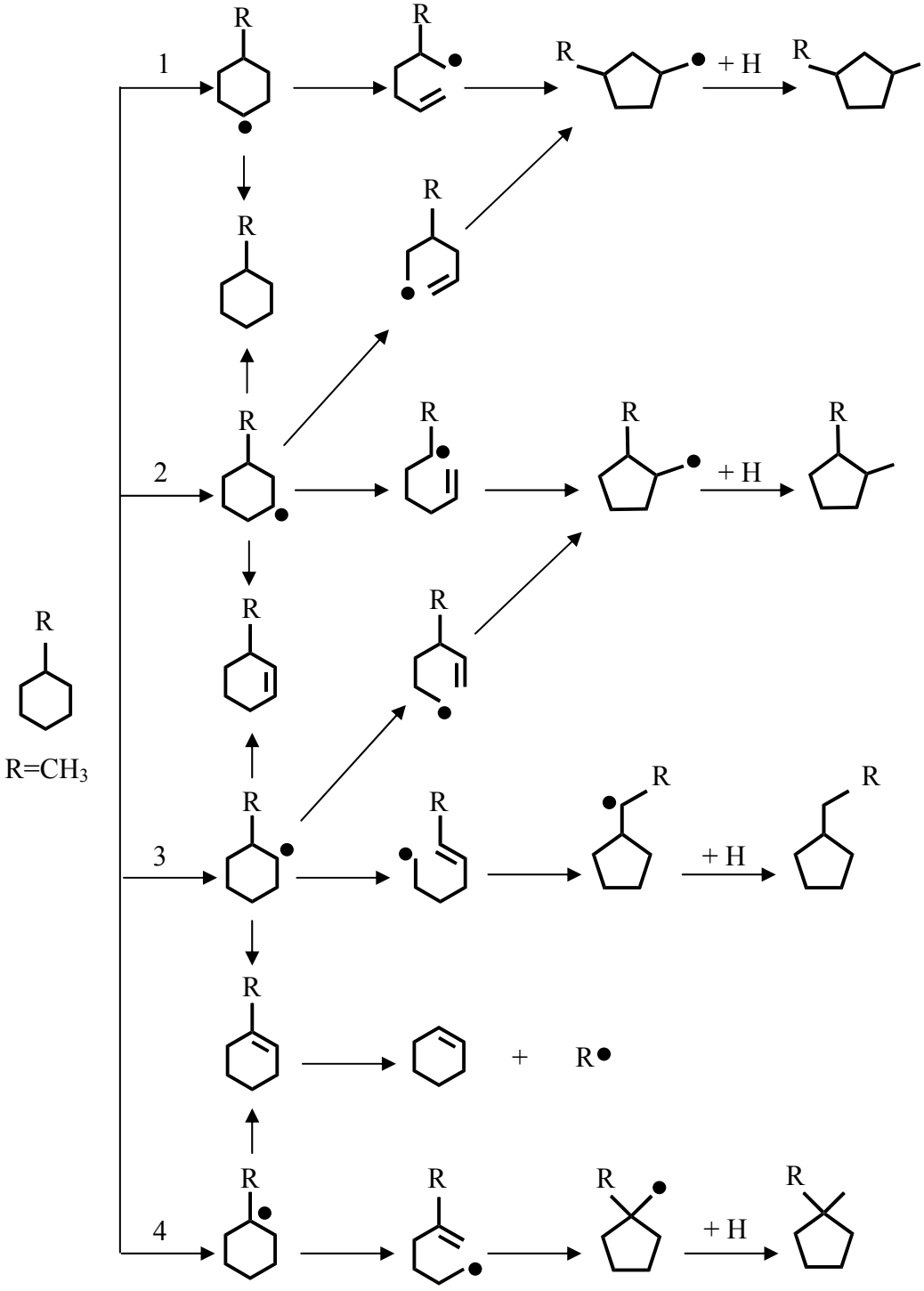


Figure 2.2. Alkylcyclopentane Formation. Extracted from Lai and Song.

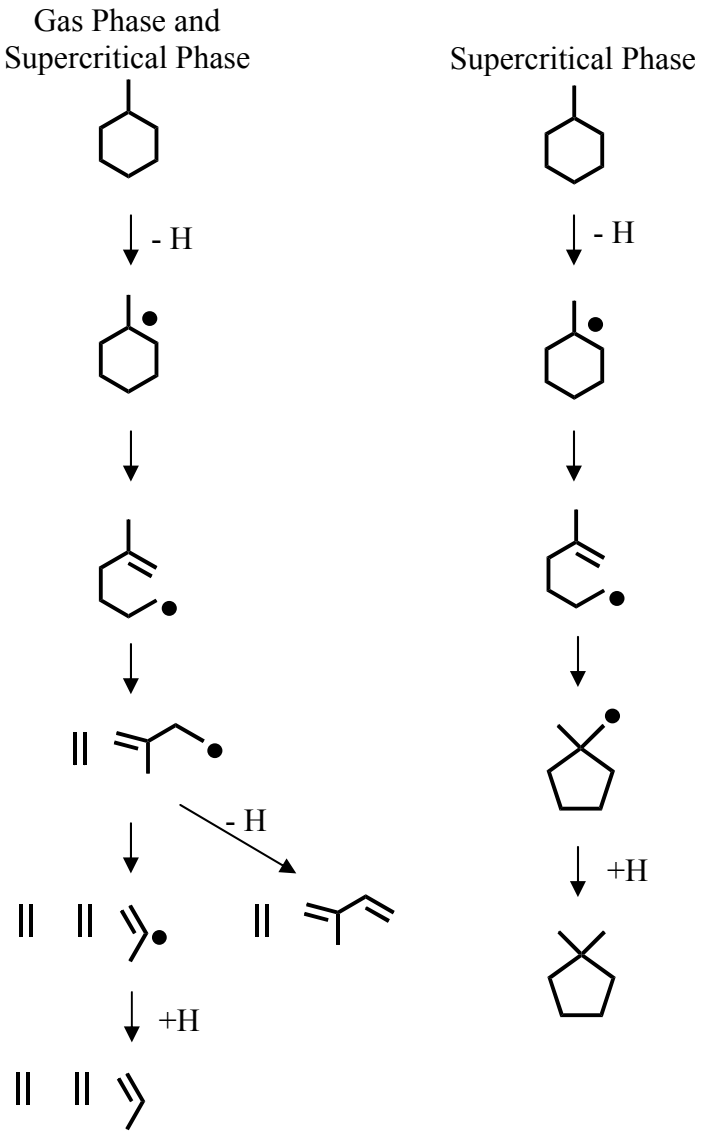


Figure 2.3. Gas Phase and Supercritical Phase Decomposition of Methylcyclohexane. Extracted from Stewart.

### 2.3.4. Toluene

The analogy between methylcyclohexane and toluene, represented in Figure 2.4., is straight-forward, toluene constitutes the dehydrogenated counterpart of methylcyclohexane. Additionally, in the supercritical pyrolysis of methylcyclohexane, toluene is present as the simplest and most abundant alkyl-substituted aromatic molecule [Stewart]. This analogy

methylcyclohexane-toluene is of primary importance for the present analysis due to the vast and valuable information reported by Ledesma et al. and McClaine et al. [McClaine et al. 2006, 2007a, 2007b] about the supercritical pyrolysis of toluene. Later in this study, it will be demonstrated that both supercritical fuel pyrolysis analyses generate very similar PAH. Using this knowledge, it will be possible to correlate the proposed mechanism for the formation of PAH from the supercritical pyrolysis of toluene [McClaine et al. 2007a] with the as-yet-unknown mechanism for the formation of PAH from the supercritical pyrolysis of methylcyclohexane. The next section of this chapter summarizes the results obtained by McClaine et al. [McClaine et al. 2007a] from the supercritical pyrolysis of toluene.

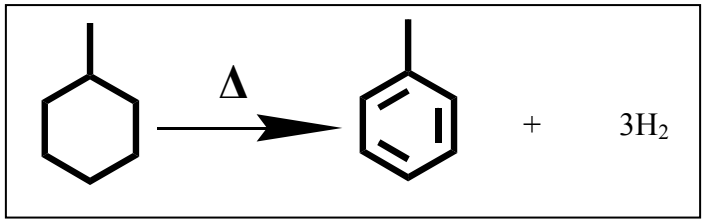


Figure 2.4. Toluene Formation

**2.4. The Supercritical Pyrolysis of Toluene**

McClaine et al. [2006, 2007a, 2007b] studied the supercritical pyrolysis of toluene with the same goal as the goal followed for the present study, i.e., the elucidation of the mechanisms of reaction of the fuel inside of the lines before the combustor in modern aircraft. The PAH identified from the study of McClaine et al. [2006, 2007a, 2007b] are presented in Figure 2.5. They reveal a product distribution very similar to the PAH product distribution found from the supercritical pyrolysis of methylcyclohexane (see Chapter 5 for a discussion of these results).

Figure 2.6. shows the mechanism proposed by McClaine et al. [2006, 2007a, 2007b] to explain the formation of the $C_{28}H_{14}$ benzenoid PAH and some other large PAH detected from the

supercritical pyrolysis of toluene. Since toluene is one of the main products observed from the pyrolysis of methylcyclohexane, it is important to refer to this mechanism as a means to explain the formation of PAH from the supercritical pyrolysis of methylcyclohexane.

This mechanism is based on a benzyl, methyl, and/or phenyl radical additions to smaller PAH products. Three reactions are the core of this mechanism: 1. a methyl and a benzyl addition, usually to a position next to a bay region, 2. a phenyl addition to a bay region, and 3. two methyl additions to a bay region [McClaine et al. 2006, 2007a, 2007b].

This mechanism makes it possible to explain why six out of the eight $C_{28}H_{14}$ benzenoid PAH: phenanthro[5,4,3,2-*efghi*]perylene, benzo[*a*]coronene, benzo[*ghi*]naphtho[8,1,2-*bcd*]-perylene, benzo[*cd*]naphtho[3,2,1,8-*pqra*]perylene, benzo[*pqr*]naphtho[8,1,2-*bcd*]perylene, and tribenzo[*cd,ghi,lm*]perylene are formed at these conditions and why the other two $C_{28}H_{14}$: bisanthene and naphthaceno[3,4,5,6,7-*defghij*]naphthacene are not formed [McClaine et al. 2007a].

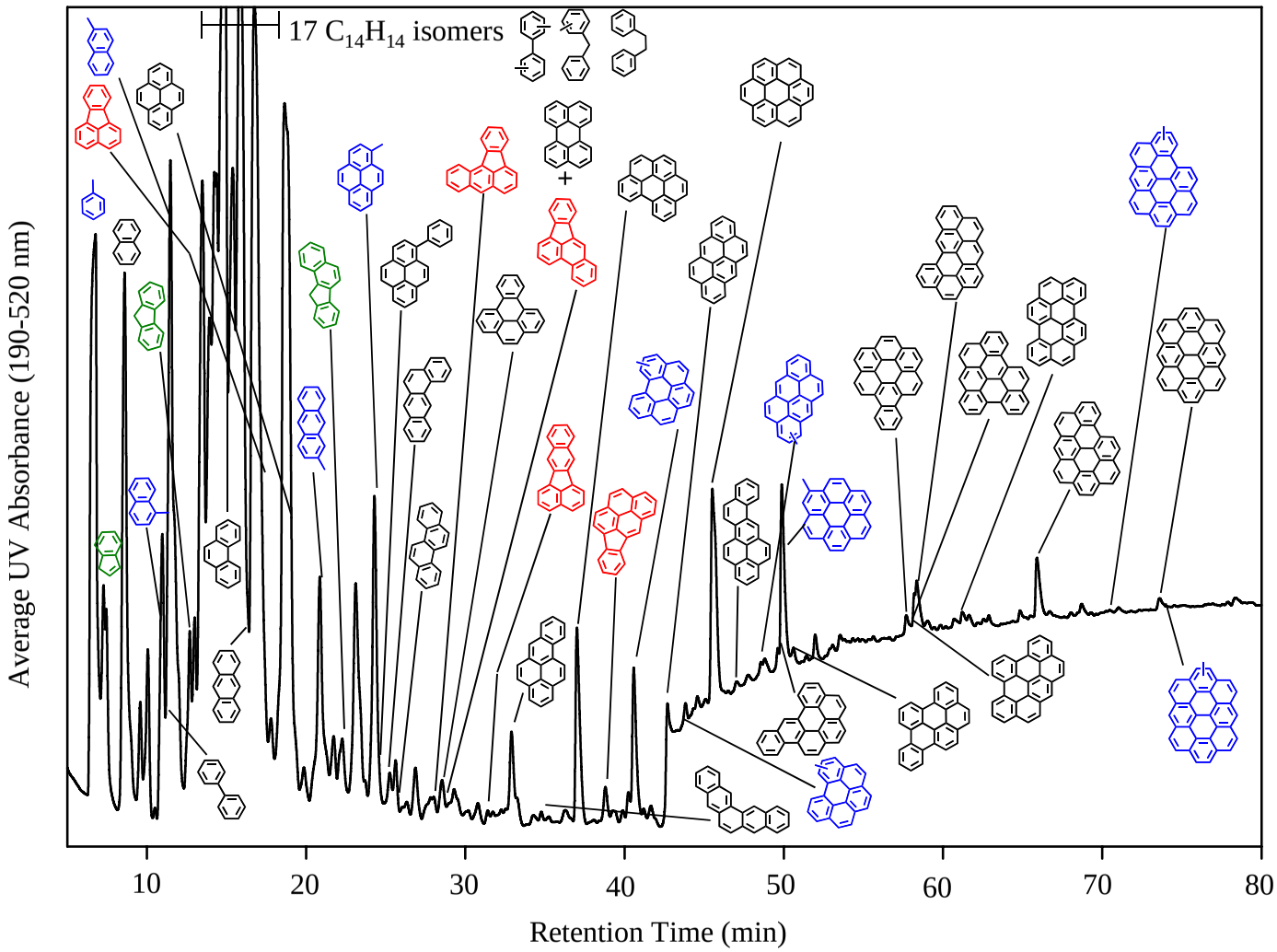


Figure 2.5. HPLC/UV Chromatogram of the Toluene Supercritical Pyrolysis Products at 535 °C, 100 atm, and 140 sec [McClaine et al. 2007a].

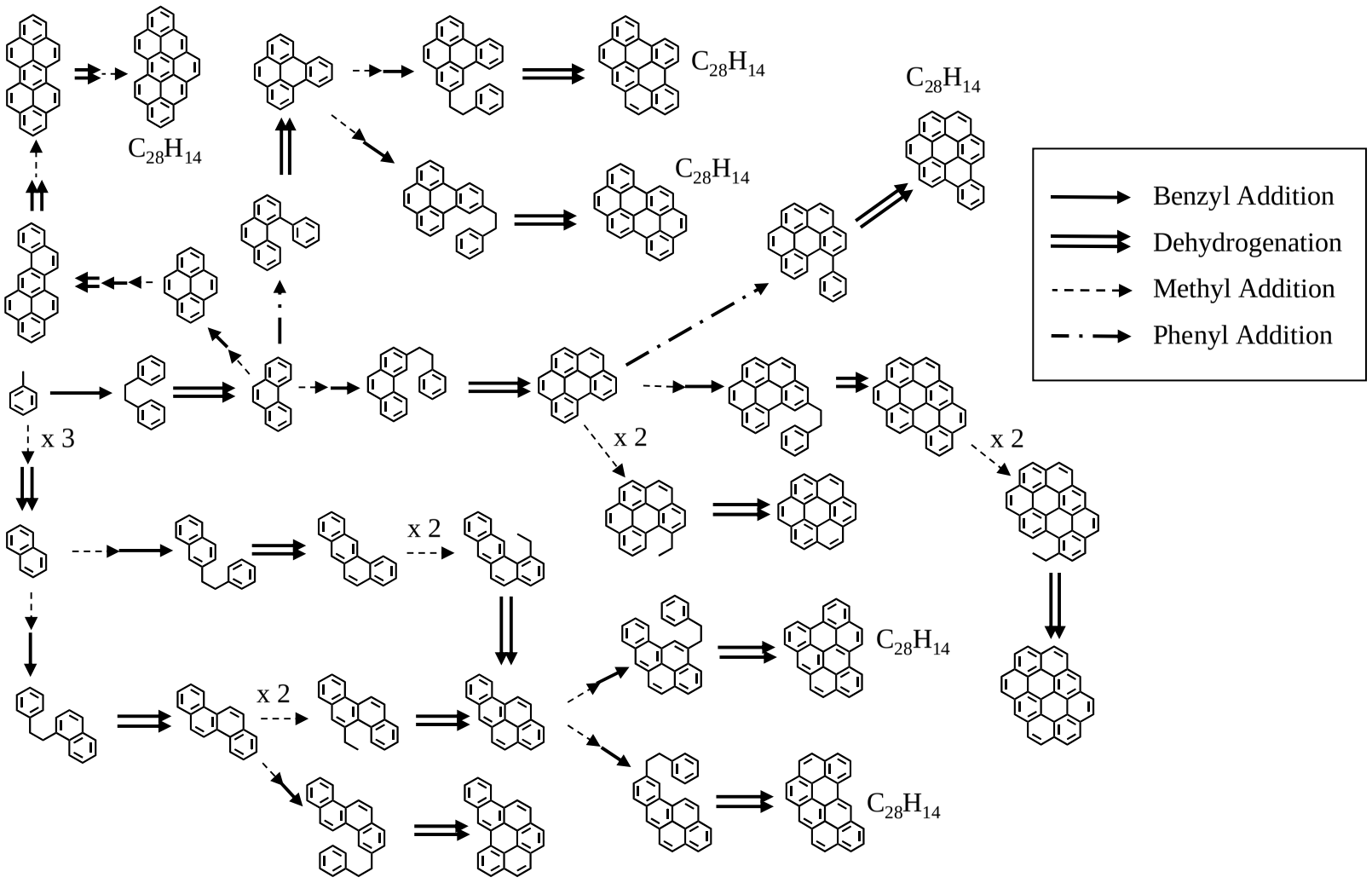


Figure 2.6. Reaction Pathways [McClaine et al. 2006, 2007a, 2007b] in the Supercritical Pyrolysis of Toluene, showing the Formation of PAH from the Addition of Benzyl (solid arrow), Methyl (dashed arrow), and Phenyl Radicals (dash-dot arrow). Dehydrogenation is shown as the double-lined arrow.

## CHAPTER 3. IDENTIFICATION OF POLYCYCLIC AROMATIC HYDROCARBONS

The identification of PAH has been accomplished using several detection techniques such as mass spectrometry (MS) [Klempier and Binder, Peaden et al.], nuclear magnetic resonance (NMR) [Weiβhoff et al.], infrared spectrometry (IR) [Hudgins and Sandford], fluorescence spectroscopy [McKay and Latham], and ultraviolet/visible (UV) absorption spectroscopy [Fetzer and Biggs 1994; Fetzer 2000; Oña and Wornat 2007, 2008c; McClaine et al. 2006, 2007b]. Moreover, certain separation techniques like gas chromatography (GC) [Lee and Hites] and liquid chromatography (LC) [Oña and Wornat 2007, 2008c; McClaine et al. 2006, 2007b] have proved to be useful prior to the detection analysis in order to make possible the identification of PAH contained in mixtures. Among the techniques above-mentioned, GC coupled with MS is one of the most used due to its lower cost, friendly operation, and high analytical sensitivities [Hites]. The GC/MS determination, however, has a big drawback; it is ineffective to distinguish among PAH isomers since it does not provide information about the exact arrangement of aromatic rings [Hites]. In opposition to the GC/MS, other techniques such as NMR, which provides information about the exact molecular conformation, and IR, which provides information on aromatic positional isomers, have demonstrated to be useful [Hites]. Both techniques, however, are 2 to 4 orders of magnitude less sensitive than GC/MS making them not valuable for certain applications [Hites]. In addition to GC/MS, high-performance liquid chromatography (HPLC) coupled with UV and MS detections has been widely accepted as the best technique for PAH detection [Fetzer and Biggs 1994; Fetzer 2000; Oña and Wornat 2007, 2008c; McClaine et al. 2006, 2007b]. HPLC/UV/MS is able to identify a particular PAH among several isomers, it is useful for the recognition of large PAH, and it is relatively easy to operate. As demonstrated by McClaine [McClaine et al. 2006, 2007b], the HPLC separates the

components of the mixture; the MS establishes the $C_xH_y$ formula of the PAH product component [Gallagher et al.]; and the UV allows the unequivocal identification of the PAH from its unique UV spectral pattern, the fingerprint that differentiates each PAH molecular structure from all others [Fetzer and Biggs 1984, 1985, 1987]. This chapter presents a description of reversed-phase high-performance liquid chromatography (RP/HPLC) coupled with UV and MS detections, which is the main technique used in this study for the identification of PAH. Later, some explanatory notes and illustrative examples about three PAH identification tools are described. These identification tools include: the alkyl substitution effect on the UV spectra of PAH, the solvent-based adjustment on the UV spectra of PAH, and the Annellation Theory.

## 3.1. Reversed-Phase High-Performance Liquid Chromatography with Ultraviolet-Visible Diode-Array and Mass Spectrometric Detections

### 3.1.1. Reversed-Phase High-Performance Liquid Chromatography

HPLC comprises all liquid chromatographic techniques that require the use of elevated pressures to force a liquid trough a packed bed of a stationary phase [Neue]. RP/HPLC, a derivation of the HPLC technique, is a technique based on a separation between a nonpolar stationary phase, e.g., a long-chain hydrocarbon attached to a support, and a polar mobile phase, e.g. mixtures of water with polar solvents [Neue]. This method has been used widely for the separation of many samples containing smaller PAH–compounds with a high solubility in polar solvents. Conversely, for the separation of the larger PAH molecules, frequently found in supercritical fuel environments, it is necessary to utilize different mobile phases. This is due to the affinity of the larger PAH for alkane solvents, e.g., the long chain alkanes of the stationary phase, which require better solvents to act as the mobile phase. In this case, nonaqueous mobile phases, e.g., ethyl acetate, dichloromethane, tetrahydrofuran, and chlorobenzene with methanol and acetonitrile acting as the weak solvent, are preferred [Fetzer 2000].

### 3.1.2. Ultraviolet-Visible Absorbance with Diode-Array Detection

One of the most important characteristics of the PAH is the unique UV spectral pattern that they describe; the UV spectrum constitutes a fingerprint that distinguishes each PAH molecular structure from all others [Oña and Wornat 2007]. According to Fetzer [Fetzer 2000], the various transitions in the UV absorbance spectrum of a PAH are classified by the electronic transition that causes them. These transitions are usually known as the α, β, and para (p) bands. This terminology was implemented by Clar in the 1930's [Vingiello and Ojakaar]. The α bands are the less intense and frequently appear at the highest wavelength. They shift to the red on linear and angular annellation in the series of the acenes and phenes, and they are hidden or partly hidden in the more intense p-bands in the higher acenes starting with anthracene [Clar 1964]. They correspond to the transition from the second highest occupied molecular orbital to the lowest unoccupied molecular orbital (LUMO) [Fetzer 2000]. The β bands are the most intense, showing the same annellation effect and in a fixed ratio to the α bands, lying more in the ultraviolet [Clar 1964]. They are the lowest wavelength bands and represent a transition from the highest occupied molecular orbital (HOMO) to the second lowest unoccupied orbital [Fetzer 2000]. Lastly, the p bands shift most strongly on linear annellation to the red [Clar 1964]. They are of intermediate wavelength and represent a transition from the HOMO to the LUMO [Fetzer 2000].

Fetzer [Fetzer 2000] emphasizes that when a group of isomers are compared, prominent differences are seen in their UV absorbance spectra, even for similar structures. These differences are related to the particular arrangement of the π electrons in each of the PAH in a particular isomer group. Despite the fact that they have the same molecular mass, their molecular shape is different and thus their UV absorbance spectra which are related to the

distribution of their π electrons. Ortho-fused PAH (known also as catacondensed PAH) produce spectra with very intense low-wavelength bands with additional less intense bands located at higher wavelengths [Fetzer 2000]. On the other hand, perifused PAH (known also as pericondensed PAH) produce spectra extremely rich in spectral bands characterized by clusters spread throughout a long spectral range [Fetzer 2000]. In the same context, Fetzer [Fetzer 2000] has defined important observations about the differences between planar and non-planar PAH. Planar PAH show spectra with very deep valleys between spectral bands and the bands themselves are very narrow. Non-planar PAH, on the other hand, show spectra with broader valleys and the bands are rounder and less distinct.

### 3.1.3. Mass Spectrometry Detection with Atmospheric-Pressure Photo-Ionization

MS detection with atmospheric-pressure photo-ionization (APPI) has been used for the identification and verification of PAH. The APPI mass spectrum helps to establish the $C_xH_y$ formula of an unknown PAH product component [Gallagher et al.].

The basic mechanism of ionization using APPI has been explained by Syage. It consists of two reactions:

$$M + h\nu \rightarrow M^+ + \bar{e} \qquad \text{Equation 3.1.}$$

and

$$M^+ + S \rightarrow M(H^+) + S(-H) \qquad \text{Equation 3.2.}$$

Where, M is the analyte, $M^+$ is the molecular ion, S is the protic molecule, $M(H^+)$ is the protonated ion, S(-H) is the hydrogen abstracted protic molecule, and hν is a light of a certain wavelength.

This analysis is consistent with the observations of Somers and Wornat and Zhang et al. According to these authors, the PAH product components that elute during the portion of the

HPLC solvent program in which the mixtures acetonitrile-dichloromethane or methanol-dichloromethane are used, yield mass spectra whose first- and second-most abundant ions are at M+H and M+2H, respectively, where M is the molecular weight of the PAH component. The reason of these ions is that acetonitrile-dichloromethane and methanol-dichloromethane, through photoionization in the mass spectrometer, are able to ionize PAH components through proton (H) transfer, yielding the M+H and M+2H peaks in the mass spectrum.

### 3.2. The Alkyl-Substitution Effect on the Ultraviolet-Visible Absorption Spectra of Polycyclic Aromatic Hydrocarbons

Several authors [Jones, Fetzer and Biggs 1984] have discussed about the effect of the alkyl substituent group on the UV spectra of PAH. Jones pointed out that the intensities and relative positions of the spectral bands in the UV spectrum of an alkyl-substituted PAH do not change very much in comparison with the spectrum of the original non-substituted PAH (as shown in Figures 3.1. and 3.2.). Fetzer and Biggs [Fetzer and Biggs 1984] have corroborated this idea emphasizing that the alkyl substitution produces small shifts of the spectra to higher wavelengths leaving the same original spectral pattern. They have argued that the location of the alkyl group in the molecule has also a distinguishable effect in the UV spectrum of an alkyl-substituted PAH. It is demonstrated in Figures 3.1. and 3.2. that noticeable differences have been found depending on the position of alkyl groups present. Shifts of 1- or 2- nm are expected for methyl or ethyl groups. In general, the alkyl substitution effect is additive; therefore, longer alkyl chains will produce even longer shifts.

### 3.3. The Ultraviolet-Visible Solvent Effect

The identification and adjustment of the solvent effect on the UV spectra of PAH constitute one of the main identification techniques used here. Several authors have discussed in some way about the influence of the solvent on the UV spectral bands [Katrizky et al., Bayliss

and McCrae, Jaffe and Orchin, LeRosen and Reid]; however, none of them have applied this effect for the identification of PAH. This section is merely devoted to the explanation of the solvent effect on the UV spectral bands of PAH. Later, in section 5.1.2.-Case C, this effect will be corrected using the "UV solvent-based adjustment" in order to verify the identity of some unknown fuel products.

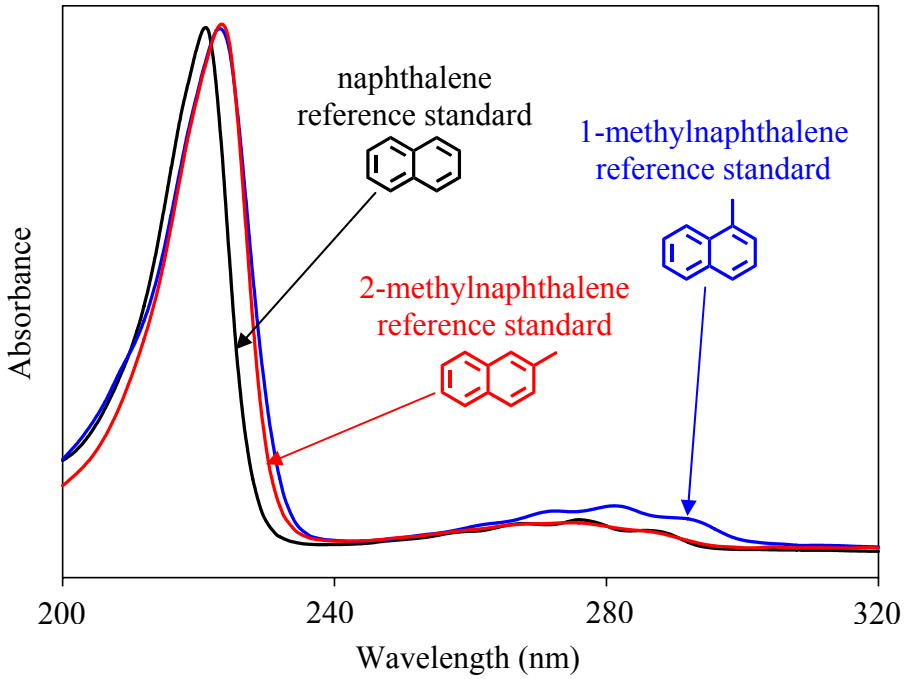


Figure 3.1. UV Absorbance Spectra for the Reference Standards of Naphthalene, 1-Methylnaphthalene, and 2-Methylnaphthalene.

The consideration of the solvent in which the sample is analyzed is a key aspect of these observations. The approach presented here follows a nineteenth century rule from Kundt. This rule asserts that an increase in the index of refraction of the solvent results in bathochromic shifts of the solute absorption bands. In spite of the macroscopic limitations associated with this rule–since it disregards microscopic intermolecular forces, solvation in multicomponent systems, and chemical solvation related to ionization and dissociation [Katrizky et al.]–this approach is justified due to the non-polar nature of the PAH molecules [Moriwaki et al., Raffaelli and Saba].

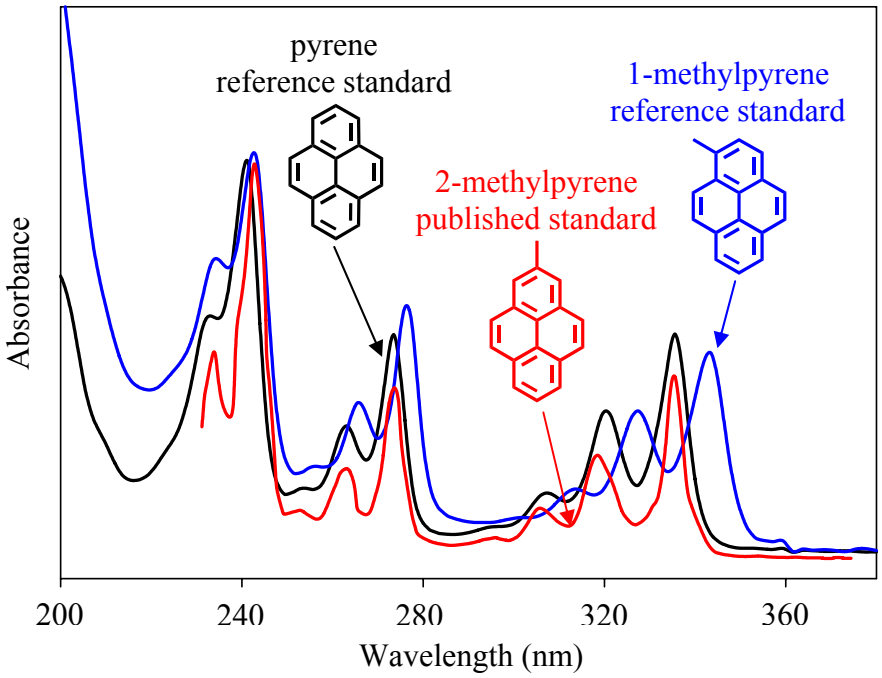


Figure 3.2. UV Absorbance Spectra for the Reference Standards of Pyrene and 1-Methylpyrene, and for the Published UV Spectrum of the Standard of 2-Methylpyrene [Friedel and Orchin].

The studies of Bayliss and McCrae, about non-polar solutes immersed in polar or non-polar solvents, pointed out that the absence of solute-solvent interactions, e.g., solute dipole moment, solute-solvent orientation forces, and orientation strain, produces a shift depending on the solvent index of refraction.

Figures 3.3. and 3.4. show two examples of the influence of the solvents on the position of the spectral bands. Figure 3.3. describes the published UV spectra of the reference standard of dibenzo[*cd,lm*]perylene in three different solvents, methanol [Jinno], tetrahydrofuran [Umemoto et al.], and benzene [Clar 1964]. In this case, the spectral bands occupy wavelength positions that are consistent with the order of the solvent index of refraction. A very similar behavior is followed by the published UV spectra of the reference standard of dibenzo[*a,cd*]naphtho[3,2,1-*lm*]perylene [Fetzer 2000] presented in Figure 3.4. in methanol, n-hexane, dichloromethane, and

chlorobenzene. The wavelength position of the spectral bands agrees well with the order of the index of refraction of the solvent. This analysis substantiates the earlier observations of Kundt, the theoretical explanations of Bayliss and McCrae, and the experimental confirmations of LeRosen and Reid, about the effect of the solvent on the position of the UV spectral bands of a compound.

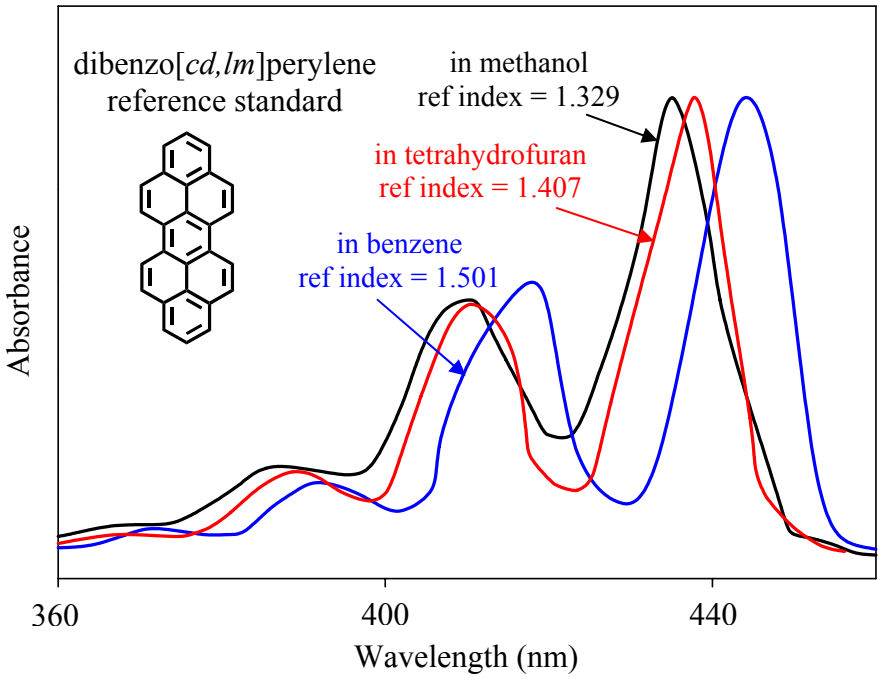


Figure 3.3. Published UV Absorbance Spectra for the Standards of Dibenzo[*cd,lm*]perylene in Methanol [Jinno], Tetrahydrofuran [Umemoto et al.], and Benzene [Clar 1964].

### 3.4. The Annellation Theory

The fundamentals of the Annellation Theory were proposed by Erich Clar in the 1930's [Vingiello and Ojakaar] when he was analyzing the UV spectra of several PAH [Clar 1952]. He observed common patterns when the UV spectra of PAH are compared using different series that contain the same structure with rings added at certain positions. Figure 3.5. shows the UV spectra of the reference standards of pyrene, benzo[*a*]pyrene, and dibenzo[*a,h*]pyrene (all of them have embedded the structure of pyrene).

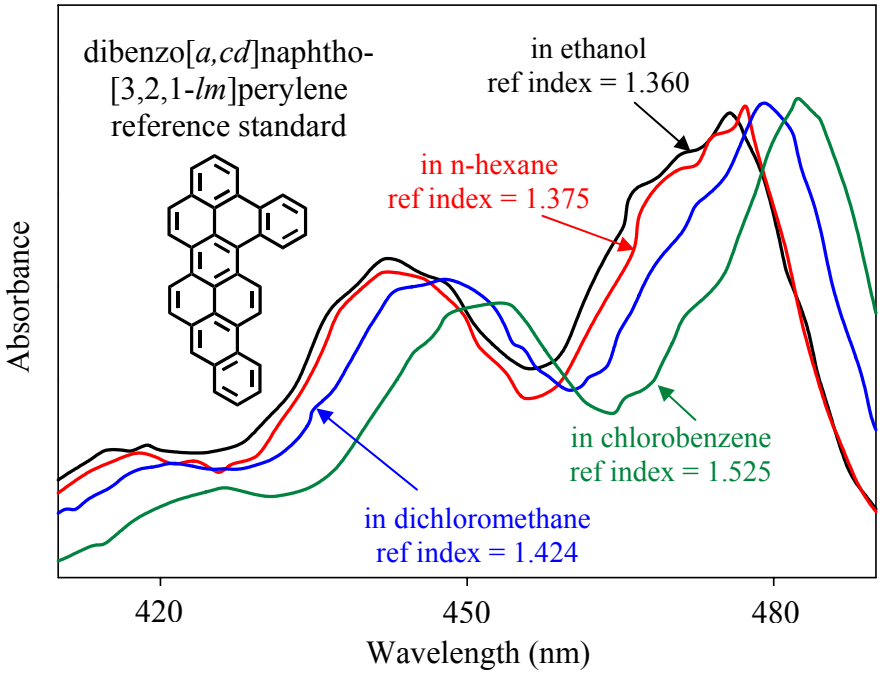


Figure 3.4. Published UV Absorbance Spectra for the Standards of Dibenzo[*a,cd*]naphtho[3,2,1-*lm*]perylene in Ethanol, n-Hexane, Dichloromethane, and Chlorobenzene [Fetzer 2000].

The spectra follow a similar pattern that varies clearly in the position of the spectral bands and somewhat noticeably in the intensity of the dominant peaks. Several rules and postulates were issued by Clar [Clar 1972] based on analogous interpretations.

The Annellation Theory explains the behavior of the UV spectra of groups of PAH that follow a common annellation, i.e., fusion of rings, pattern. Its main purpose is the prediction of the UV spectrum of an unknown PAH based on the observed patterns in the UV spectra of previously known PAH and on the arrangement of the aromatic sextets in the molecule. Fetzer and Biggs [Fetzer and Biggs 1994] and McClaine et al. [McClaine et al. 2006], for example, have used the Annellation Theory for the identification of phenanthro[5,4,3,2-*efghi*]perylene and benzo[*ghi*]naphtho[8,1,2-*bcd*]perylene, respectively.

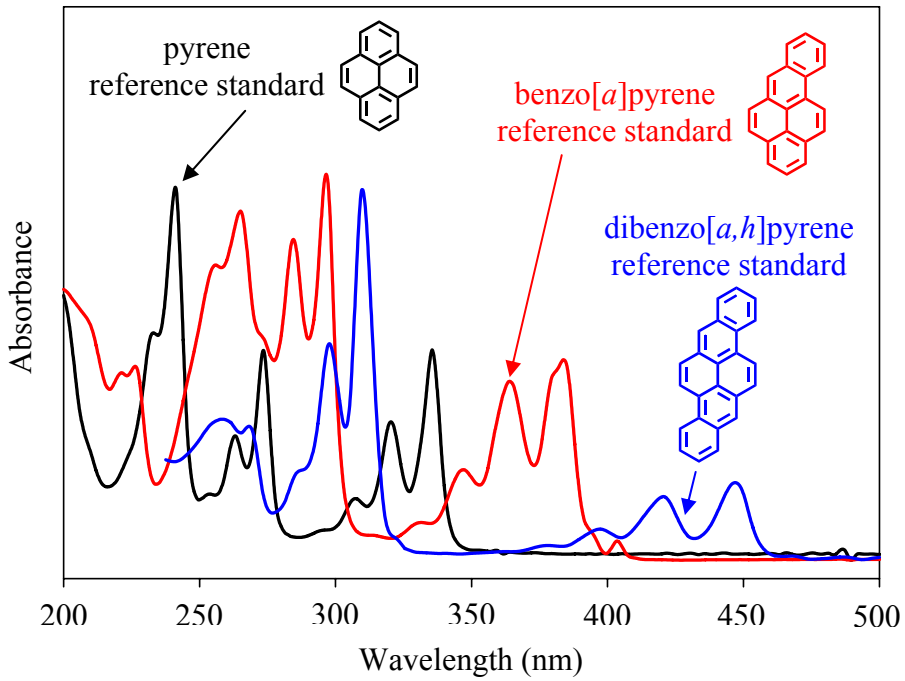


Figure 3.5. UV Absorbance Spectra for the Reference Standards of Pyrene, Benzo[*a*]pyrene, and Dibenzo[*a,h*]pyrene.

The sextets are located in particular hexagons of the molecule, indicating domains of increased π-electron contents and/or local aromaticity [Gutman and Ruiz-Morales]. It is therefore possible, by means of the Annellation Theory, not only the elucidation of the molecular structure that generates a certain UV spectrum but also the identification of the areas of a molecular structure with a higher degree of aromaticity.

Two rules taken from the numerous observations collected and published by Clar about the Annellation Theory [Clar 1964, 1972] have been considered and applied in this study. These two rules describe the effect on the UV spectra of a PAH due to the addition of a benzenoid ring in a particular position of its molecular structure. Informative examples are presented in each case to make the explanation clearer. In chapter 5, these two rules will be applied for the identification of unknown PAH present in the supercritical pyrolysis products of synthetic jet fuel S-8 and in the supercritical pyrolysis products methylcyclohexane.

### 3.4.1. Rule 1: Effects on the Ultraviolet-Visible Spectrum due to the Addition of a Benzenoid Ring to a Fixed Double Bond

Out of the several observations extracted from the Annellation Theory [Clar 1972], one excels due to its simplicity and straight-forward applicability. This observation asserts that the fusion of a new ring onto a ring of a PAH in which a fixed double bond is present causes either no shift or a weak one towards shorter wavelength keeping a similar shape for both UV spectra [Clar 1972]. This effect is explained due to the formation of a sextet in the new benzenoid ring. The addition of a new sextet limits the shift of the UV spectral bands due to the increase of the aromaticity in the molecule. This increase in the aromaticity decreases the movement of the electrons between the electronic orbitals which are related to the transitions that define the absorbance intensity and shape of the spectral bands.

To prove this observation, let's examine the case of the two PAH: benzo[*pqr*]naphtho[8,1,2-*bcd*]perylene and dibenzo[*ghi,k*]phenanthro[9,10,1-*cde*]perylene, presented in Figure 3.6. Benzo[*pqr*]naphtho[8,1,2-*bcd*]perylene has two fixed double bonds located in terminal rings of the molecule [Clar 1972]. The addition of two rings at each of these terminal rings produces the PAH dibenzo[*ghi,k*]phenanthro[9,10,1-*cde*]perylene. As a difference with benzo[*pqr*]napthho[8,1,2-*bcd*]perylene and observed in Figure 3.6., dibenzo[*ghi,k*]-phenanthro[9,10,1-*cde*]perylene shows two additional sextets (six in total) located at each side of the molecule [Clar 1972].

The correspondent spectral analysis presented in Figure 3.7. verifies this postulate. The addition of two benzenoid rings to two fixed double bonds produces almost no variation in the position and shape of the β and p spectral bands. The absorbance intensity of the p bands is also maintained. There is, however, a very small variation in the intensity of the β bands.

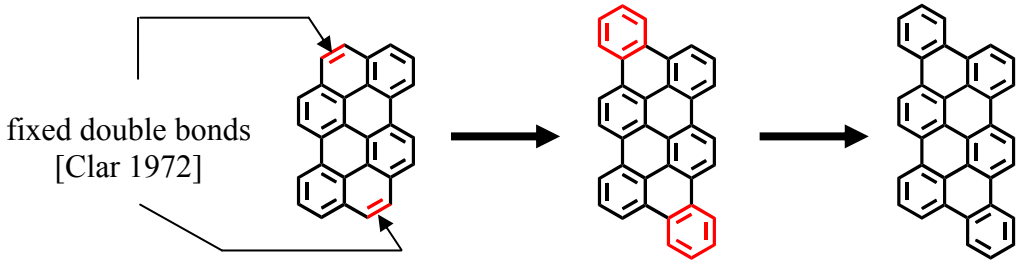


Figure 3.6. Addition of two Benzenoid Rings to the two Fixed Double Bonds of Benzo[*pqr*]naphtho[8,1,2-*bcd*]perylene to form Dibenzo[*ghi,k*]phenanthro[9,10,1-*cde*]perylene.

Figure 3.8. presents an additional example of the same principle. The case under analysis is the addition of a benzenoid ring to the fixed double bond of benz[*a*]anthracene to form dibenz[*a,c*]anthracene. As it is observed in Figure 3.8., this addition does not produce substantial shifts, changes in the spectral pattern, or changes in the absorbance intensities of the spectral bands.

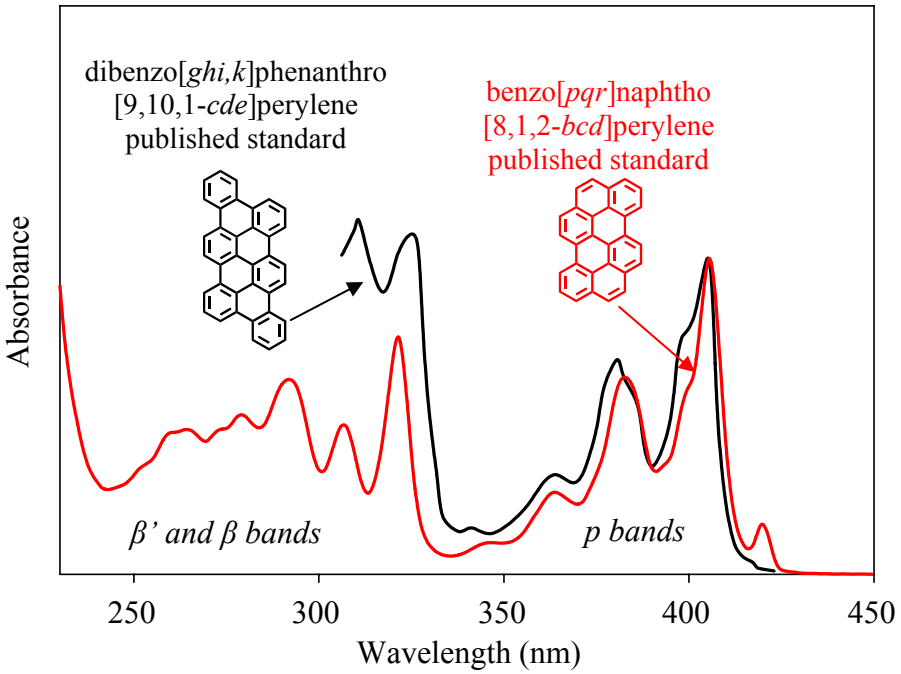


Figure 3.7. UV Absorbance Spectrum for the Reference Standard of Benzo[*pqr*]naphtho[8,1,2-*bcd*]perylene (black line) and for the Published UV Spectrum of Dibenzo[*ghi,k*]-phenanthro[9,10,1-*cde*]perylene (red line) [Clar 1964].

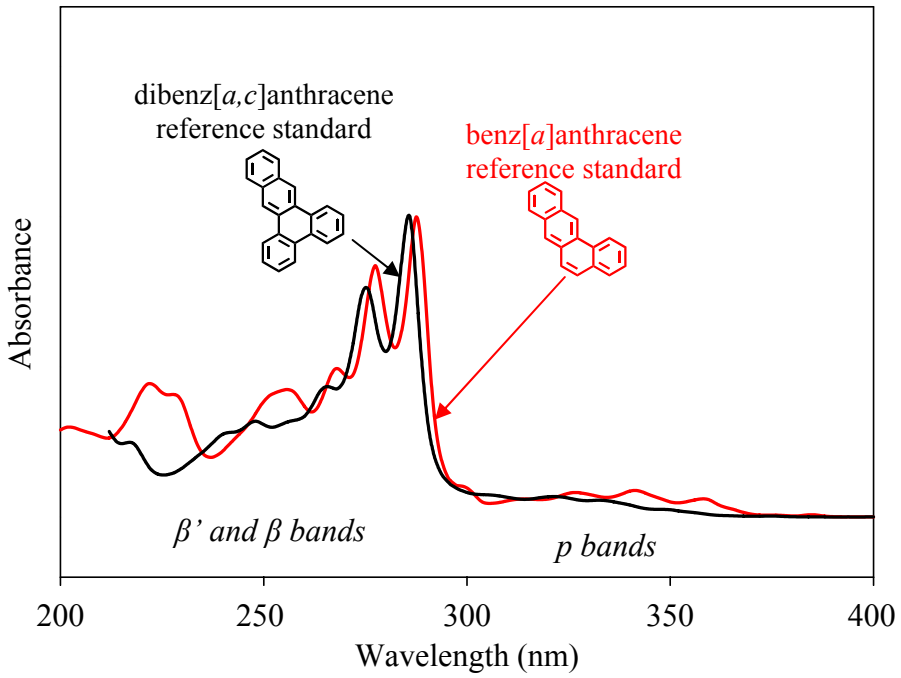


Figure 3.8. UV Absorbance Spectra for the Reference Standards of Benz[*a*]anthracene and Dibenz[*a,c*]anthracene.

In chapter 5, the preceeding observations about the effect on the UV spectrum of a PAH due to the addition of a benzenoid ring to a fixed double bond will be used so as to demonstrate the presence of one of the unknown PAH products from the supercritical pyrolysis of synthetic jet fuel S-8.

### 3.4.2. Rule 2: Effects on the Ultraviolet-Visible Spectrum due to the Addition in an Angular Position of a Benzenoid Ring to a Benzenoid Ring with a High-Sextet Character

A benzenoid ring with a high-sextet character is a ring that shares a sextet with a neighboring ring in such a way that the electrons can move freely from one ring to the other [Clar 1972]. The ring addition in an angular position to a benzenoid ring with a high-sextet character has very much the same effect on the p bands of the UV spectrum of a PAH as the effect already discussed in Rule 1, i.e., due to the addition of a benzenoid ring to a fixed double bond. There is a very small, if any, shift of the p bands that characterize the spectrum. Also, the

intensities and shape of the p bands are preserved as in the spectrum of the original compound. The reason of this behavior is the formation of a new sextet in the new benzenoid ring. The increase in the number of sextets restricts the mobility of the p bands due to the increase of the aromaticity in the molecule. This aromaticity's increase diminishes the chances of the electrons to move between the HOMO and the LUMO which is related to the transitions that define the absorbance intensity and shape of the p bands [Fetzer 2000].

To examine this postulate, Figure 3.9. shows the addition of a benzenoid ring to the benzenoid ring with a high-sextet character of benzo[*a*]pyrene in angular positions. The new PAH molecules formed are naphtho[1,2-*a*]pyrene and naphtho[2,1-*a*]pyrene. The effect of this addition is elucidated in Figure 3.10. Figure 3.10. shows the UV spectra of the reference standards of benzo[*a*]pyrene, naphtho[1,2-*a*]pyrene, and naphtho[2,1-*a*]pyrene. In agreement with the arguments presented above, the p bands (383.5 nm, 363.5, and 347.5 nm for benzo[*a*]pyrene; 382.0 nm, 364.0 nm, and 345.0 nm for naphtho[1,2-*a*]pyrene, and 381.0 nm, 364.0 nm, and 346.0 nm for naphtho[2,1-*a*]pyrene) show almost the same behavior in terms of intensity, position and shape. In chapter 5, these observations will be used so as to demonstrate the presence of one of the unknown synthetic jet fuel S-8 supercritical pyrolysis products.

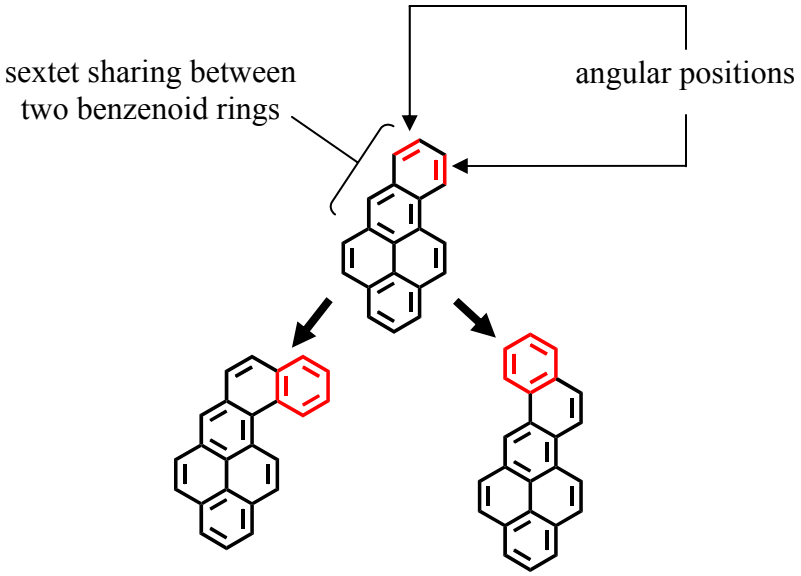


Figure 3.9. Addition of a Benzenoid Ring to the two Angular Positions of Benzo[*a*]pyrene to form Naphtho[1,2-*a*]pyrene and Naphtho[2,1-*a*]pyrene.

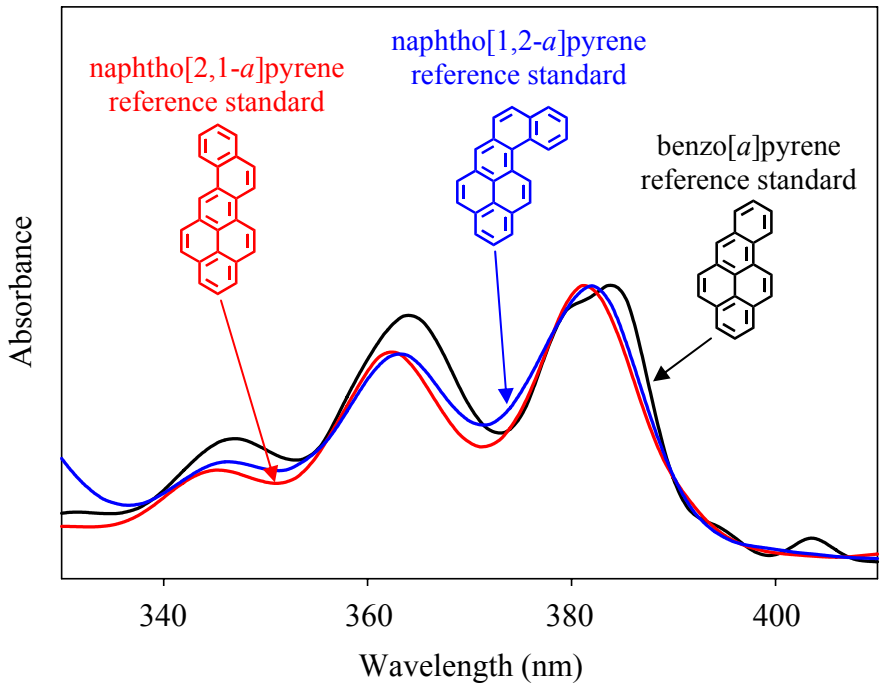


Figure 3.10. p Bands of the UV Absorbance Spectra for the Reference Standards of Benzo[*a*]pyrene, Naphtho[1,2-*a*]pyrene, and Naphtho[2,1-*a*]pyrene.

# CHAPTER 4. METHODOLOGY

## 4.1. Pyrolysis of Methylcyclohexane

### 4.1.1. Equipment Diagram

The supercritical pyrolysis reactor design shown in Figure 4.1. was proposed by Davis and adapted by Stewart.

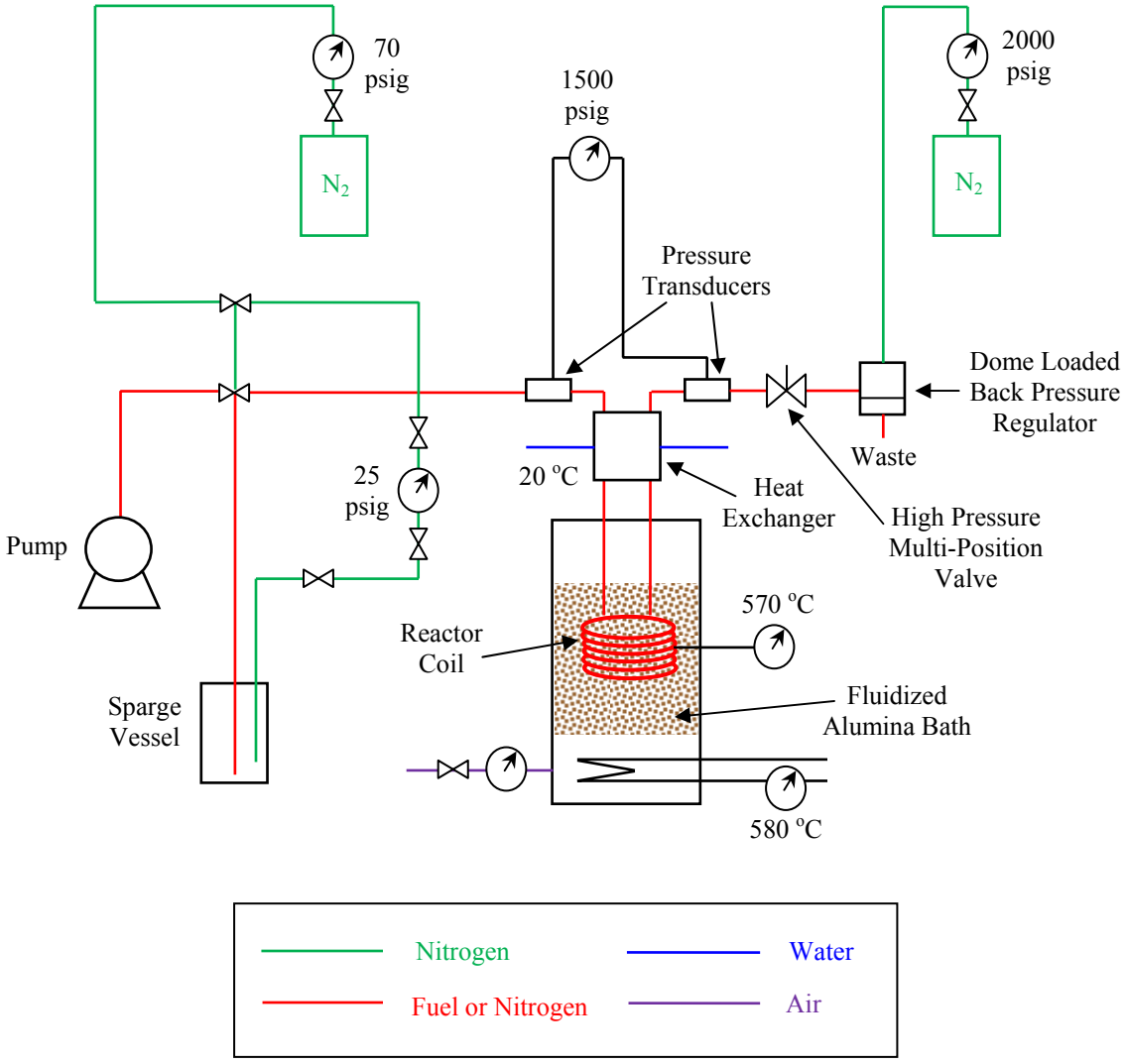


Figure 4.1. Supercritical Pyrolysis Reactor

### 4.1.2. Experimental Procedure

Figure 4.1. shows the supercritical pyrolysis reactor designed by Davis to conduct isothermal and isobaric studies using methylcyclohexane. Prior to an experiment, liquid methylcyclohexane (99.9+% pure) purchased from Sigma-Aldrich (St. Louis, MO, USA) is sparged with nitrogen for three hours, as described by Stewart, to get rid of any dissolved oxygen that could introduce auto-oxidative effects [Edwards]. The sparged fuel is then loaded into a high-pressure nonreciprocating pump, which delivers the fuel to the reactor. The reactor itself is a coil of 1-mm i.d., 1.59-mm o.d. capillary tube made of silica-lined stainless steel. (The silica lining prevents wall-catalyzed deposit formation that occurs with unlined stainless steel [Edwards, Stewart, Davis].) The reactor coil is immersed in a temperature-controlled fluidized-alumina bath, which ensures isothermality throughout the reactor length. As indicated in Figure 4.1., the entrance and exit lines of the reactor are passed through a water-cooled (20 °C) heat exchanger to ensure a controlled thermal history and residence time. Exiting the heat exchanger, the quenched reaction products pass through a stainless steel filter (hole size, 5 μm) and on to a six-position high-pressure valve, for product collection. A dome-loaded back-pressure regulator, downstream of the valve, controls the system pressure, to within ± 0.2 atm, up to a maximum of 110 atm.

As documented by Stewart and Davis, the reactor has been designed to meet the criteria for idealization as plug flow of Cutler et al. and Lee, with regard to species concentration profiles—criteria concerning the product of the Reynolds and Schmidt numbers [Lee], criteria for fast radial species diffusion relative to forced convection, and criteria for minimum axial diffusion relative to axial convection [Cutler et al.]. The resulting radially uniform species concentrations, coupled with the reactor's constant-temperature and constant-pressure operation,

render this reactor ideal for supercritical pyrolysis kinetics experiments. The reactor system is capable of operating at temperatures up to 590 °C, pressures up to 110 atm, and residence times up to 3600 sec—operating ranges relevant to those envisioned for fuel systems in future hypersonic aircraft [Heneghan et al.]. The methylcyclohexane pyrolyses experiments reported here are conducted at three different set of conditions: First, constant temperature (570 $^{o}$C), variable pressure (20 atm, 40 atm, 60 atm, 80 atm, and 100 atm), and constant residence time (140 sec); second, constant pressure (100 atm), variable temperature (560 $^{o}$C, 570 $^{o}$C, and 580 $^{o}$C), and constant residence time (140 sec); and third, constant temperature (570 $^{o}$C), constant pressure (100 atm), and variable residence time (70 sec and 140 sec).

At the conclusion of each methylcyclohexane pyrolysis experiment, the reaction products are removed from the high-pressure collection valve and transferred to a vial. To analyze the smaller aromatic products, a 10-μL aliquot of the product solution is removed for injection onto a GC/MS. The remainder of the product solution (~1 mL) is prepared for HPLC to analyze the larger aromatic products.

**4.2. Supercritical Pyrolysis of Synthetic Jet Fuel S-8**

The synthetic jet fuel S-8 supercritical pyrolysis products analyzed here have been obtained at two conditions: First, 710 $^{o}$C and 42 atm; and second, 666 $^{o}$C and 42 atm. These supercritical pyrolysis tests have been performed in a bench-scale test rig [Huang et al. 2002, 2004] located in the United Technologies Research Center of Hartford (Connecticut) that simulates the actual conditions in heat exchangers for aircraft and missile applications.

**4.3. Analysis of the Pyrolysis Products of Synthetic Jet Fuel S-8 and Methylcyclohexane**

The following solvents are used in the preparation for GC and HPLC analysis of the synthetic jet fuel S-8 and methylcyclohexane product mixtures: dichloromethane ($CH_2Cl_2$),

water ($H_2O$), acetonitrile ($CH_3CN$), and methanol ($CH_3OH$)–all Calledon brand, distilled-in-glass, purchased from KSE Scientific (Durham, NC, USA); benzene ($C_6H_6$) (Chromasolv Plus 99.9+% purity), purchased from Sigma-Aldrich (St. Louis, MO, USA); dimethylsulfoxide (99.9+% purity), purchased from American Bioanalytical (Natick, MA, USA).

### 4.3.1. Gas Chromatography with Mass Spectrometry

GC analysis of the supercritical pyrolysis products of synthetic jet fuel S-8 and methylcyclohexane is performed on an Agilent Model 6890 gas chromatograph with an Agilent Model 5973 mass spectrometer. For the analysis of the products, a sample volume of 10 μL is injected by syringe, through a split injector, onto an HP-5 fused silica capillary column of length, 30 m; diameter, 0.25 mm; and film thickness, 0.1 μm. The column temperature is programmed to hold at 40 °C for the first 3 minutes; it is then ramped at 4 °C /min to 300 °C, where it is held for 15 minutes. The GC/MS instrument is used to identify alkanes, alkenes, alkynes, naphthenes, and 1- to 3-ring aromatic products. The products are identified by matching retention times and mass spectra with those of reference standards.

### 4.3.2. High-Performance Liquid Chromatography with Ultraviolet-Visible Detection

For analysis of the synthetic jet fuel S-8 and methylcyclohexane products by HPLC/UV, a 20-μL aliquot of the product/dimethyl sulfoxide solution is injected onto a Hewlett–Packard Model 1050 high-pressure liquid chromatograph, coupled to a diode-array UV absorbance detector. The chromatographic separation method [Ledesma et al.] utilizes a reversed-phase Vydac 201-TP octadecylsilica column of length, 250 mm; inner diameter, 4.6 mm; particle size, 5 μm; and pore size, 300 Å; with a solvent flow rate of 1.5 mL/min and a temperature of 25 ºC. UV absorbance spectra (from 190-520 nm) are taken, every 0.6 s, of the exiting components. The components are then identified by matching HPLC elution times and UV absorbance spectra

(unique to each PAH) with those of PAH reference standards. As it will be documented in the papers about the identification of the supercritical pyrolysis products of synthetic jet fuel S-8 [Oña and Wornat 2008b] and methylcyclohexane [Oña and Wornat 2008a], the reference standards include both commercially available compounds as well as PAH specially synthesized.

### 4.3.3. High-Performance Liquid Chromatography with Ultraviolet-Visible and Mass Spectrometric Detections

For HPLC/UV/MS analysis of the synthetic jet fuel S-8 products, a 20-μL aliquot of the product/dimethylsulfoxide solution is injected onto an Agilent 1100 Series LC/MSD SL (Palo Alto, CA, USA) high-pressure liquid chromatograph, coupled to a diode-array UV absorbance detector and a mass spectrometric detector (MSD Model G1956B). The chromatographic separation method utilizes a reversed-phase Pinnacle-II PAH octadecylsilica column (Restek, Bellefonte, PA, USA) of length, 250 mm; inner diameter, 4.6 mm; particle size, 5 μm; and pore size, 110 Å; with a solvent flow rate of 1.0 mL/min and a temperature of 30 ºC. UV absorbance spectra (from 190-520 nm) are taken, every 0.4 s, of the product components as they exit the HPLC column. The components are then identified by matching HPLC elution times and UV absorbance spectra (unique to each PAH) with those of PAH reference standards. As it will be documented in the paper about the identification of the supercritical pyrolysis products of synthetic jet fuel S-8 [Oña and Wornat 2008b], the reference standards include both commercially available compounds as well as PAH specially synthesized.

After passing through the UV detector, the separated product components in the eluent are directly introduced into a PhotoMate APPI source (Syagen Technology Inc., Tustin, CA, USA), which uses photo-ionization energies of 10.0 eV and 10.6 eV. The ions are detected by a high-energy dynode detector in the mass spectrometer. The MS is operated in the positive-ion mode with vaporizer and drying gas temperatures of 350 ºC, capillary voltage of 3000 V, drying

gas flow rate of 13 L/min, nebulizer pressure of 60 psig, and cycle time of 0.94 sec/cycle (solvent program of Figure 4.2.B.) or 1.02 sec/cycle (solvent program of Figure 4.2.E.). One MS signal optimized for large PAH is acquired, using a scan range of 273-550 m/z. The signal has a 100% cycle time (solvent program of Figure 4.2.B.) or 50% cycle time (solvent program of Figure 4.2.E.). The fragmentor is set to 200 V, the gain to 1.5, the signal level threshold to 25, and the stepsize to 0.1.

**4.3.4. HPLC Solvent Programs**

The synthetic jet fuel S-8 and methylcyclohexane supercritical pyrolysis product mixtures are each subjected to the time sequence of solvent for HPLC/UV analysis detailed in Figure 4.2.A.

Additionally, the synthetic jet fuel S-8 products are subjected to four separate analyses (two HPLC/UV and two HPLC/UV/MS), each using a different time sequence and series of solvents, as detailed in Figures 4.2.C. and 4.2.D, and in Figures 4.2.B. and 4.2.E., respectively.

The five HPLC solvent programs employ different combinations of five different solvents. The organic solvents, of interest in this work, have different indices of refraction, as reported by Timmermans and Washburn et al. and listed in Table A.1. (Appendix A) and Table B.3. (Appendix B).

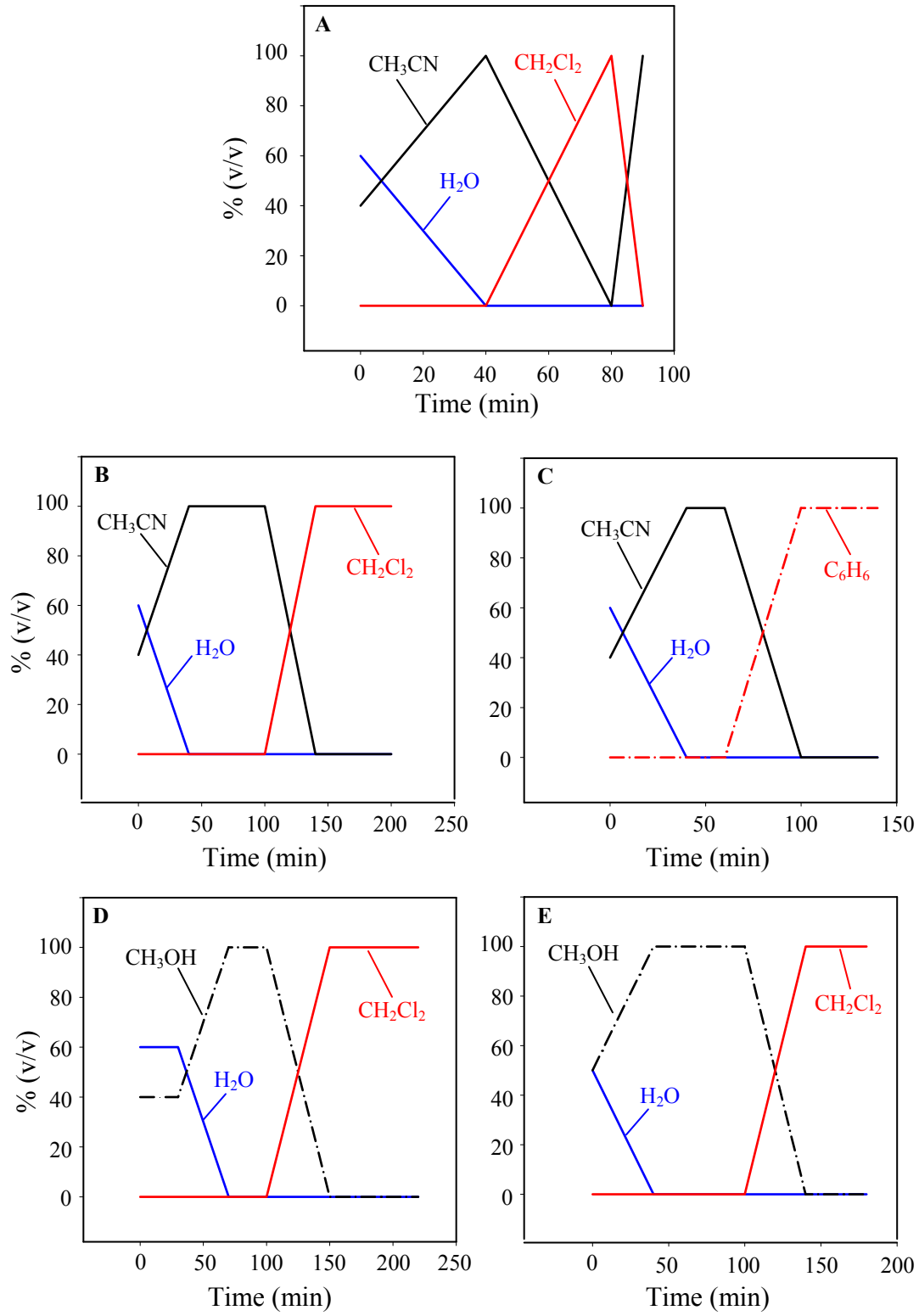


Figure 4.2. Time-Programmed Sequences of Solvents Applied in the HPLC Analyses. $H_2O$, Water; $CH_3CN$, Acetonitrile; $CH_2Cl_2$, Dichloromethane; $C_6H_6$, Benzene; $CH_3OH$, Methanol

# CHAPTER 5. RESULTS AND DISCUSSION

This chapter is divided in two parts: the identification of PAH from the supercritical pyrolysis products of synthetic jet fuel S-8 and the identification of PAH from the supercritical pyrolysis products of methylcyclohexane. To begin this chapter, GC/MS and HPLC/UV/MS results are indicated to substantiate the presence of PAH products from the supercritical pyrolysis of synthetic jet fuel S-8 at a fixed condition. In addition to these results, PAH identifications are reported from the supercritical pyrolysis products of synthetic jet fuel S-8 applying the following identification tools to the HPLC/UV/MS data: the alkyl-substitution effect on the UV spectra of a PAH, the UV solvent-based adjustment, and the Annellation Theory. To supplement this material, a section that explains the effect of the change of temperature in the formation of PAH from the supercritical pyrolysis of synthetic jet fuel S-8 has been added. Later, GC/MS and HPLC/UV results are shown to certify the presence of PAH products from the supercritical pyrolysis of methylcyclohexane at a fixed condition. Finally, the HPLC/UV results collected at several experimental conditions from the supercritical pyrolysis products of methylcyclohexane are shown to demonstrate the influence of the pressure, the temperature, and the residence time in the formation of PAH. Many PAH detected in the products of synthetic jet fuel S-8 and of methylcyclohexane have been identified for the first time as products in the pyrolysis or combustion of a hydrocarbon fuel in any context.

## 5.1. Supercritical Pyrolysis of Synthetic Jet Fuel S-8

### 5.1.1. Identification of Polycyclic Aromatic Hydrocarbons Using Gas Chromatography with Mass Spectrometry

Figure 5.1. shows the GC/MS chromatogram of the supercritical pyrolysis products of synthetic jet fuel S-8 subjected at 710 $^{o}$C and 42 atm. A total of eleven different peaks have been identified based on the comparison of the elution time of the unknown compounds with the

respective elution time of authentic standards. In addition to the solvent, i.e., $CH_2Cl_2$, the following small compounds have been fully identified in the GC/MS chromatogram: benzene, toluene, styrene, indene, 2-methylindene, and naphthalene. The full identification of several of these molecules, e.g., xylenes, ethylbenzenes, methylethylbenzenes, and methylstyrenes, has not been possible due to the lack of standards to recognize the correct retention time of each compound and due to the inability of the GC/MS technique to distinguish between isomeric molecules with similar mass spectra.

### 5.1.2. Identification of Polycyclic Aromatic Hydrocarbons Using High-Performance Liquid Chromatography with Ultraviolet-Visible Spectroscopy and Mass Spectrometric Detections

**• Case A: Identification Based on Comparison with Ultraviolet-Visible Spectra from Authentic Standards**

Figure 5.2. shows the first version of the HPLC/UV chromatogram of the supercritical pyrolysis products of synthetic jet fuel S-8 at 710 $^oC$ and 42 atm using the solvent program described in Figure 4.2.-A. Theoretically, Figure 4.2.A. shows a change of solvent at 40 minutes from $CH_3CN$ to $CH_2Cl_2$, experimentally, however, this change is evidenced by a rise in the baseline in the chromatogram of Figure 5.2. at approximately 42 minutes. This difference of about 2 minutes is due to the delay time between the preset solvent program in the computer and the actual chromatographic signal. The hump observed in the chromatogram at approximately 42 minutes indicates a gradual change from the UV-nonabsorbing solvent ($CH_3CN$) to the UV-absorbing solvent ($CH_2Cl_2$).

Sixty-one different peaks have been identified based on the UV spectral comparison with the spectral information of authentic standards commercially available and with the spectral information collected from the literature [Graselli and Ritchey, Friedel and Orchin, Fetzer and Biggs 1994, Lang and Buffleb, and Ojakaar].

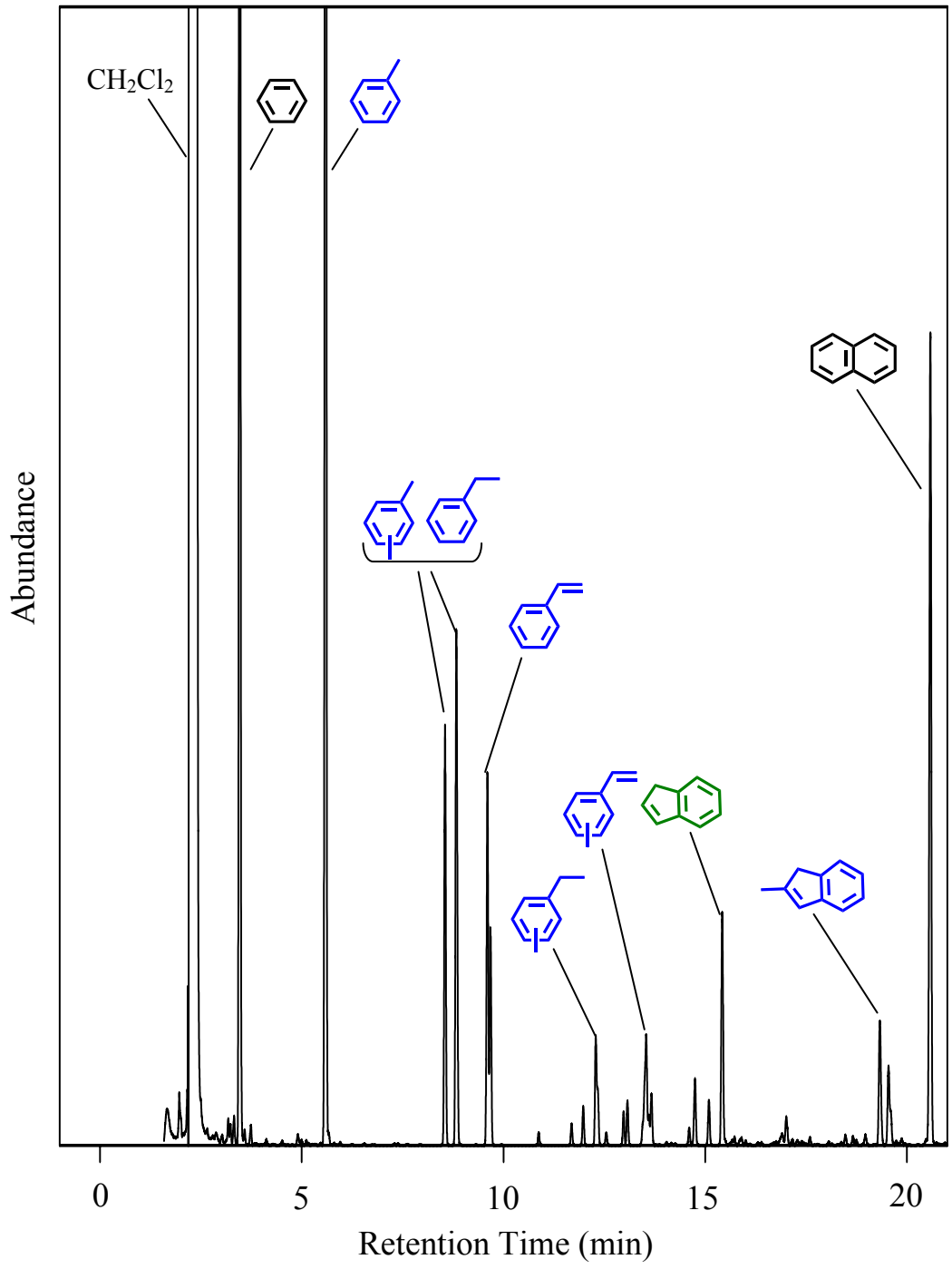


Figure 5.1. GC/MS Chromatogram of the Synthetic Jet Fuel S-8 Supercritical Pyrolysis Products at 710 $^{o}$C and 42 atm.

The PAH identified can be grouped into: methylated PAH (blue), indene benzologues (green), fluoranthene benzologues (red), and benzenoid PAH (black). The following is the list of the identified PAH in their respective elution order: phenalenone, indene, naphthalene, 2-methylindene, acenaphthylene, 1-methylnaphthalene, 2-methylnaphthalene, acenaphthene, fluorene, phenanthrene, anthracene, cyclopenta[*def*]phenanthrene, 9-phenylfluorene, 9-methyl-phenanthrene, fluoranthene, 1-methylphenanthrene, 1,1'-naphthylanthracene, 1-methyl-anthracene, pyrene, 2-methylanthracene, benzo[*a*]fluorene, 4-methylpyrene, 1-methylpyrene co-eluting with 1-phenylpyrene, benz[*a*]anthracene, 2-methylpyrene, chrysene, benzo[*a*]-fluoranthene, benzo[*j*]fluoranthene, benzo[*e*]pyrene, benzo[*b*]fluoranthene, perylene, benzo[*k*]-fluoranthene, benzo[*a*]pyrene, dibenz[*a,h*]anthracene, benzo[*ghi*]perylene, indeno[1,2,3-*cd*]-pyrene, naphtho[2,3-*e*]pyrene, naphtho[1,2-*a*]pyrene, dibenzo[*a,e*]pyrene, naphtho[1,2-*k*]-fluoranthene, benzo[*b*]perylene, anthanthrene, picene, benzo[*b*]chrysene, dibenzo[*b,k*]-fluoranthene, naphtho[2,3-*b*]fluoranthene, coronene, naphtho[2,1-*a*]pyrene, dibenzo[*a,i*]pyrene, phenanthro[2,3-*a*]pyrene, naphtho[2,3-*a*]pyrene, dibenzo[*a,h*]pyrene, 2,2'-bianthryl, dibenzo-[*cd,lm*]perylene co-eluting with benzo[*a*]coronene, phenanthro[5,4,3,2-*efghi*]perylene co-eluting with benzo[*cd*]naphtho[3,2,1,8-*pqra*]perylene, benzo[*pqr*]naphtho[8,1,2-*bcd*]perylene, naphtho-[8,1,2-*abc*]coronene, and ovalene.

Representative identifications are presented in Figures 5.3. through 5.6. Figures 5.3., 5.4., 5.5., and 5.6. show the UV spectral matches between the spectra of the reference standards of benzo[*ghi*]perylene, indeno[1,2,3-*cd*]pyrene, dibenzo[*a,i*]pyrene, and naphtho[8,1,2-*abc*]-coronene (in red) and their respective spectra from the supercritical pyrolysis products of synthetic jet fuel S-8 (in black). Similar procedure has been followed to identify the remainder of the PAH discussed in this section.

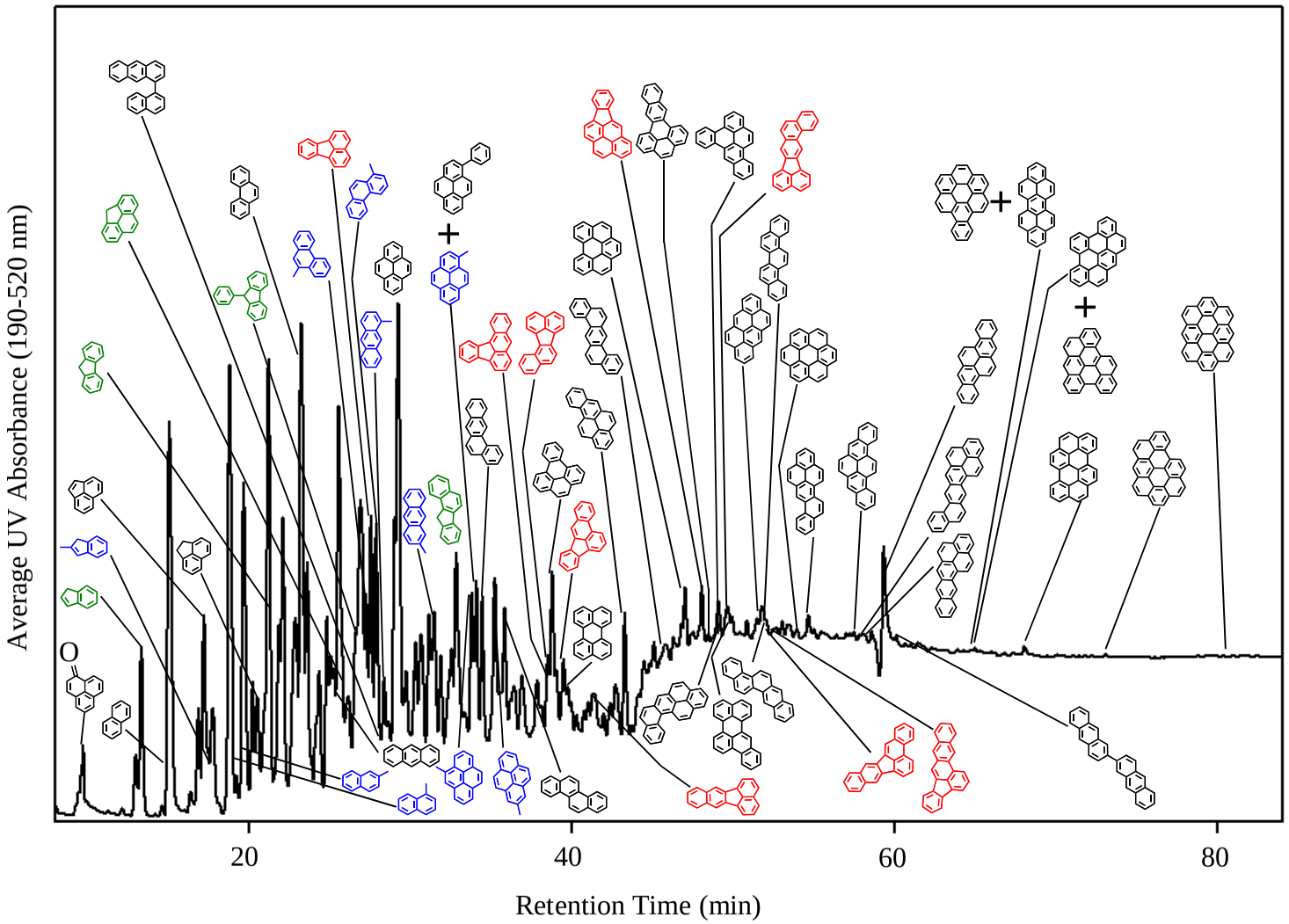


Figure 5.2. HPLC/UV Chromatogram (First Version) of the Synthetic Jet Fuel S-8 Supercritical Pyrolysis Products at 710 °C and 42 atm.

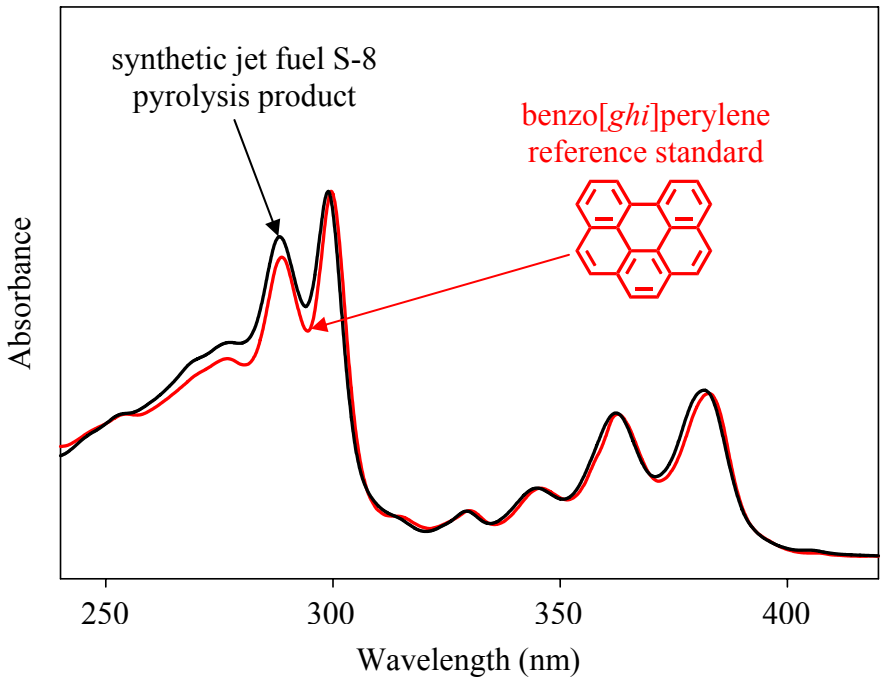


Figure 5.3. UV Absorbance Spectra for the Reference Standard of Benzo[*ghi*]perylene and for a Synthetic Jet Fuel S-8 Supercritical Pyrolysis Product having the same HPLC Retention Time.

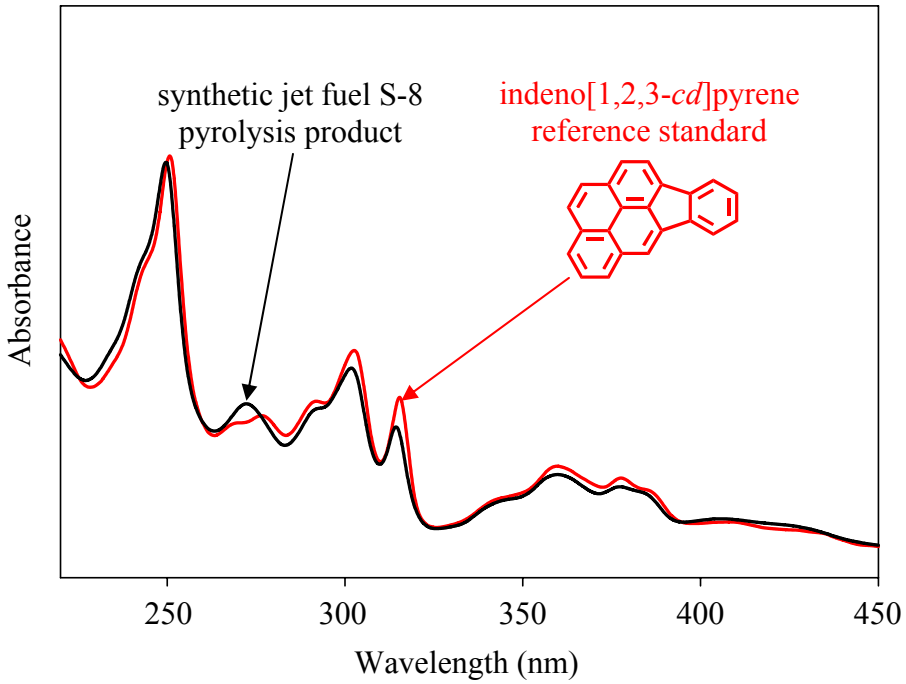


Figure 5.4. UV Absorbance Spectra for the Reference Standard of Indeno[1,2,3-*cd*]pyrene and for a Synthetic Jet Fuel S-8 Supercritical Pyrolysis Product having the same HPLC Retention Time.

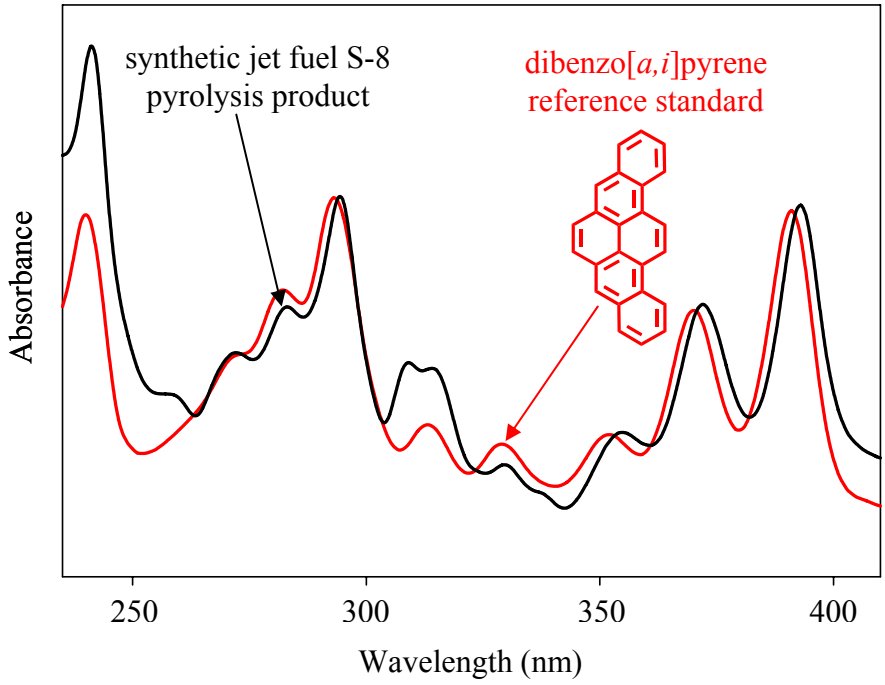


Figure 5.5. UV Absorbance Spectra for the Reference Standard of Dibenzo[*a,i*]pyrene and for a Synthetic Jet Fuel S-8 Supercritical Pyrolysis Product having the same HPLC Retention Time.

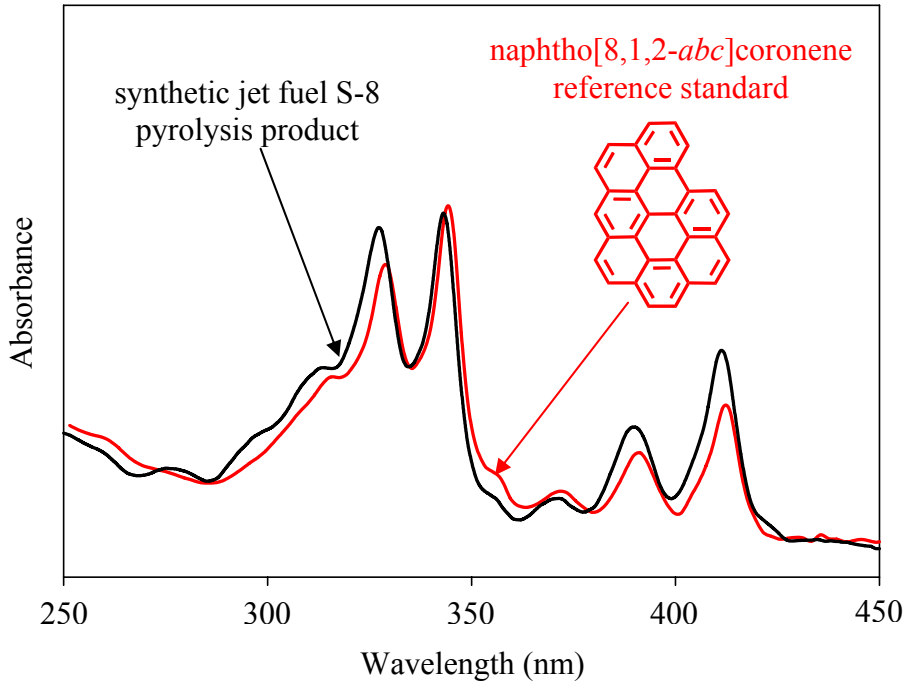


Figure 5.6. UV Absorbance Spectra for the Reference Standard of Naphtho[8,1,2-*abc*]coronene and for a Synthetic Jet Fuel S-8 Supercritical Pyrolysis Product having the same HPLC Retention Time.

**• Case B: Identification Based on the Alkyl Substituent Effect on the UV Spectra**

Section 3.2. discusses about the effect of an alkyl substituent on the UV spectra of PAH. These arguments have been used to identify alkylated products both from the supercritical pyrolysis of synthetic jet fuel S-8 and from the supercritical pyrolysis of other fuels, e.g., methylcyclohexane, toluene [McClaine et al. 2006], and *n*-decane [Bagley and Wornat]. The present section describes the identification of: methylphenalenone, methylfluoranthene, methylchrysene, methylbinaphthyl, methylbenzo[*e*]pyrene, methylbenzo[*a*]pyrene, methylbenzo-[*ghi*]perylene, methylbenzo[*b*]chrysene, 1-methylcoronene, methylnaphtho[2,1-*a*]pyrene, methyldibenzo[*cd,lm*]perylene, and methylnaphtho[8,1,2-*abc*]coronene, based on these principles.

Like in the previous case, the HPLC/UV results obtained with the solvent program 4.2.-A have been employed. Furthermore, to verify the presence of methylated PAH in opposition to the presence of other kinds of alkylated PAH with similar UV spectral behavior, the MS results obtained with the solvent program 4.2.-E have been used.

Figures 5.7., 5.9., and 5.11. show the UV spectral identification of methylbenzo-[*b*]chrysene, 1-methylcoronene, and methylnaphtho[2,1-*a*]pyrene, respectively, from the supercritical pyrolysis products of synthetic jet fuel S-8 based on the arguments of Section 3.2. As it is evidenced from Figures 5.7., 5.9., and 5.11., there are perceptible shifts of 2, 0.5, and 3.0 nm from the UV spectral bands of the unknown compounds (in black) to the bands of the standards of benzo[*b*]chrysene, coronene, and naphtho[2,1-*a*]pyrene (in red), respectively.

Furthermore, the mass spectra of Figures 5.8., 5.10., and 5.12. demonstrate the presence of compounds with the same molecular mass of methylbenzo[*b*]chrysene, 1-methylcoronene, and methylnaphtho[2,1-*a*]pyrene.

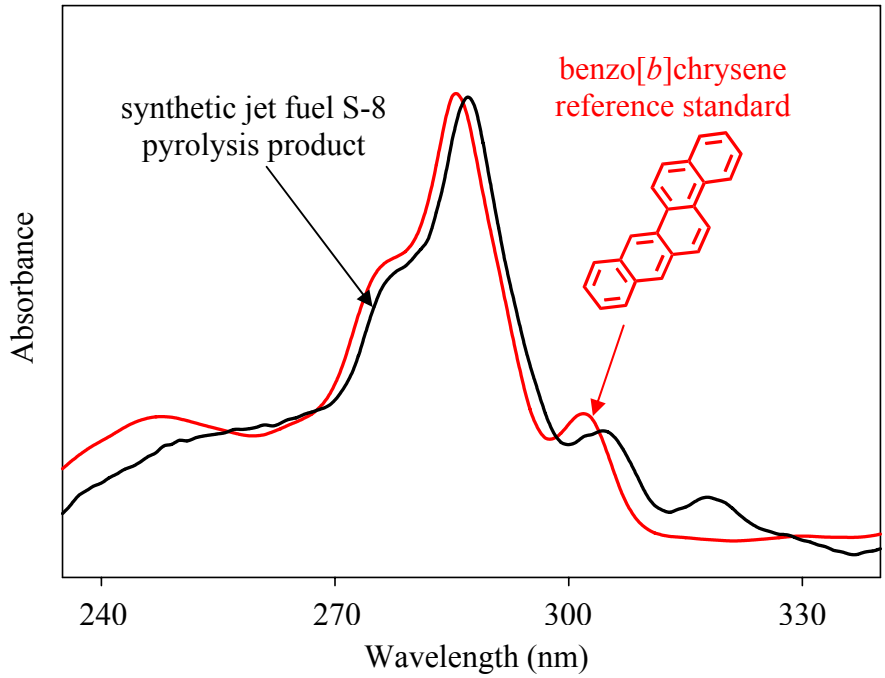


Figure 5.7. UV Absorbance Spectra for the Reference Standard of Benzo[*b*]chrysene and for a Synthetic Jet Fuel S-8 Supercritical Pyrolysis Product.

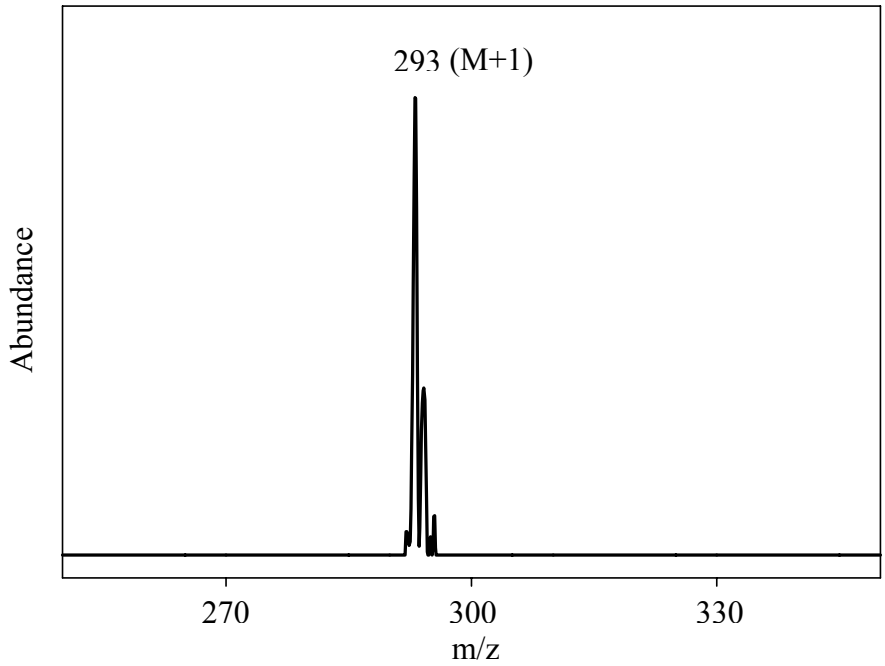


Figure 5.8. Mass Spectrum of the Synthetic Jet Fuel S-8 Supercritical Pyrolysis Product presented in Figure 5.7.

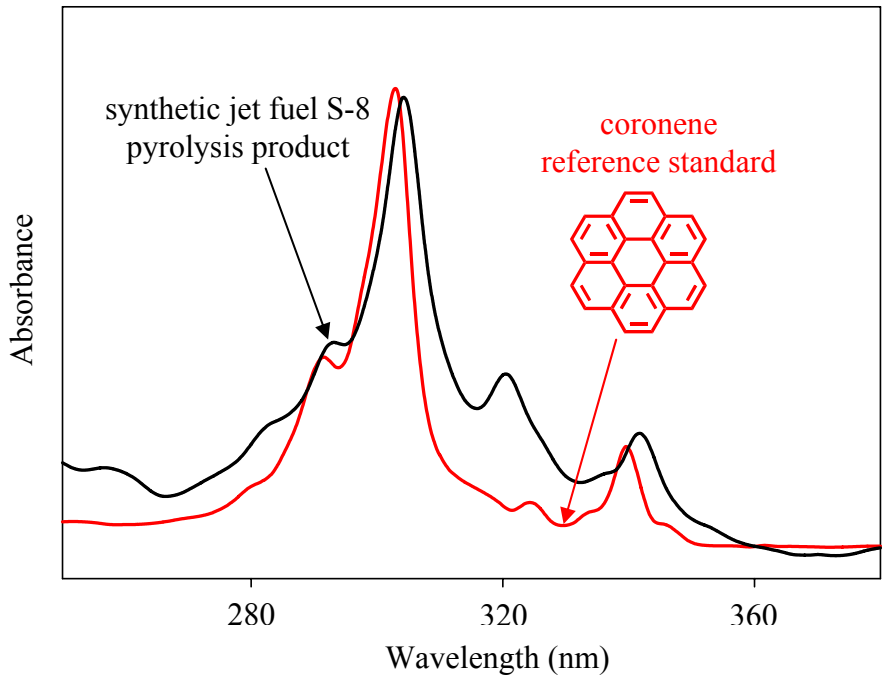


Figure 5.9. UV Absorbance Spectra for the Reference Standard of Coronene and for a Synthetic Jet Fuel S-8 Supercritical Pyrolysis Product.

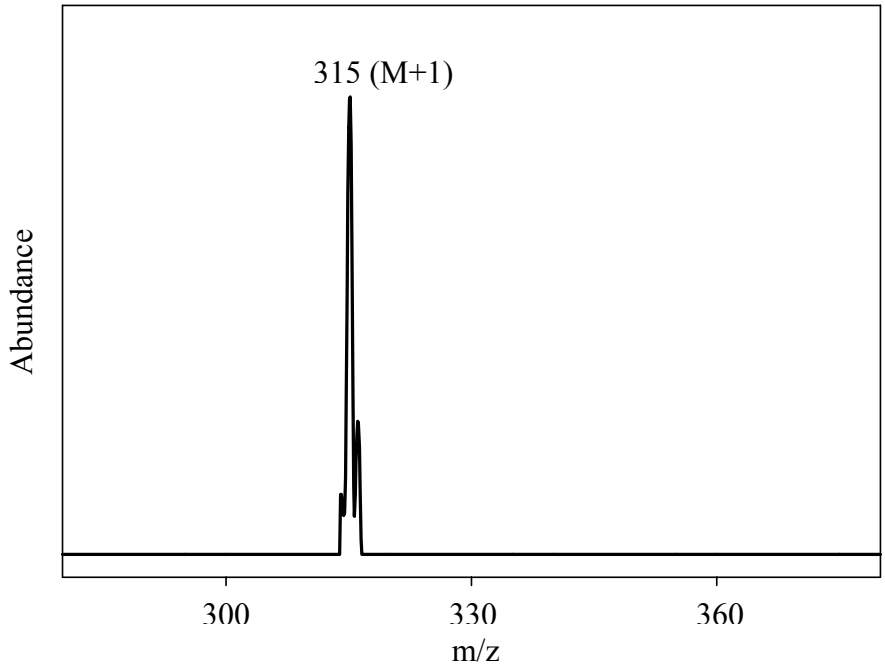


Figure 5.10. Mass Spectrum of the Synthetic Jet Fuel S-8 Supercritical Pyrolysis Product presented in Figure 5.9.

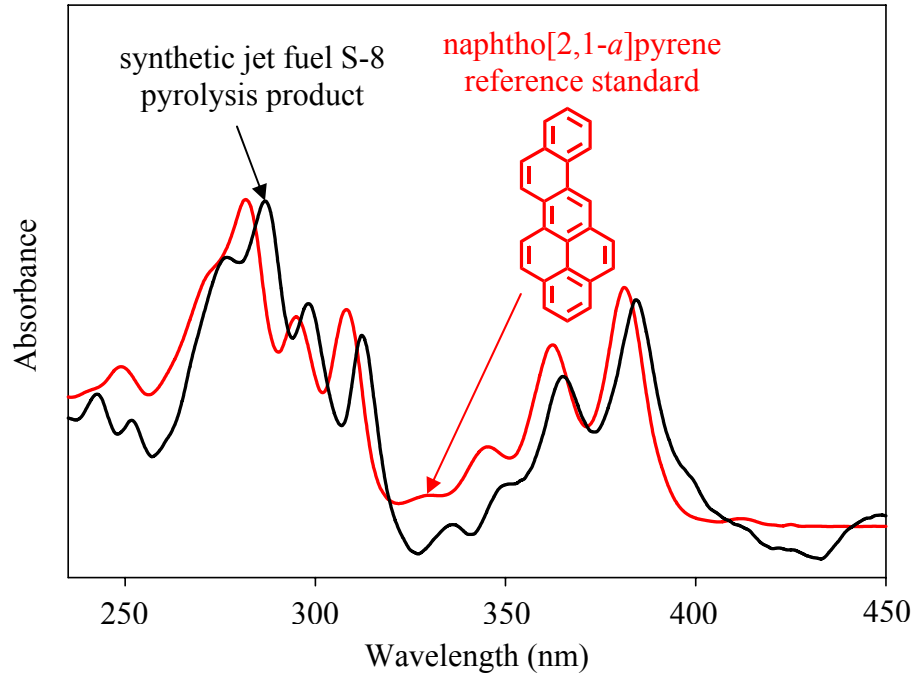


Figure 5.11. UV Absorbance Spectra for the Reference Standard of Naphtho[2,1-*a*]pyrene and for a Synthetic Jet Fuel S-8 Supercritical Pyrolysis Product.

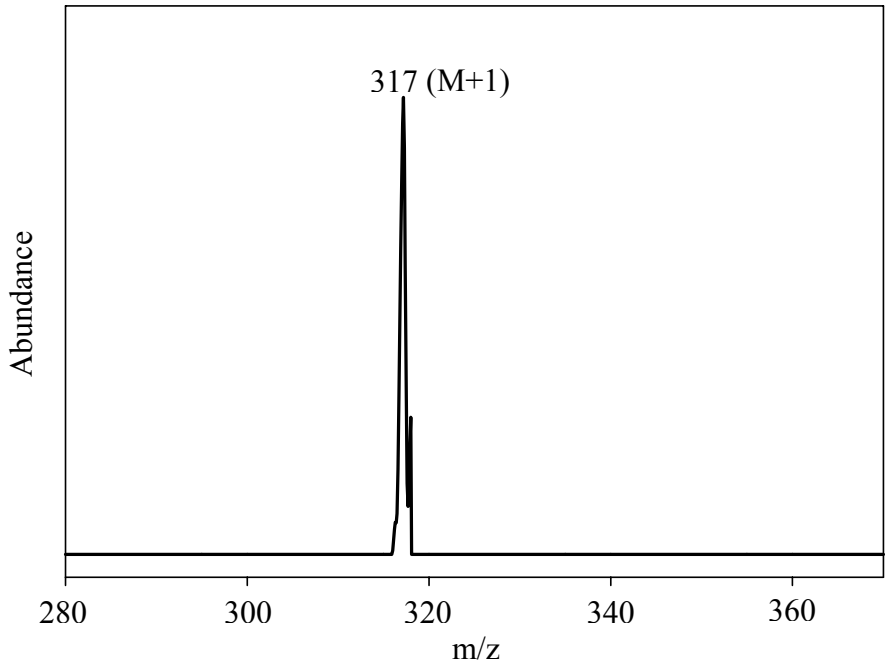


Figure 5.12. Mass Spectrum of the Synthetic Jet Fuel S-8 Supercritical Pyrolysis Product presented in Figure 5.11.

The UV analyses show that in addition to the spectral shifts, there are noticeable similarities in shape, position, and intensity of the spectral bands in each case. In Section 3.2., those evidences have been associated with the presence of alkylated PAH. Based on these observations, the unknown compounds have been labeled as methylbenzo[*b*]chrysene, 1-methylcoronene, and methylnaphtho[2,1-*a*]pyrene, respectively. Similar analyses have been followed to identify the remainder of the methylated PAH discussed in this section. To sum up, Figure 5.13. shows the second version of the HPLC/UV chromatogram of the synthetic jet fuel S-8 products using the solvent program from Figure 4.2.-A. Seventy-three compounds have been detected so far including the new methylated PAH recently identified.

**• Case C: Identification Using the Ultraviolet-Visible Solvent-Based Adjustment**

The identifications of benzo[*cd*]naphtho[1,2,3-*lm*]perylene, dibenzo[*b,ghi*]perylene, 8H-dibenzo[*a,jk*]pyrene, and benzo[*pqr*]dinaphtho[8,1,2-*bcd*:2',1',8'-*lmn*]perylene presented in this section constitute summaries of two papers already published in the literature [Oña and Wornat 2007, Oña and Wornat 2008c]. These identifications have been performed using the arguments and observations about the solvent-based adjustment on the UV spectra of a PAH delineated in Section 3.3.

**Identification of Benzo[*cd*]naphtho[1,2,3-*lm*]perylene:** As a first step for the UV spectral identification of benzo[*cd*]naphtho[1,2,3-*lm*]perylene [Oña and Wornat 2007], the information obtained with the solvent program 4.2.-A. has been used. The identification of benzo[*cd*]naphtho[1,2,3-*lm*]perylene starts with the designation of the unknown component as **I** in Figure 5.13. Figure 5.14. shows the UV spectrum of compound **I** and the UV spectrum of dibenzo[*cd,lm*]perylene, a PAH with a high length-to-breadth (L/B) ratio [Wise et al.] for which a reference standard is available.

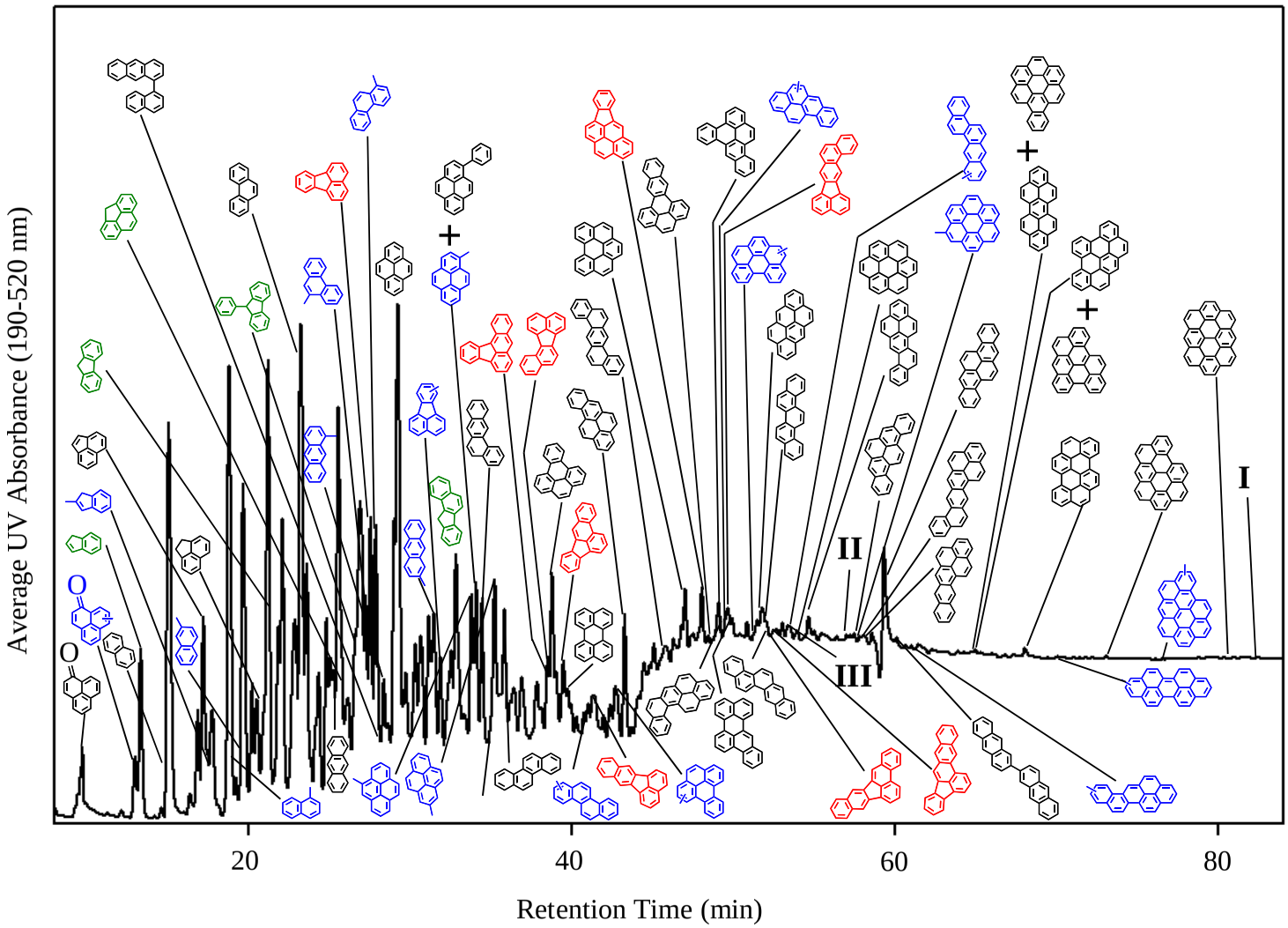


Figure 5.13. HPLC/UV Chromatogram (Second Version) of the Synthetic Jet Fuel S-8 Supercritical Pyrolysis Products at 710 ºC and 42 atm.

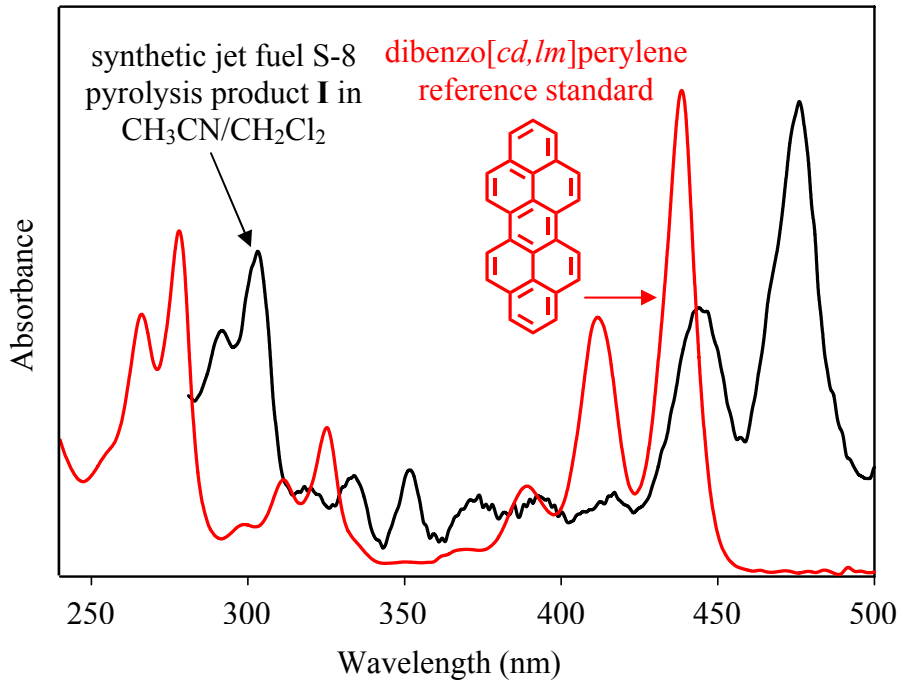


Figure 5.14. UV Absorbance Spectra for Compound **I** (black line) in the Solvent Program 4.2.-A and for the Reference Standard of Dibenzo[*cd,lm*]perylene (red line) in $CH_3CN/CH_2Cl_2$.

This UV spectral analysis has been carried out in order to establish common spectral behaviors and determine the PAH family of compound **I**. Figure 5.14. reveals that the UV spectrum of compound **I** is extremely similar in band shape features to the UV spectrum of dibenzo[*cd,lm*]perylene; only the positions of the bands are shifted. Consequently, it is feasible to deduce that the structure of compound **I** should be very closely related to that of this reference PAH.

One of the distinctive analogies between both UV spectra is the presence of the long-wavelength (> 385 nm) bands of increasing intensity, which are characteristic of benzenoid compounds, particularly those with a base structure of perylene [McClaine et al. 2006], e.g., benzo[*a*]perylene, benzo[*ghi*]perylene, dibenzo[*e,ghi*]perylene, tribenzo[*b,ghi,k*]perylene, and dibenzo[*b,k*]perylene [Clar 1964].

Figure 5.15 shows the mass spectrum of compound **I**, obtained from the HPLC/MS analysis using the solvent program of Figure 4.2.-B. Since the mass spectrum in Figure 5.15. is taken when acetonitrile and dichloromethane compose the HPLC mobile phase, the first- and second- most abundant ions in the spectrum, as demonstrated by Zhang et al., are at M + H and M + 2H, respectively─where M is the molecular weight of the PAH analyte. Therefore the primary ion at M + H = 377 and the secondary ion at M + 2H = 378 in the mass spectrum of Figure 5.15. reveal that product **I** is an unsubstituted PAH of molecular weight 376 and molecular formula $C_{30}H_{16}$.

The MS analysis of Figure 5.15., the UV absorbance characteristics in Figure 5.14., and the HPLC elution behavior in Figure 5.13. lead us to deduce that compound **I** is a planar benzologue of perylene, having a high L/B, a molecular weight of 376, and thus a molecular formula of $C_{30}H_{16}$.

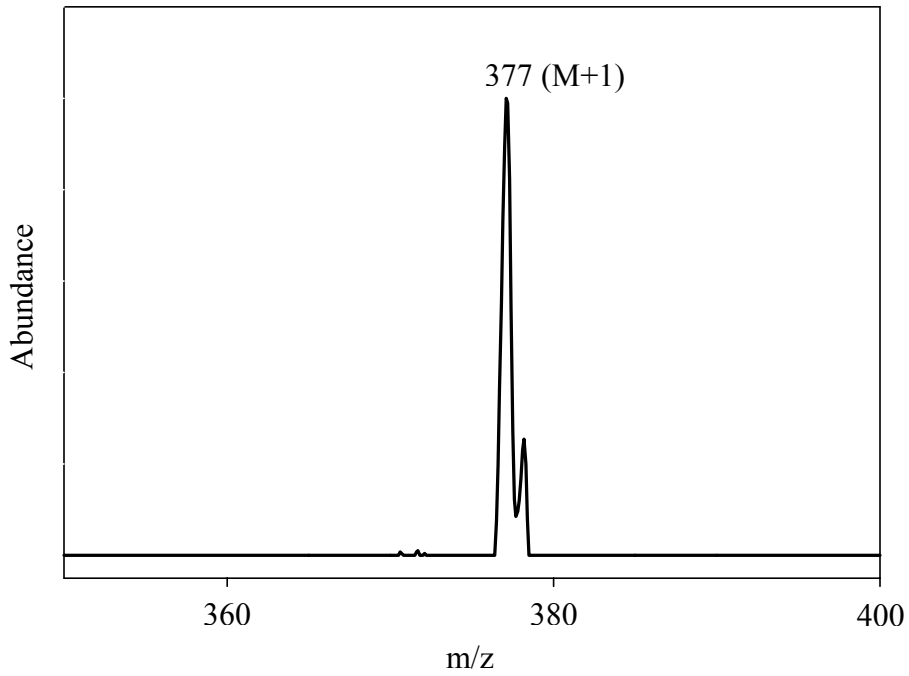


Figure 5.15. The Mass Spectrum of Compound **I**, taken during the Solvent Program 4.2.-B.

One such $C_{30}H_{16}$ PAH for which the UV spectrum is available [Fetzer and Biggs 1985, Fetzer 2000] is benzo[*cd*]naphtho[1,2,3-*lm*]perylene. (It should be noted that in their initial paper [Fetzer and Biggs 1985], Fetzer and Biggs mistakenly attributed the UV spectrum to phenaleno[1,9-*ab*]perylene, but subsequently Fetzer [Fetzer 2000] corrected the error, clarifying that the UV spectrum was that of benzo[*rst*]naphtho[8,1,2-*cde*]pentaphene, which is also called benzo[*cd*]naphtho[1,2,3-*lm*]perylene.) Consistent with its planarity, benzo[*cd*]naphtho[1,2,3-*lm*]perylene has been shown to exhibit a long HPLC elution time [Fetzer and Biggs 1985], as it is evidenced for compound **I** in Figure 5.13., as well as sharp UV spectral peaks [Fetzer and Biggs 1985, Fetzer 2000], as it is noted for compound **I** in Figure 5.14. Neither of these characteristics is displayed by non-planar $C_{30}H_{16}$ isomers such as tribenzo[*a,cd,lm*]perylene, tribenzo-[*b,n,pqr*]perylene, benzo[*ghi*]naphtho[2,1-*a*]perylene, benzo[*b*]naphtho[1,2,3,4-*ghi*]perylene, and phenanthro[1,2,3,4-*ghi*]perylene, which have earlier HPLC elution times [Fetzer and Biggs 1985, Sander and Wise] and whose UV spectral bands are rounder and less distinct [Fetzer 2000] than those of compound **I**.

Figure 5.16. shows the published UV spectrum of benzo[*cd*]naphtho[1,2,3-*lm*]perylene [Fetzer and Biggs 1985, Fetzer 2000], taken in $CH_3OH/CH_2Cl_2$, along with the UV spectrum of the unknown compound **I,** taken in $CH_3CN/CH_2Cl_2$. Three different groups of bands are delineated in these UV spectra: *s*, short wavelength, before 310 nm; *m*, medium wavelength, between 310 and 385 nm; and *l*, long wavelength, after 385 nm. Comparison of the two spectra in Figure 5.16. shows that the magnitudes of the two sets of *s* bands and *l* bands match quite well, but the wavelengths of the peaks do not fully coincide. The two sets of *m* band peaks, in contrast, match fairly well in wavelength but not in magnitude.

The UV spectrum of compound **I** and the UV spectrum of benzo[*cd*]naphtho[1,2,3-*lm*]perylene [Fetzer and Biggs 1985, Fetzer 2000] in Figure 5.16. have been obtained in different mixtures of solvents: $CH_3OH/CH_2Cl_2$ for benzo[*cd*]naphtho[1,2,3-*lm*]perylene and $CH_3CN/CH_2Cl_2$ for compound **I**. It is therefore reasonable to suppose that the differences between the two spectra in Figure 5.16. could indicate the influence of solute-solvent interactions, through solvatochromism shifts [Bayliss and McCrae, LeRosen and Reid]. If such shifts are responsible for the spectral differences in Figure 5.16., a simple shifting of one of the spectra would cancel out the presumed solvatochromic effect of the solvent on the position of the spectral bands. To test this idea, the whole UV spectrum of benzo[*cd*]naphtho[1,2,3-*lm*]perylene in Figure 5.16. has been shifted until its *l* bands coincide with the *l* bands of the UV spectrum of compound **I**—a shift of approximately 3.4 nm.

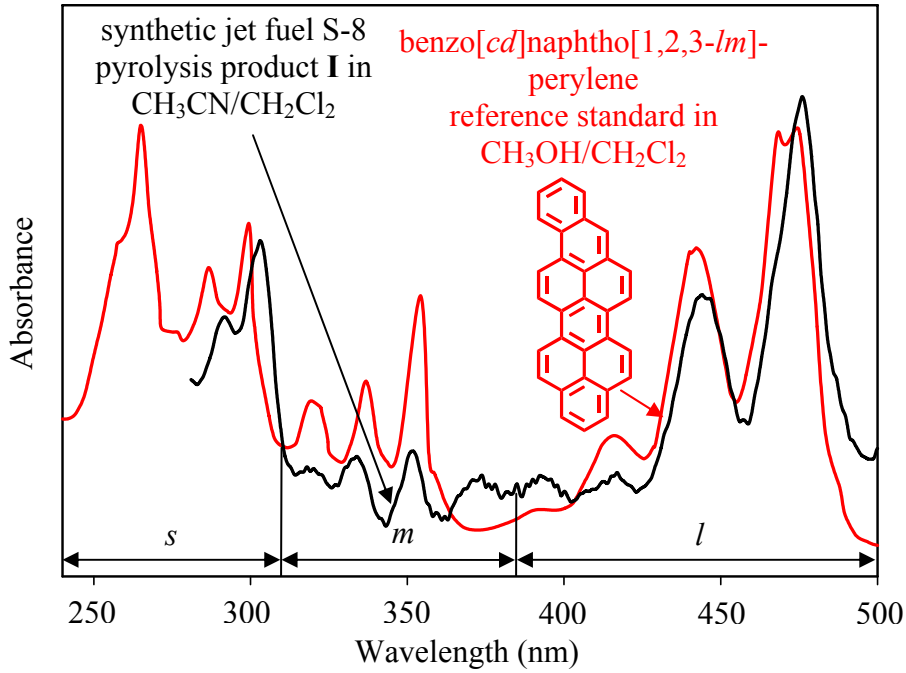


Figure 5.16. UV Absorbance Spectra for Compound **I** (black line), taken during the Solvent Program 4.2.-A, and for the Reference Standard of Benzo[*cd*]naphtho[1,2,3-*lm*]perylene [Fetzer and Biggs 1985, Fetzer 2000] (red line), in $CH_3OH/CH_2Cl_2$.

Figure 5.17. portrays this newly shifted UV spectrum of benzo[*cd*]naphtho[1,2,3-*lm*]perylene, with the UV spectrum of compound **I** from Figure 5.14. The new spectral comparison indicates that the wavelengths of the *l* bands and the *s* bands now match quite well. However, the *m* bands do not behave similarly, and they do not match after the adjustment, either in peak size or in peak position (wavelength).

The fact that the two spectra in Figure 5.17. do look so similar suggests that compound **I** is very likely benzo[*cd*]naphtho[1,2,3-*lm*]perylene, but the differences in the *m* bands—and the 3.4 nm shift necessary to achieve agreement in the *s* and *l* bands—suggest that there are complex solvent effects that need to be accounted for before the identity of compound **I** can be established.

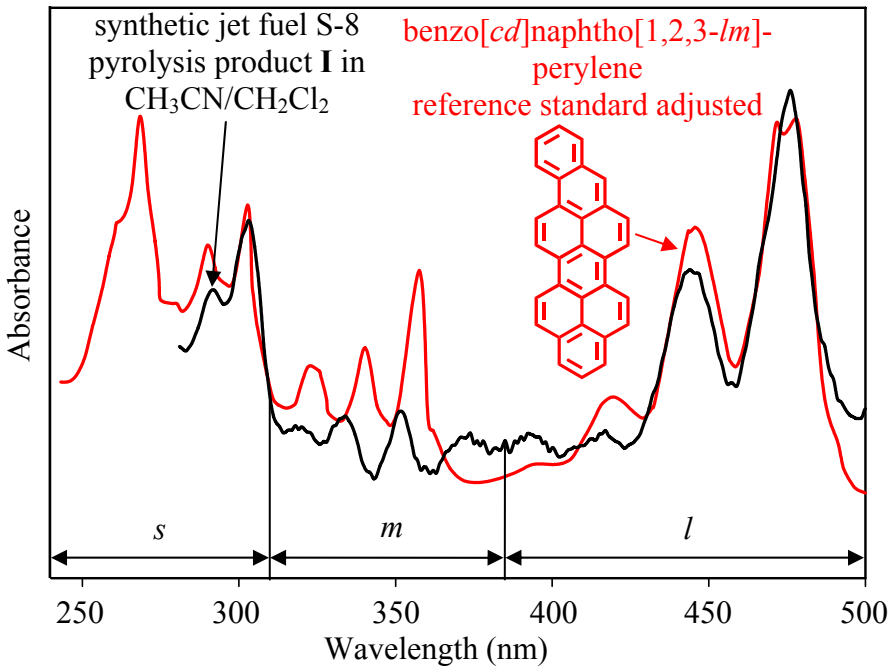


Figure 5.17. UV Absorbance Spectrum for Compound **I** (black line), taken during the Solvent Program 4.2.-A, and the adjusted UV Absorbance Spectrum (shifted by 3.4 nm) for the Reference Standard of Benzo[*cd*]naphtho[1,2,3-*lm*]perylene [Fetzer and Biggs 1985, Fetzer 2000] (red line).

To further explore these solvent effects, the synthetic jet fuel products have been analyzed with the HPLC solvent program of Figure 4.2.-C, which utilizes $H_2O$, $CH_3CN$ and $C_6H_6$ as solvents. The resulting UV spectrum of compound **I**, in $CH_3CN/C_6H_6$, appears in Figure 5.18., along with that published [Fetzer and Biggs 1985, Fetzer 2000] for benzo[*cd*]naphtho[1,2,3-*lm*]perylene, in $CH_3OH/CH_2Cl_2$. In this case, the magnitudes of all the peaks match quite well, and the *s* and the *m* bands of the UV spectrum of compound **I** match quite well with their respective bands of benzo[*cd*]naphtho[1,2,3-*lm*]perylene [Fetzer and Biggs 1985, Fetzer 2000]; however, the *l* bands still present a bathochromic shift due to the influence of the solvent.

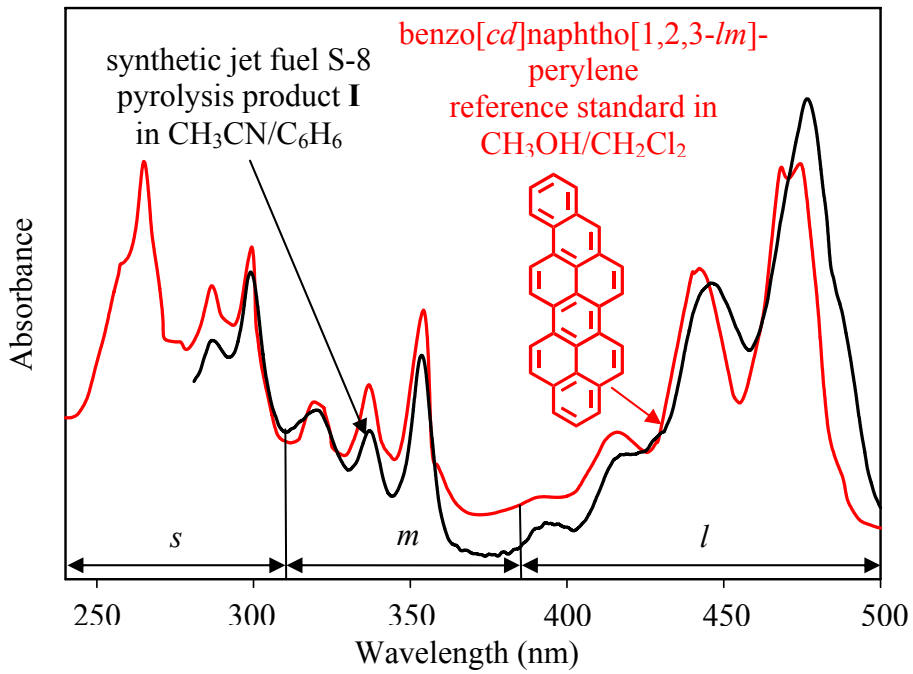


Figure 5.18. UV Absorbance Spectra for Compound **I** (black line), taken during the Solvent Program 4.2.-C, and for the Reference Standard of Benzo[*cd*]naphtho[1,2,3-*lm*]perylene [Fetzer and Biggs 1985, Fetzer 2000] (red line), in $CH_3OH/CH_2Cl_2$.

In order to establish that the differences between the UV spectra of compound **I** and benzo[*cd*]naphtho[1,2,3-*lm*]perylene, in both Figure 5.16. and Figure 5.18., are due to solvent

effects, the synthetic jet fuel products have also been analyzed with the solvent program of Figure 4.2.-D, which utilizes water, methanol and dichloromethane. The purpose of this solvent program is to emulate the conditions of the analysis carried out by Fetzer et al. [Fetzer and Biggs 1985, Fetzer 2000]. The resulting UV spectrum of compound **I**, in $CH_3OH/CH_2Cl_2$, appears in Figure 5.19., along with that published for benzo[*cd*]naphtho[1,2,3-*lm*]perylene [Fetzer and Biggs 1985, Fetzer 2000], in $CH_3OH/CH_2Cl_2$. Readily apparent from Figure 5.19. is the great consistency of the match of all of the spectral bands (*s*, *m*, and *l*) that define the two spectra, in terms of both peak magnitude and position (wavelength). The very slight differences between the two spectra in Figure 5.19. are due to the different concentrations of dichloromethane in the two analyses. Nevertheless, the virtual coincidence of the two spectra in Figure 5.19. represents the undeniable verification that compound **I** is indeed benzo[*cd*]naphtho[1,2,3-*lm*]perylene.

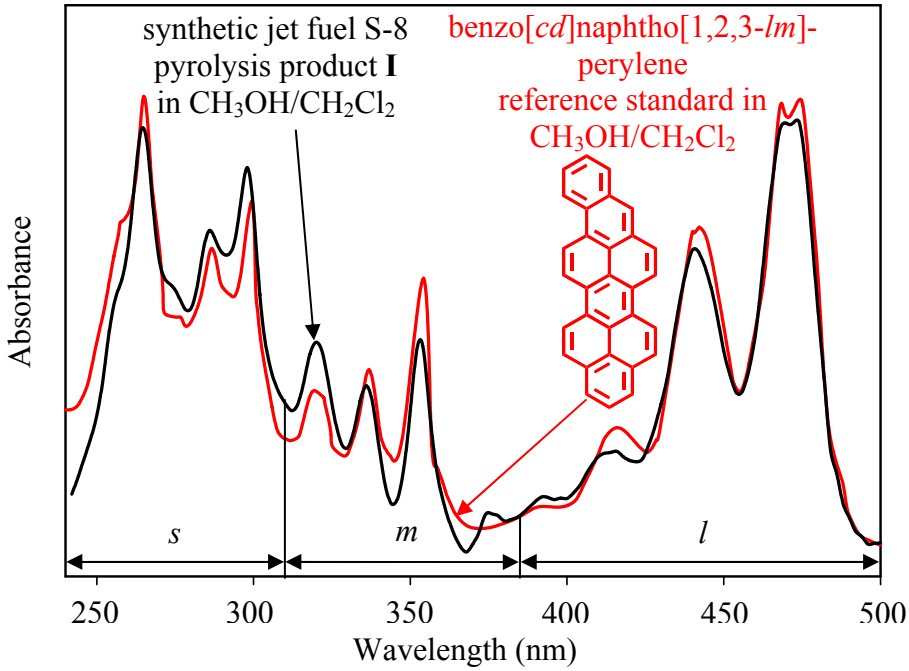


Figure 5.19. UV Absorbance Spectra for Compound **I** (black line), taken during the Solvent Program 4.2.-D, and for the Reference Standard of Benzo[*cd*]naphtho[1,2,3-*lm*]perylene [Fetzer and Biggs 1985, Fetzer 2000] (red line), in $CH_3OH/CH_2Cl_2$.

With the identity of compound **I** established as benzo[*cd*]naphtho[1,2,3-*lm*]perylene, the solvent-associated differences in the UV spectra of this compound are now examined. Since Kundt has related solvent-associated effects in UV spectra with the solvents' indices of refraction, it is important to calculate, for each solvent program, the refractive index *n* of the mobile phase at the time of compound **I**'s elution. The results of these calculations appear in Table A.2. (Appendix A). In calculating the refractive index *n* of each binary solvent mixture, the equation of Venables and Schmuttenmaer has been used:

$$n = a_1 n_1 + a_2 n_2 \qquad \text{Equation 5.1.}$$

where $n_i$ and $a_i$ are the refractive index and volume fraction, respectively, of each organic solvent i composing the HPLC mobile phase at the time of the component's elution. The computed refractive index *n* from Equation 5.1. is designated as "ideal" by Venables and Schmuttenmaer since their equation assumes that the solvent mixture behaves as a volume-fraction-weighted sum of its components. The values of the $a_i$ needed for Equation 5.1. come from the third column of Table A.2. (Appendix A), and the values of the $n_i$ are taken from the last column of Table A.1. (Appendix A). The resulting values of *n*, computed for each mobile phase composition at the time of compound **I**'s elution, appear in the last column of Table A.2. (Appendix A).

Figure 5.20. presents the three UV spectra of compound **I** (now determined to be benzo[*cd*]naphtho[1,2,3-*lm*]perylene), taken in the three mobile phases: $CH_3CN/CH_2Cl_2$ (Solvent Program 4.2.-A); $CH_3CN/C_6H_6$ (Solvent Program 4.2.-C); and $CH_3OH/CH_2Cl_2$ (Solvent Program 4.2.-D). Each spectrum in Figure 5.20. is labelled with the computed index of refraction (from Table A.2.)that is associated with the respective mobile phase at the time each spectrum is taken. As Figure 5.20. reveals, the solvent effects are different for the different UV spectral bands. In accordance with the postulate of Kundt, the *l* bands exhibit a sequential bathochromic shift as the

refractive index is increased from 1.405 to 1.413 to 1.463, although the initial shift is greater than the latter. The magnitudes of the *l*-band peaks are affected very little by the change in solvent. In contrast, the magnitudes of the *m*-band peaks vary with solvent, but these peaks exhibit very little shift with changing solvent. Lastly, the *s* bands exhibit the most complex behavior: an increase in refractive index from 1.405 to 1.413 brings about a bathochromic shift and a reduction in peak intensity; a further increase in refractive index from 1.413 to 1.463, however, brings about a hypsochromic shift and a minor decrease in peak intensity. Therefore, it is reasonable to conclude that Kundt's postulate—that a bathochromic shift is associated with an increase in the solvent index of refraction—holds for the *l* bands of the UV spectrum of benzo[*cd*]naphtho[1,2,3-*lm*]perylene, but that it does not adequately account for the more complex behavior in the *m* and *s* bands.

**Identification of Dibenzo[*b,ghi*]perylene:** For the UV spectral analysis and identification of dibenzo[*b,ghi*]perylene [Oña and Wornat 2008c], the information obtained with the solvent program 4.2.-A has been used. The identification of dibenzo[*b,ghi*]perylene starts with the designation of the unknown component as **II** in the chromatogram shown in Figure 5.13.

Figure 5.21. shows the mass spectrum of compound **II** obtained with the solvent program 4.2.-E. As it was explained in Section 3.1.3., the first- and second- most abundant ions in the PAH mass spectrum are at M + H and M + 2H, respectively, where M is the molecular weight of the PAH analyte. Therefore, the primary ion at M + H = 327 and the secondary ion at M + 2H = 328, in the mass spectrum of Figure 5.21., reveal that product **II** is an unsubstituted PAH of molecular weight 326 and molecular formula $C_{26}H_{14}$.

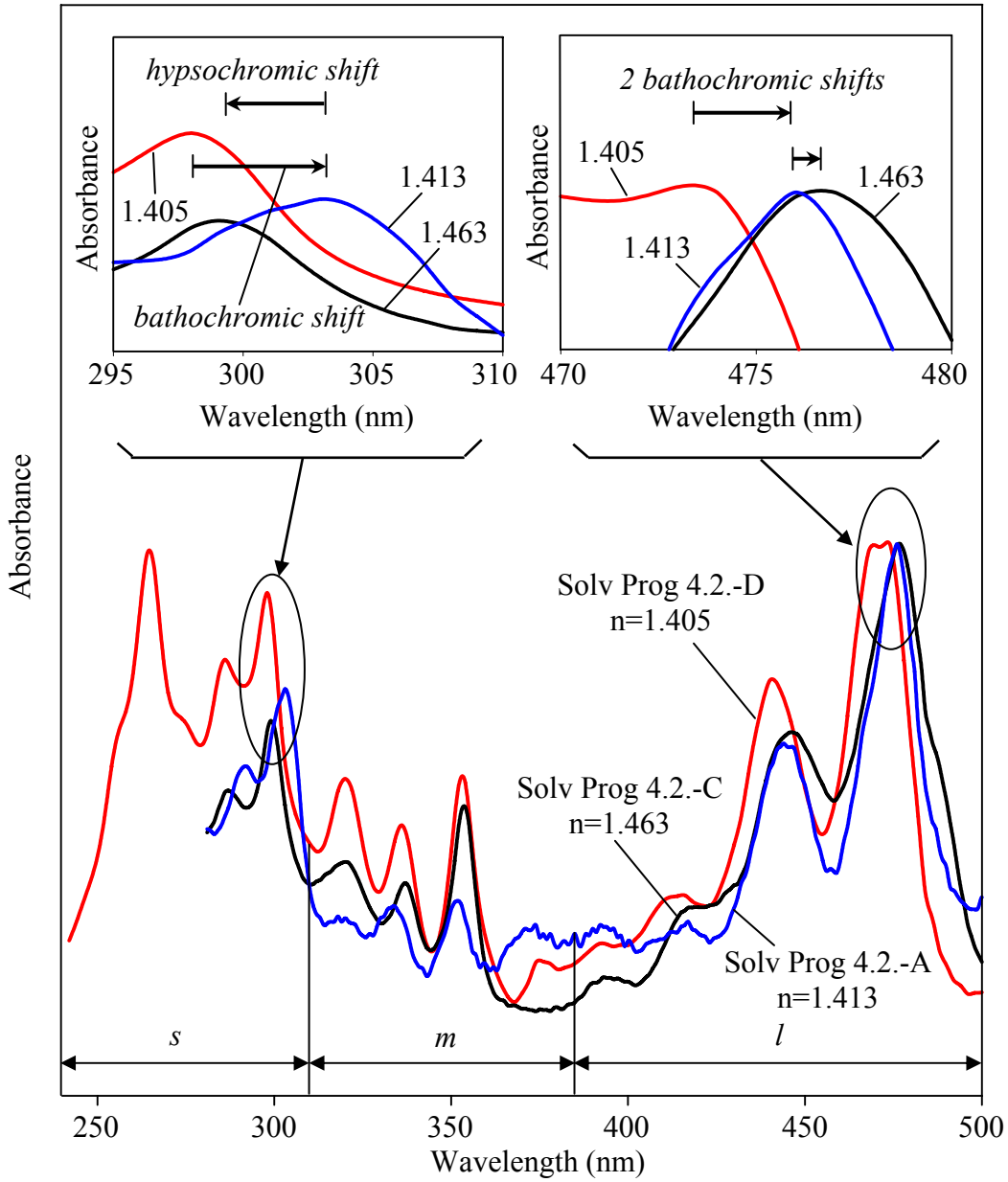


Figure 5.20. Comparison of the UV Absorbance Spectra for Compound **I** in the Solvent Programs 4.2.-A (blue line), 4.2.-C (black line), and 4.2.D (red line). Each Spectrum is labeled with the Index of Refraction *n*, computed for each Mobile Phase at the Time the Spectrum is taken.

PAH in the $C_{26}H_{14}$ family include 9 benzenoid compounds [Dias] and numerous compounds with one or more non-benzenoid rings [Dias]. As benzenoid and non-benzenoid PAH exhibit different UV absorbance characteristics, it is logical to examine the UV absorbance

features of the $C_{26}H_{14}$ compound **II** in order to gain further information on its identity. (The UV spectrum of compound **II** from the supercritical synthetic jet fuel pyrolysis products is shown as the black solid line in Figure 5.22.)

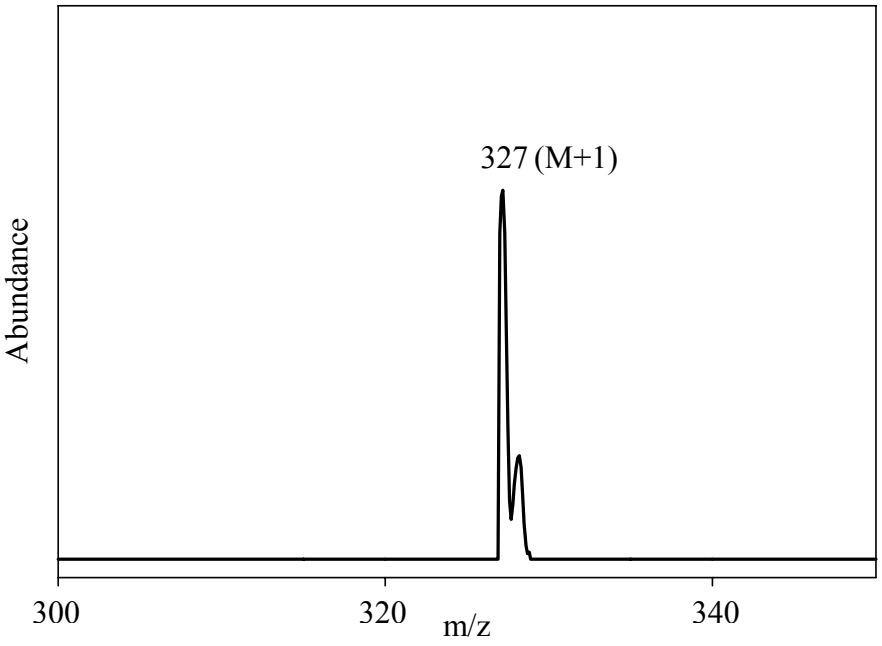


Figure 5.21. The Mass Spectrum of Compound **II**, the Product Component eluting at 57.0 min in Figure 5.13.

As indicated in Table B.1. (Appendix B), the UV spectra of at least 17 $C_{26}H_{14}$ PAH, both benzenoid [Zander and Franke, Clar et al. 1948, 1956, 1958, 1960] and non-benzenoid [Clar et al. 1959, 1964, Lang et al., Aitken and Reid, Cho and Harvey, Wilcox and Farley, Jessup and Reiss], have been reported in the literature. Except for the UV spectrum of dibenzo[*b,ghi*]-perylene, reproduced as the red solid and red dashed lines in Figure 5.22. (from the paper of Zander and Franke), none of the UV spectral features of the compounds in Table B.1. match those in Figure 5.22. for compound **II**.

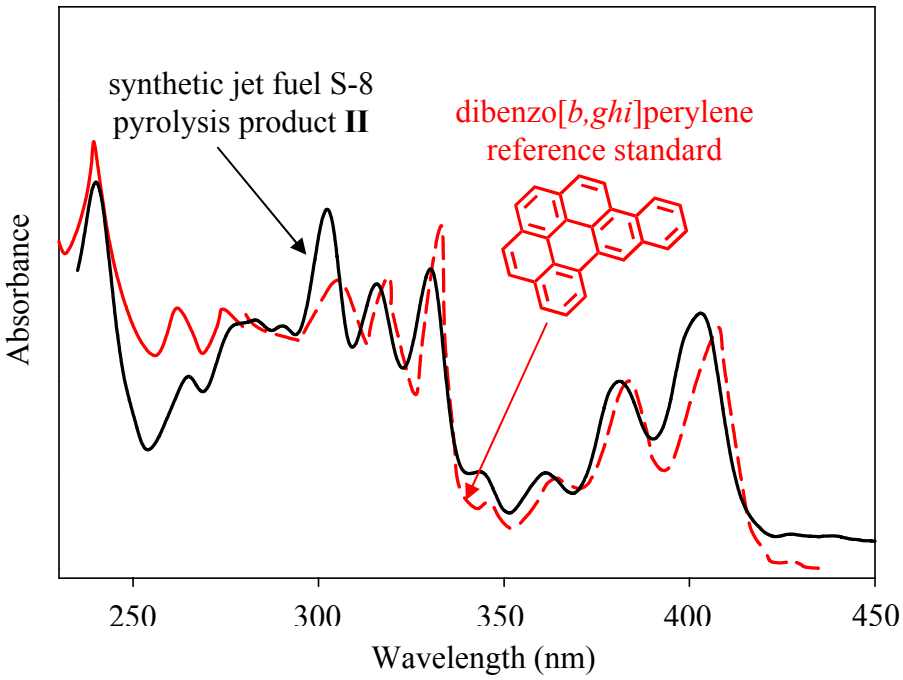


Figure 5.22. UV Absorbance Spectra for Compound **II** (black solid line), the Product Component eluting at 57.0 min in Figure 5.13., in $CH_3CN/CH_2Cl_2$, and for the Reference Standard of Dibenzo[*b,ghi*]perylene [Zander and Franke] in $C_2H_5OH$ (red solid line up to 280 nm) and $C_6H_6$ (red dashed line after 280 nm).

The UV spectrum of **II** in Figure 5.22. clearly indicates that **II** is a benzenoid PAH. As reported by McClaine et al. [McClaine et al. 2006], four well-defined peaks of the p band that increase in height with increasing wavelength (as shown by the UV spectrum of **II** at wavelengths of 345 nm, 361 nm, 381 nm, and 403 nm) are characteristic of benzenoid compounds, particularly those with a base structure of perylene, for example, benzo[*a*]perylene, benzo[*ghi*]perylene, dibenzo[*e,ghi*]perylene, tribenzo[*b,ghi,k*]perylene, and dibenzo[*b,k*]perylene [Clar 1964]. Other $C_{26}H_{14}$ PAH with one or more five-membered rings, e.g., acenaphtho[1,2-*k*]-fluoranthene and acenaphtho[1,2-*j*]fluoranthene [Clar 1964], fluoreno[1,9-*ab*]fluoranthene and benzo[*a*]indeno[1,2,3-*cd*]fluoranthene [Clar and Willicks 1958], fluoreno[9,1-*ab*]fluoranthene [Lang et al.], fluoreno[3,2,1,9-*defg*]chrysene [Aitken and Reid], benz[*def*]indeno[1,2,3-

*hi*]chrysene and benz[*def*]indeno[1,2,3-*qr*]chrysene [Cho and Harvey], seldom present distinct peaks that show this type of stair-step increase within the p band of the UV spectrum. Therefore, the UV spectral features of **II** and the close similarity, in Figure 5.22., between the UV spectrum of **II** and the published UV spectrum of dibenzo[*b,ghi*]perylene strongly suggest that compound **II** is dibenzo[*b,ghi*]perylene. However, there are differences between the two spectra in Figure 5.22., so in order to obtain more evidence to support compound **II**'s identity, the explanation of these differences have to be adressed. To do so, the effects of solvent on the UV spectrum are examined.

The published UV spectrum of dibenzo[*b,ghi*]perylene [Zander and Franke] in Figure 5.22. has been taken in two different solvents, ethanol ($C_2H_5OH$) up to 280 nm (represented as the red solid line) and $C_6H_6$ after 280 nm (represented as the red dotted line). The UV spectrum of compound **II** in Figure 5.22., however, has been taken in a solvent mixture of $CH_3CN/CH_2Cl_2$. Up to 280 nm, the two UV spectra in Figure 5.22. match quite well in terms of shape, magnitude, and position of the spectral bands. The consistency in shape and magnitude holds after 280 nm; however, a shift in the positions of the spectral bands appears in the published [Zander and Franke] UV spectrum of dibenzo[*b,ghi*]perylene, compared to the UV spectrum of compound **II**.

As it was previously explained in this section during the identification of the $C_{30}H_{16}$ benzo[*cd*]naphtho[1,2,3-*lm*]perylene, the observed coincidences and differences in the two spectra of Figure 5.22. can be attributed to solvatochromic effects associated with the refractive index of the solvent. The segment of Figure 5.22. up to 280 nm indicates a similar solvatochromic effect in the two solute-solvent couples: dibenzo[*b,ghi*]perylene-$C_2H_5OH$ and compound **II**-$CH_3CN/CH_2Cl_2$. The segment after 280 nm, on the other hand, indicates a dissimilar solvatochromic effect in the two solute-solvent couples: dibenzo[*b,ghi*]perylene-

$C_6H_6$, and compound **II**-$CH_3CN/CH_2Cl_2$. The solvents $C_2H_5OH$ and $CH_3CN/CH_2Cl_2$ thus appear to behave similarly, whereas $C_6H_6$ is different from both.

The segment of the dibenzo[*b,ghi*]perylene spectrum taken in $C_6H_6$, in Figure 5.22., can be corrected, however, based on the empirical findings in Table B.2. (Appendix B). Table B.2. reports the wavelength of maximum absorption, in both $C_6H_6$ and $CH_3OH$ (The refractive index of $CH_3OH$ is very close to that of $C_2H_5OH$, as shown in Table B.3.), for p-band peaks in the UV spectrum of seven different PAH [Clar 1964, Jinno]. As indicated in Table B.2. (Appendix B) for anthanthrene, coronene, benzo[*ghi*]perylene, benzo[*a*]coronene, benzo[*a*]naphthacene, picene, and benzo[*ghi*]fluoranthene, there is an average shift to longer wavelengths of approximately 4 nm in the position of the p band when $C_6H_6$ is used as the solvent, compared to when $CH_3OH$ is used. Following this analysis, it is reasonable to shift the $C_6H_6$ segment (the part after 280 nm) of the published dibenzo[*b,ghi*]perylene UV spectrum in Figure 5.22. by approximately 4 nm to shorter wavelengths, and the results appear in Figure 5.23.

Figure 5.23. portrays this newly shifted UV spectrum of dibenzo[*b,ghi*]perylene, with the UV spectrum of compound **II** from the supercritical synthetic jet fuel products. Readily apparent from Figure 5.23. is the good match between the pairs of spectra in terms of the shape, magnitude, and position of the spectral bands. The peak at 304 nm in the UV spectrum of compound **II** in Figure 5.23. is due to 1-methylcoronene, which elutes very close to **II** (as Figure 5.13. shows) and exhibits maximum absorbance at 304 nm. Nevertheless, with this minor interference taken into account, the virtual coincidences of the pairs of spectra in Figures 5.23., along with the mass spectral information in Figure 5.21., verify that **II** is indeed the $C_{26}H_{14}$ PAH dibenzo[*b,ghi*] perylene.

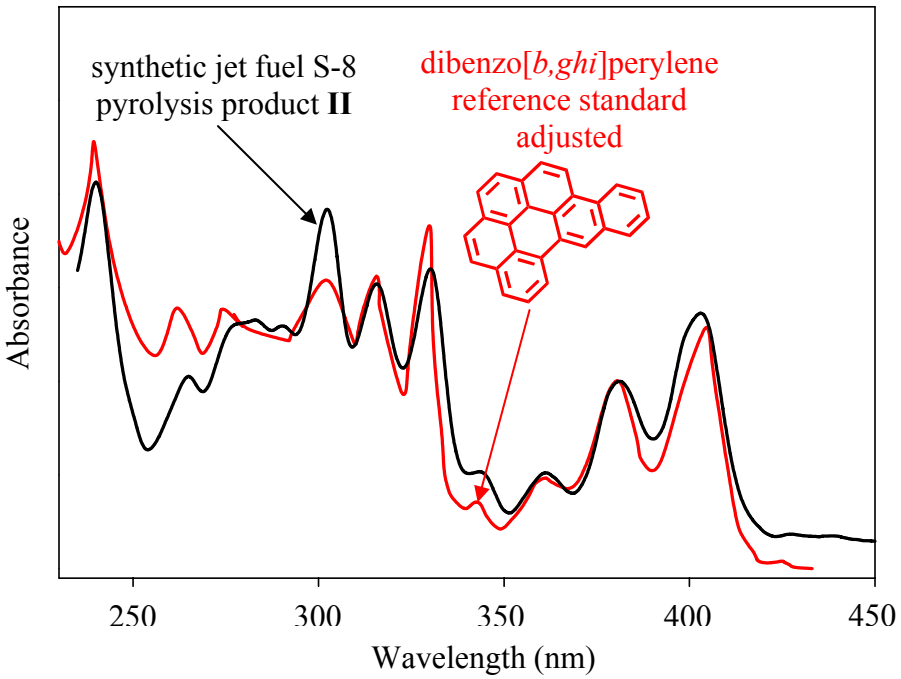


Figure 5.23. UV Absorbance Spectra for Compound **II** (black line), the Product Component eluting at 57.0 min in Figure 5.13., in $CH_3CN/CH_2Cl_2$, and for the Reference Standard of Dibenzo[*b,ghi*]perylene [Zander and Franke] in $C_2H_5OH$ (red line up to 280 nm) and $C_6H_6$ with the 4-nm Adjustment in the Spectral Bands (red line after 280 nm).

The above-observed differences in the UV spectrum of dibenzo[*b,ghi*]perylene, taken in different solvents, can be explained by the studies of Kundt, Bayliss and McRae, and LeRosen and Reid, which established a relation between the solvent effects in UV spectra and the solvents' indices of refraction. Following the procedure and arguments employed previously for the identification of benzo[*cd*]naphtho[1,2,3-*lm*]perylene, the refractive indices of the solvent mixtures employed in our HPLC analyses of the supercritical pyrolysis products have been computed. The values, used in the calculation, of the mobile phase composition and individual solvents' indices of refraction come from the fourth column of Table B.4. (Appendix B) and the fifth and sixth columns of Table B.3. (Appendix B), respectively. The resulting value of *n*, 1.35470, computed for the mobile phase composition at the time of compound **II**'s elution in Figure 5.13., appears in the top row and last column of Table B.4.

The two UV spectra presented in Figure 5.22., one of compound **II**, now identified as dibenzo[*b,ghi*]perylene, and the other of the standard of dibenzo[*b,ghi*]perylene [Zander and Franke], agree with the behavior explained by Kundt. For the first segment of Figure 5.22., up to 280 nm, the two spectra do not exhibit any appreciable differences in wavelength since the refractive indices of the solvents, 1.36367 (from Table B.4.) for $CH_3CN$-$CH_2Cl_2$ and 1.35950 (from Table B.3.) for $C_2H_5OH$, are very close in value. After 280 nm, however, the spectral bands exhibit the aforementioned bathochromic shift of 4 nm, as the refractive index of the solvent increases from 1.36367 for $CH_3CN$-$CH_2Cl_2$ to 1.49322 (from Table B.3.) for $C_6H_6$. In addition to this spectral wavelength shift, Figure 5.22. indicates that there are minor but perceptible differences in the intensities of some of the lower- to medium- wavelength spectral bands, due to the difference in solvent. These minor effects of solvent on UV spectral peak intensity are similar to those observed during the identification of benzo[*cd*]naphtho[1,2,3-*lm*]perylene.

**Identification of 8H-Dibenzo[*a,jk*]pyrene:** For the UV spectral identification of 8H-dibenzo[*a,jk*]pyrene [Oña and Wornat 2008c], the information obtained with the solvent program delineated in Figure 4.2.-A has been used. The spectral identification of 8H-dibenzo[*a,jk*]pyrene starts with the designation of the unknown component as **III** in the chromatogram shown in Figure 5.13.

Figure 5.24. shows the mass spectrum of compound **III** taken with the solvent program 4.2.-E. The first- and second- most abundant ions at M + H = 291 and M + 2H = 292, respectively, in the mass spectrum of Figure 5.24., reveal that the unknown compound **III** in Figure 5.13. is an unsubstituted polycyclic hydrocarbon of molecular weight 290 and molecular formula $C_{23}H_{14}$.

Figure 5.25. presents the UV spectrum of the $C_{23}H_{14}$ product compound **III**, taken in a solvent mixture of $CH_3CN/CH_2Cl_2$, along with the published [Clar 1964] UV spectrum of a reference standard of the $C_{23}H_{14}$ 8H-dibenzo[*a,jk*]pyrene, taken in $C_6H_6$.

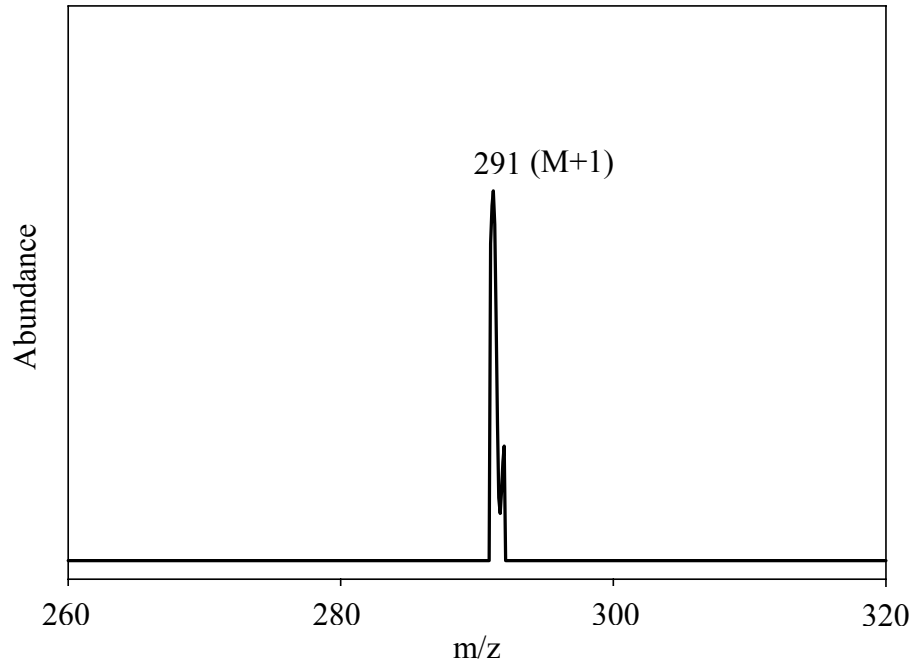


Figure 5.24. The Mass Spectrum of Compound **III**, the Product Component eluting at 53.0 min in Figure 5.13.

The two UV spectra of Figure 5.25. exhibit the same solvatochromic spectral band shift already observed in Figure 5.22. for the published [Zander and Franke] UV spectrum of dibenzo[*b,ghi*]perylene and the UV spectrum of compound **II** after 280 nm. This similarity in shift is due to the use of the same two solvents in both cases, $CH_3CN/CH_2Cl_2$ and $C_6H_6$. Therefore, the steps used to elucidate the identity of compound **II** in the previous analysis have also been taken to elucidate the identity of compound **III**, using the empirical findings in Table B.2. (Appendix B).

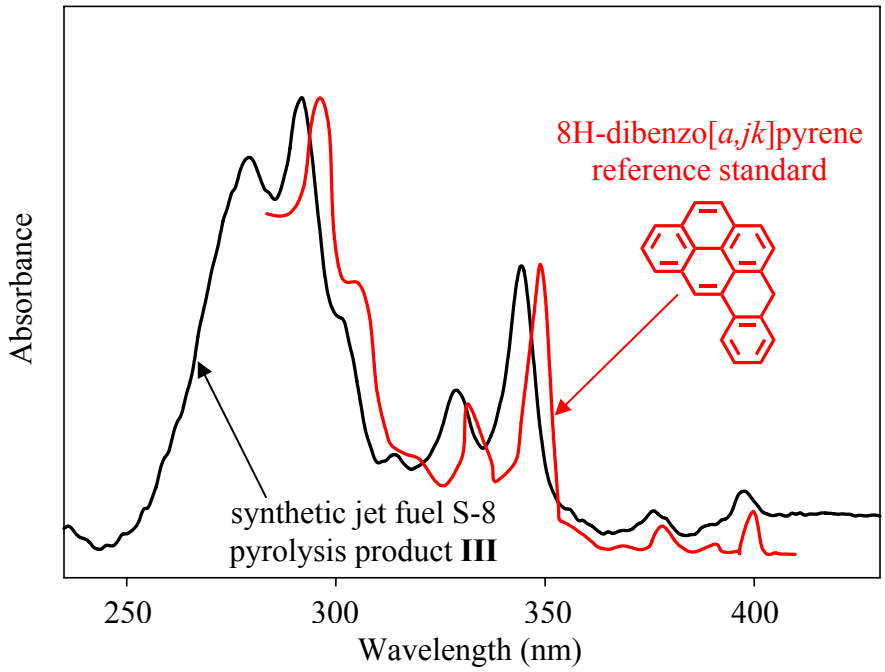


Figure 5.25. UV Absorbance Spectra for Compound **III** (black line), the Product Component eluting at 53.0 min in Figure 5.13., in $CH_3CN/CH_2Cl_2$, and for the Reference Standard of 8H-Dibenzo[*a,jk*]pyrene [Clar 1964] in $C_6H_6$ (red line).

Analogous to the shift of approximately 4 nm applied for the benzene portion of the published UV spectrum of dibenzo[*b,ghi*]perylene in Figure 5.22., a shift of about 4 nm has been applied to the published 8H-dibenzo[*a,jk*]pyrene UV spectrum in Figure 5.25. to shorter wavelengths, and the results appear in Figure 5.26. Figure 5.26. portrays this newly shifted UV spectrum of 8H-dibenzo[*a,jk*]pyrene, with the UV spectrum of compound **III** from the supercritical synthetic jet fuel pyrolysis products. Readily apparent is the good match between the two spectra in Figure 5.26., in terms of shape, magnitude, and position. The virtual coincidence of the pair of spectra in Figure 5.26., along with the mass spectral information in Figure 5.24., verify that **III** is indeed the $C_{23}H_{14}$ PAH 8H-dibenzo[*a,jk*]pyrene.

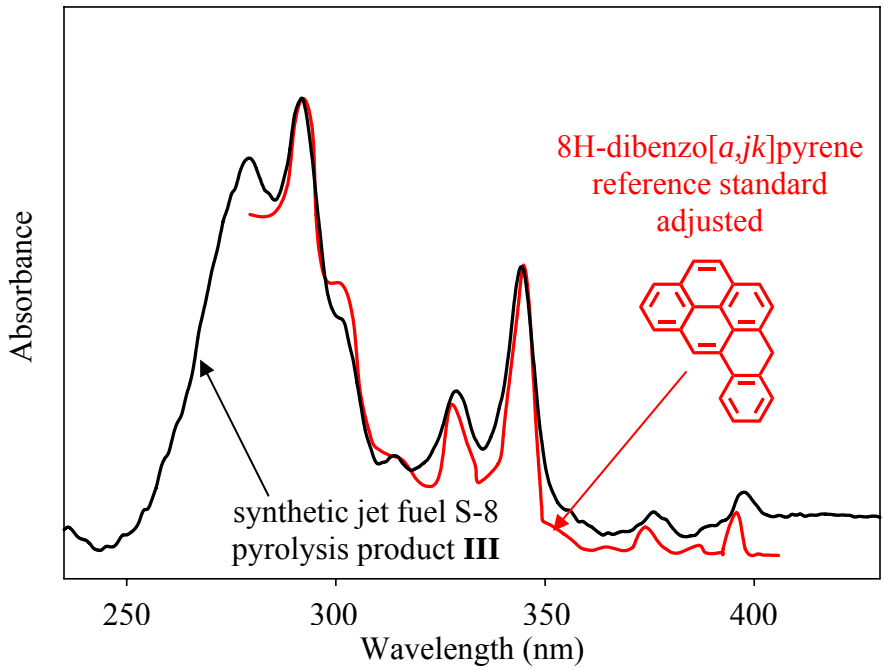


Figure 5.26. UV Absorbance Spectra for Compound **III** (black line), the Product Component eluting at 53.0 min in Figure 5.13., in $CH_3CN/CH_2Cl_2$, and for the Reference Standard of 8H-Dibenzo[*a,jk*]pyrene [Clar 1964] in $C_6H_6$ with the 4-nm Adjustment in the Spectral Bands (red line).

Just as the findings of Kundt, Bayliss and McRae, and LeRosen and Reid (on the effects of the solvent's index of refraction) explained the solvent-associated differences in the UV spectra of dibenzo[*b,ghi*]perylene in Figure 5.22., they also explain the differences in the UV spectra of 8H-dibenzo[*a,jk*]pyrene that are observed in Figure 5.25. Following the same procedure used to identify compound **II**, the refractive index for the HPLC mobile phase composition at the time of compound **III**'s elution was computed, and the resulting value of *n*, 1.35579, appears in the middle row and last column of Table B.4. (Appendix B).

Since a UV spectrum shifts bathochromically with an increase in the solvent's refractive index [Kundt], the spectral bands of 8H-dibenzo[*a,jk*]pyrene in Figure 5.25. exhibit a bathochromic shift of 4 nm, as the refractive index of the solvent increases from 1.35579 for $CH_3CN$-$CH_2Cl_2$ to 1.49007 for $C_6H_6$—just as the spectral bands of dibenzo[*b,ghi*]perylene in

Figure 5.22. exhibited a 4-nm bathochromic shift when the solvent index of refraction increased from 1.35470 to 1.49322. Moreover, Figure 5.25. indicates small but perceptible changes in the intensities of some medium- to long- wavelength spectral bands, due to the difference in solvent. These solvent effects on UV spectral intensity are analogous to those previously noted for dibenzo[*b,ghi*]perylene in Figure 5.22. and for benzo[*cd*]naphtho[1,2,3-*lm*]perylene in Figures 5.16., 5.18., and 5.19.

**Identification of Benzo[*pqr*]dinaphtho[8,1,2-*bcd*:2',1',8'-*lmn*]perylene:** For the UV and MS identification of benzo[*pqr*]dinaphtho[8,1,2-*bcd*:2',1',8'-*lmn*]perylene [Oña and Wornat 2008c], the information obtained with the solvent program 4.2.-E has been used. The identification of benzo[*pqr*]dinaphtho[8,1,2-*bcd*:2',1',8'-*lmn*]perylene starts with the designation of the unknown component as **IV** in Figure 5.27. Figure 5.28. shows the mass spectrum of compound **IV**. The first- and second- most abundant ions in the spectrum are at M + H = 425 and M + 2H = 426, respectively. The unknown compound **IV** is therefore an unsubstituted PAH of molecular weight 424 and molecular formula $C_{34}H_{16}$.

Figure 5.29. presents the UV spectrum of the $C_{34}H_{16}$ product compound **IV**, taken in $CH_2Cl_2$, along with the published [Clar 1964] UV spectrum of a reference standard of the $C_{34}H_{16}$ benzo[*pqr*]dinaphtho[8,1,2-*bcd*:2',1',8'-*lmn*]perylene, taken in 1,2,4-trichlorobenzene (1,2,4-$C_6H_3Cl_3$). A preliminary comparison between these two UV spectra shows a solvatochromic spectral band shift similar to the ones already observed in Figure 5.22. and Figure 5.25.

Data are not readily available on the UV spectral bands of large benzenoid PAH in both 1,2,4-$C_6H_3Cl_3$ and $CH_2Cl_2$, the two solvents of Figure 5.29. Data are available in Table B.5. (Appendix B), however, for two large benzenoid PAH [Wornat et al. 2001,2008] in 1,2,4-$C_6H_3Cl_3$ and two $CH_3CN/CH_2Cl_2$ mixtures, each of which has a refractive index (1.38740 and

1.39291, from Table B.3.) close to that of $CH_2Cl_2$ (1.41656, from Table B.3.). As indicated in Table B.5., there is an average shift to longer wavelengths of approximately 6 nm in the position of the p band when 1,2,4-$C_6H_3Cl_3$ is used as solvent, compared to when 37:63 $CH_3CN$:$CH_2Cl_2$ or 30:70 $CH_3CN$:$CH_2Cl_2$ is used.

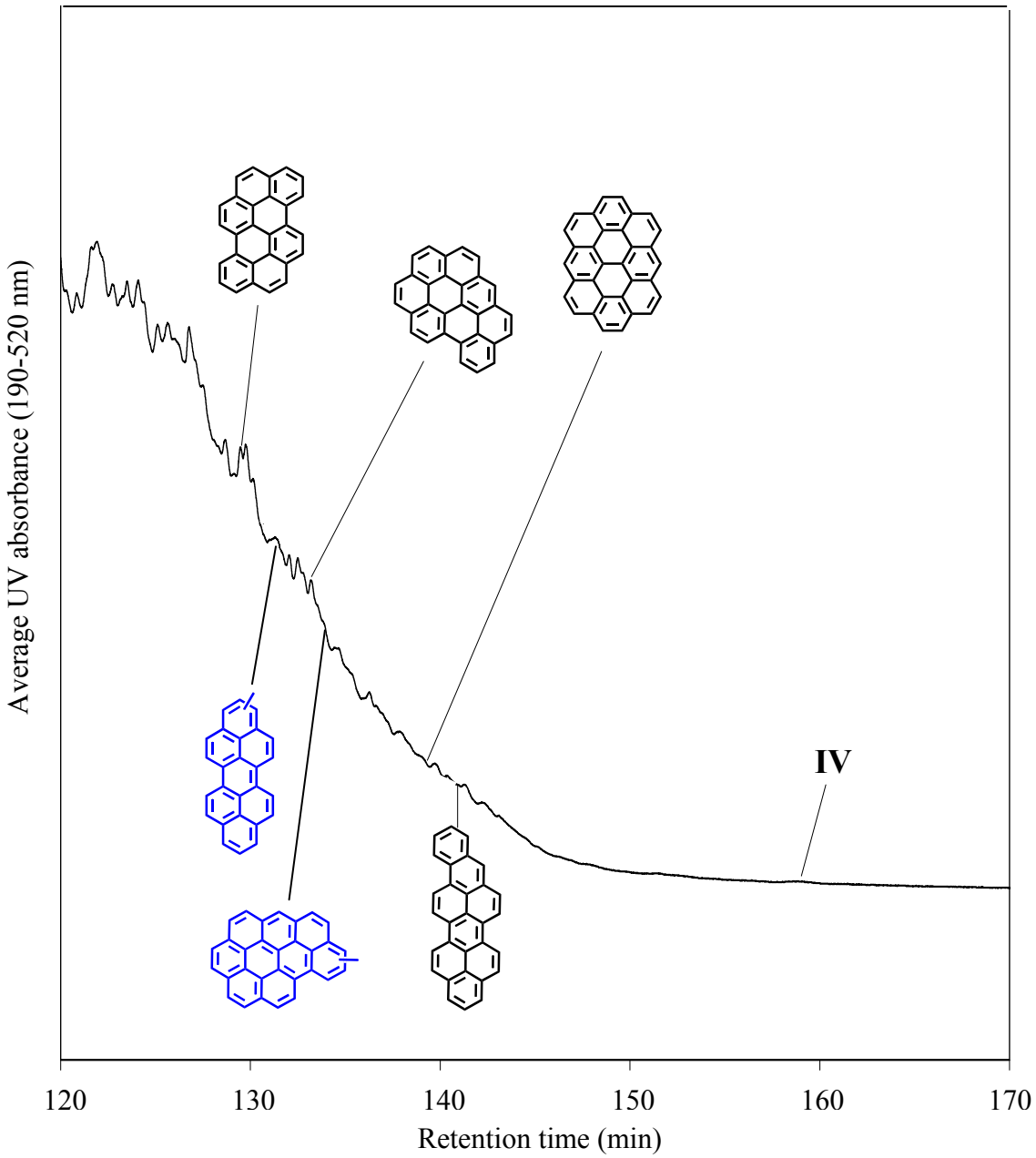


Figure 5.27. Portion of the HPLC/UV Chromatogram from 120 to 170 minutes, showing the Retention Times of six identified Products and one unidentified Product from the Supercritical Synthetic Jet Fuel S-8 Pyrolysis at 710 $^{o}$C and 42 atm Using the Solvent Program 4.2.-E.

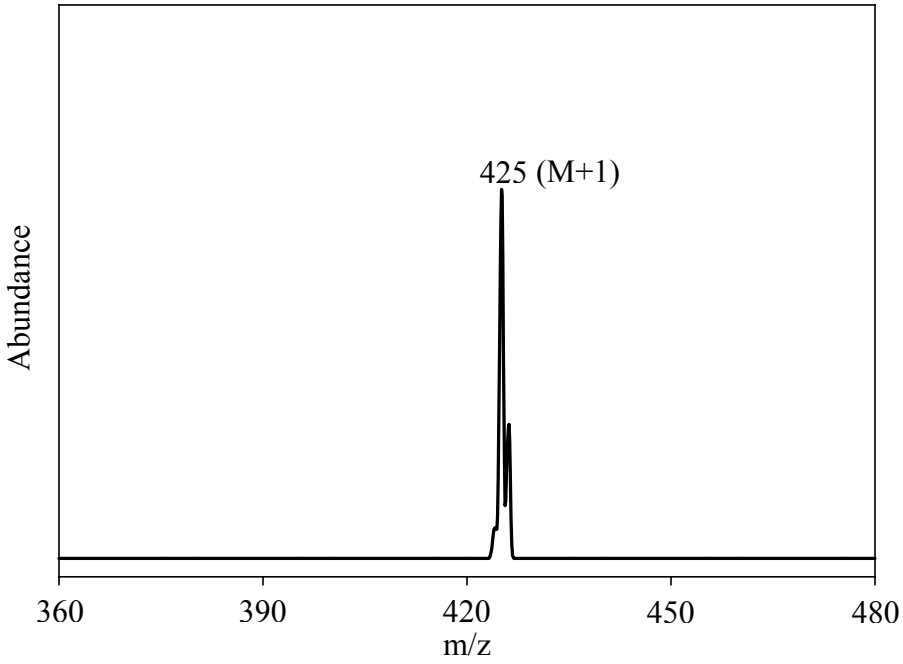


Figure 5.28. The Mass Spectrum of Compound **IV**, the Product Component eluting at 159.0 min in Figure 5.27.

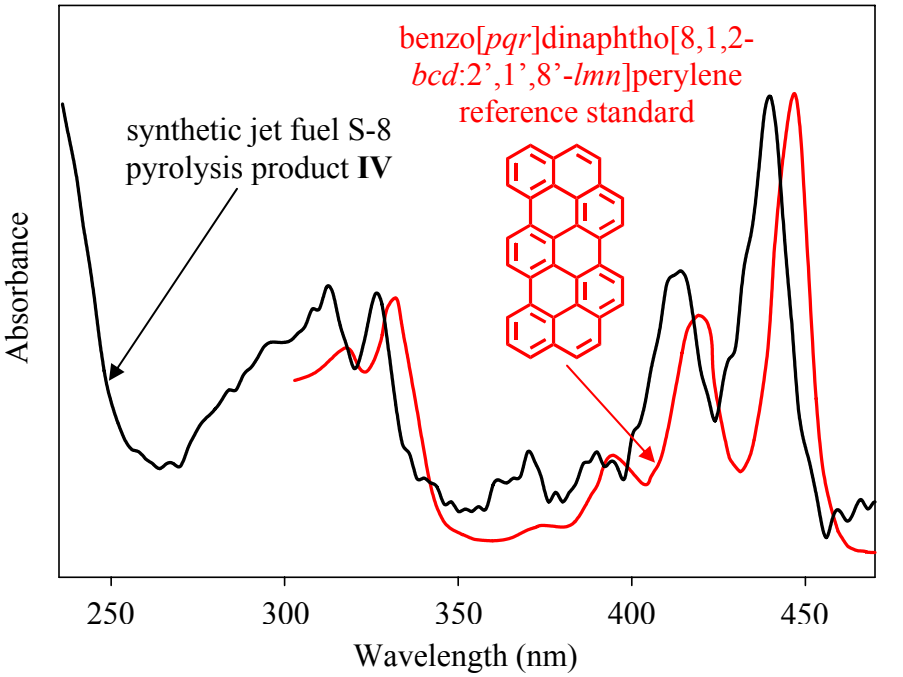


Figure 5.29. UV Absorbance Spectra for Compound **IV** (black line), the Product Component eluting at 159.0 min in Figure 5.27., in $CH_2Cl_2$, and for the Reference Standard of Benzo[*pqr*]dinaphtho[8,1,2-*bcd*:2',1',8'-*lmn*]perylene [Clar 1964] in 1,2,4-$C_6H_3Cl_3$ (red line).

Following this analysis, the published benzo[*pqr*]dinaphtho[8,1,2-*bcd*:2',1',8'-*lmn*]perylene UV spectrum in Figure 5.29. has been shifted by approximately 6 nm to shorter wavelengths. Figure 5.30. portrays this newly shifted UV spectrum of benzo[*pqr*]dinaphtho[8,1,2-*bcd*:2',1',8'-*lmn*]perylene, with the UV spectrum of compound **IV** from the supercritical synthetic jet fuel pyrolysis products. Readily apparent from Figure 5.30. is the good match between the two spectra, in terms of shape, magnitude and position. There is some spectral interference at 360-375 nm from an unidentified isomeric co-eluting species, but the virtual coincidence of the two spectra in Figure 5.30., along with the mass spectral information in Figure 5.28., verify that **IV** is indeed the $C_{34}H_{16}$ PAH benzo[*pqr*]dinaphtho[8,1,2-*bcd*:2',1',8'-*lmn*]perylene.

It is possible to see again that the findings of Kundt, Bayliss and McRae, and LeRosen and Reid, with regard to the solvatochromic shift, have been substantiated. As it is observable in Figure 5.29., similar to the cases of Figure 5.22. and Figure 5.25., there are small solvent-induced differences in the intensities and shape of several of the UV spectral bands.

**Identification of Other PAH according to the UV Solvent-Based Adjustment:** The same procedure applied for the identification of benzo[*cd*]naphtho[1,2,3-*lm*]perylene, dibenzo[*b,ghi*]perylene, 8H-dibenzo[*a,jk*]pyrene, and benzo[*pqr*]dinaphtho[8,1,2-*bcd*:2',1',8'-*lmn*]perylene has been used for the identification of dibenzo[*e,ghi*]perylene, naphtho[8,1,2-*bcd*]perylene, and benzo[*b*]picene from the synthetic jet fuel products [Oña and Wornat 2008b]. The UV spectral identifications of these PAH products has been achieved by application of the UV solvent-based adjustment discussed previously.

Figure 5.31. shows the third version of the HPLC/UV chromatogram of the synthetic jet fuel S-8 supercritical pyrolysis products using the solvent program described in Figure 4.2.-A.

The total number of products detected so far is eighty (seventy-nine from Figure 5.31. and one more, benzo[*pqr*]dinaphtho[8,1,2-*bcd*:2',1',8'-*lmn*]perylene, from Figure 5.32.).

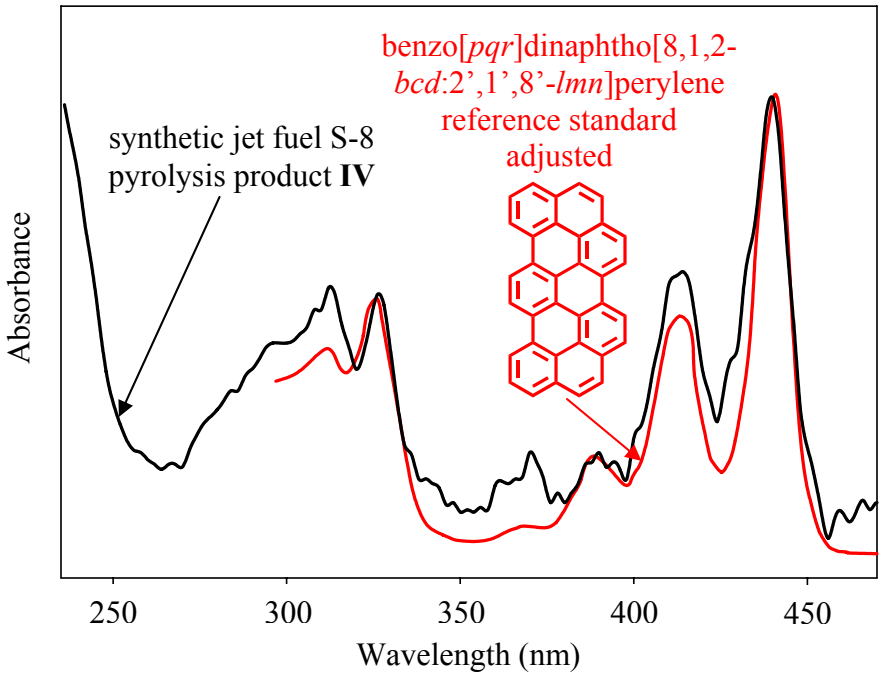


Figure 5.30. UV Absorbance Spectra for Compound **IV** (black line), the Product Component eluting at 159.0 min in Figure 5.27., in $CH_2Cl_2$, and for the Reference Standard of Benzo[*pqr*]dinaphtho[8,1,2-*bcd*:2',1',8'-*lmn*]perylene [Clar 1964] in 1,2,4-$C_6H_3Cl_3$ with the 6-nm Adjustment in the Spectral Bands (red line).

**• Case D: Identification Using the Annellation Theory**

**Identification of Benzo[*ghi*]phenanthro[9,10,1-*cde*]perylene:** For the UV spectral identification of benzo[*ghi*]phenanthro[9,10,1-*cde*]perylene, the information obtained with the solvent program 4.2.-A has been used. The detection of benzo[*ghi*]phenanthro[9,10,1-*cde*]perylene starts with the designation of the unknown component as **V** in the chromatogram of Figure 5.31. Figure 5.33. shows the mass spectrum of compound **V** obtained with the solvent program described in Figure 4.2.-E.

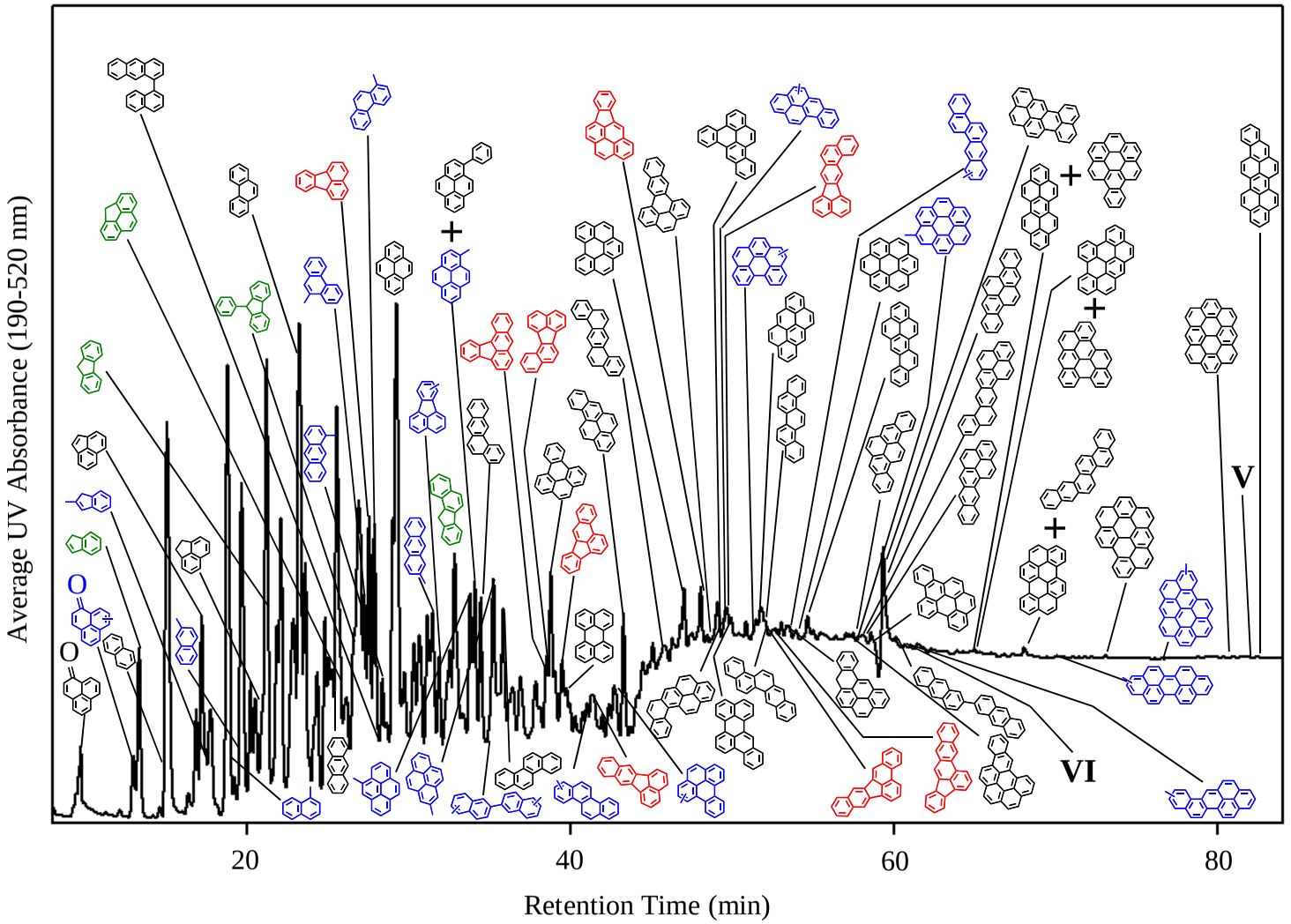


Figure 5.31. HPLC/UV Chromatogram (Third Version) of the Synthetic Jet Fuel S-8 Supercritical Pyrolysis Products at 710 ºC and 42 atm.

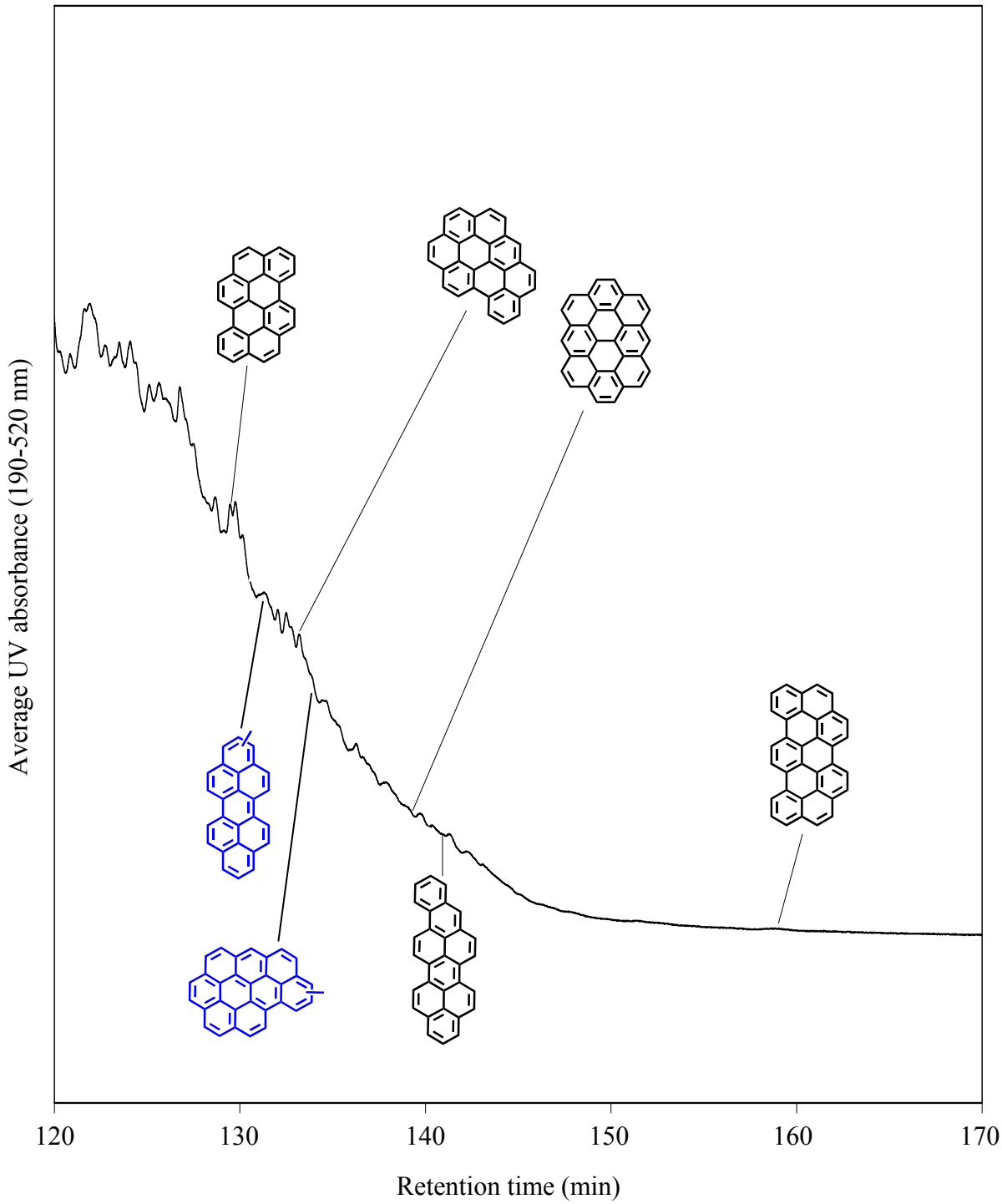


Figure 5.32. Portion of the HPLC/UV Chromatogram from 120 to 170 minutes, showing the Retention Times of seven Products from the Supercritical Synthetic Jet Fuel S-8 Pyrolysis at 710 $^{o}$C and 42 atm Using the Solvent Program 4.2.-E.

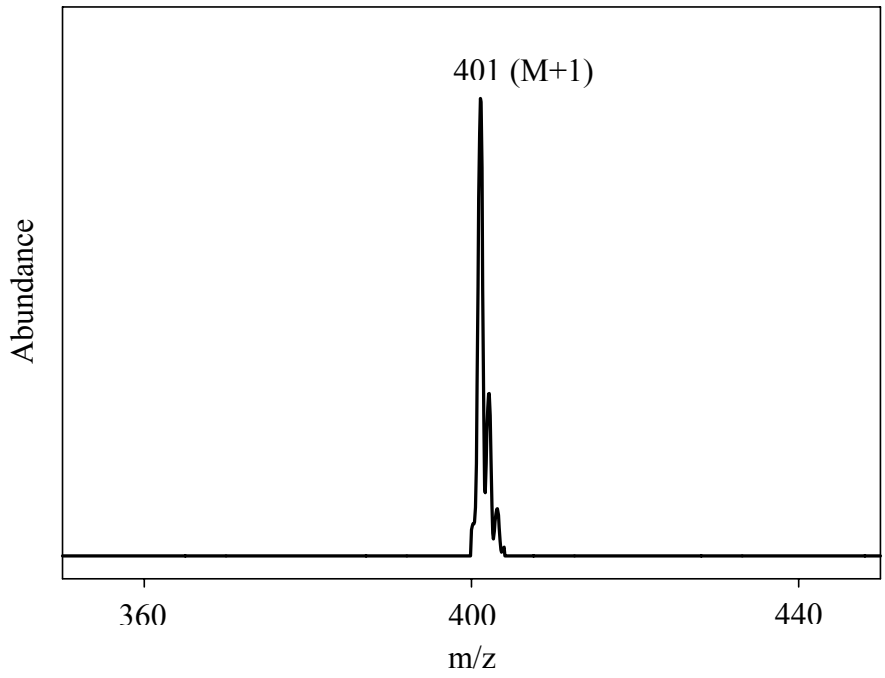


Figure 5.33. The Mass Spectrum of Compound **V**, the Product Component eluting at 81.4 min in Figure 5.31.

As it has been explained in Section 3.1.3., the first- and second- most abundant ions in the PAH mass spectrum are at M + H and M + 2H, respectively, where M is the molecular weight of the PAH analyte. Therefore, the primary ion at M + H = 401 and the secondary ion at M + 2H = 402, in the mass spectrum of Figure 5.33., reveal that product **V** is an unsubstituted PAH of molecular weight 400 and molecular formula $C_{32}H_{16}$.

Figure 5.34. shows the UV spectrum of **V** and the UV spectra of benzo[*pqr*]naphtho[8,1,2-*bcd*]perylene, a PAH for which a reference standard is available, and dibenzo[*ghi,k*]phenanthro[9,10,1-*cde*]perylene [Clar 1964], a PAH with a published UV spectrum. The spectral comparison between the UV spectra of benzo[*pqr*]naphtho[8,1,2-*bcd*]perylene and dibenzo[*ghi,k*]phenanthro[9,10,1-*cde*]perylene has been presented, as an example, during the explanation of the first rule of the Annellation Theory in Section 3.4.1. For

the present case, this rule has been evoked in order to show the identification of benzo[*ghi*]phenanthro[9,10,1-*cde*]perylene.

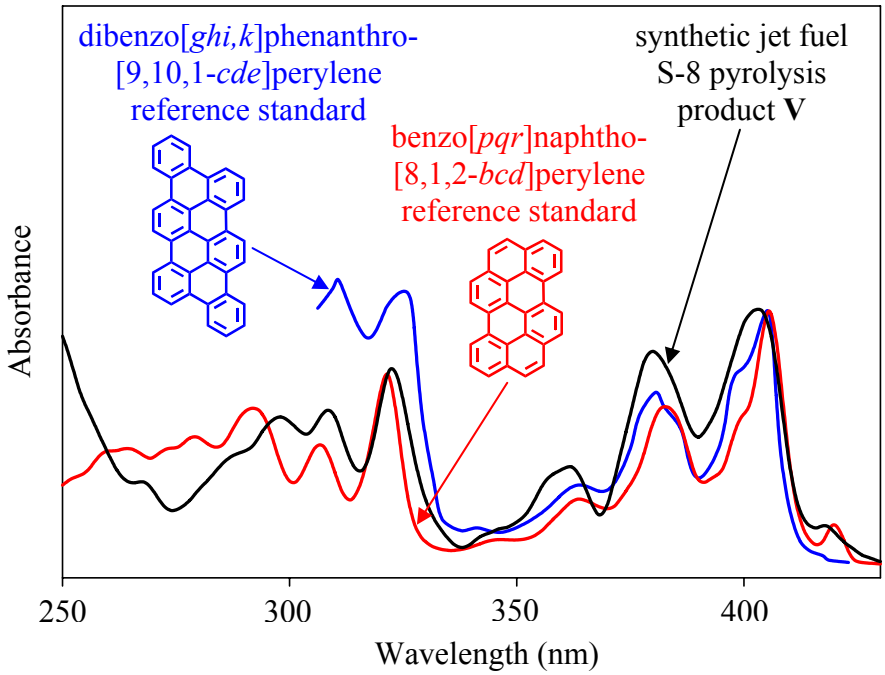


Figure 5.34. UV Absorbance Spectrum for Compound **V** (black line), the Product Component eluting at 81.4 min in Figure 5.31., in $CH_3CN/CH_2Cl_2$, UV Absorbance Spectrum for the Reference Standard of Benzo[*pqr*]naphtho[8,1,2-*bcd*]perylene (red line) and Published UV Absorbance Spectrum for the Reference Standard of Dibenzo[*ghi,k*]phenanthro[9,10,1-*cde*]perylene [Clar 1964] (blue line).

Figure 5.34. reveals that the UV spectrum of **V** is very similar in band shape features and in band shape positions to the UV spectra of benzo[*pqr*]naphtho[8,1,2-*bcd*]perylene and dibenzo[*ghi,k*]phenanthro[9,10,1-*cde*]perylene. The spectral coincidences are especially notorious in the positions and shape of the last p bands of the UV spectra which present a stair-step increase in height with increasing wavelength—this behavior has been linked to the presence of benzenoid compounds, particularly those with a base structure of perylene [McClaine et al. 2006]. Consequently, it is valid to suppose that the structure of compound **V** should be very closely related to that of these two PAH.

Based on these observations, the first rule of the Annellation Theory described in Chapter 3 has been applied. According to this rule, the fusion of a ring in an area of low aromaticity of a PAH, i.e., over an isolated double bond, produces despicable changes in the UV spectral bands in terms of intensity, position, and shape.

Figure 5.35. shows the positions of the aromatic sextets and isolated double bonds in benzo[*pqr*]naphtho[8,1,2-*bcd*]perylene, benzo[*ghi*]phenanthro[9,10,1-*cde*]perylene, and dibenzo-[*ghi,k*]phenanthro[9,10,1-*cde*]perylene established by application of the Y-Rule [Gutman and Ruiz-Morales] which is valid for perifused PAH.

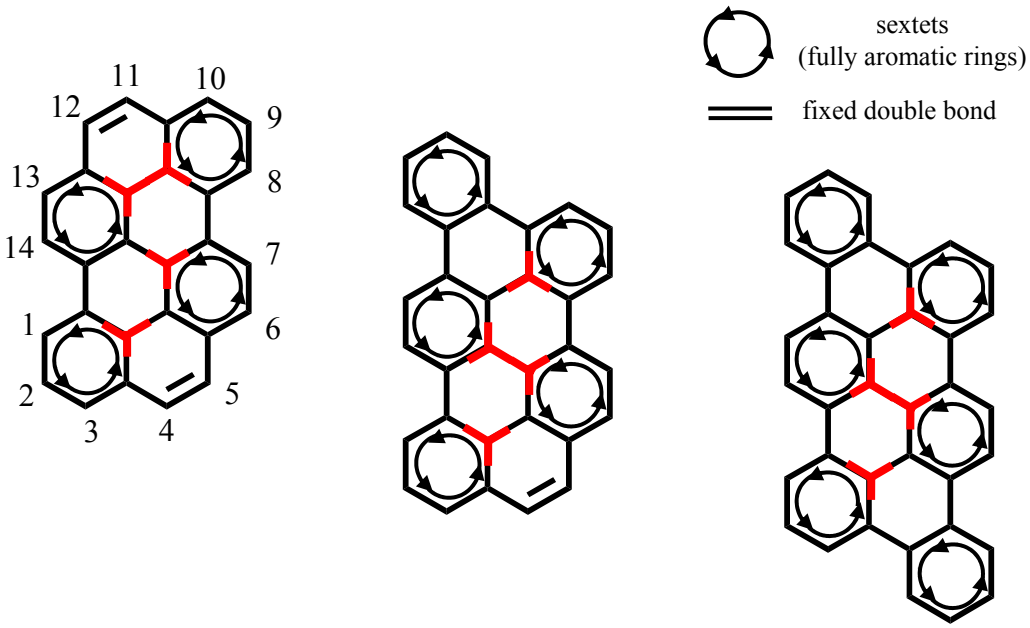


Figure 5.35. Sextets Locations in the Molecules of Benzo[*pqr*]naphtho[8,1,2-*bcd*]perylene, Benzo[*ghi*]phenanthro[9,10,1-*cde*]perylene, and Dibenzo[*ghi,k*]phenanthro[9,10,1-*cde*]perylene by Application of the Y-Rule [Gutman and Ruiz-Morales].

From Figure 5.35. is evident that the double bonds located in positions 4:5 and 11:12 of benzo[*pqr*]naptho[8,1,2-*bcd*]perylene are the only isolated double bonds that can hold a new fused ring in such a way to accomplish the above-indicated postulate of the Annellation Theory.

Two cases have been analyzed. The first case, the fusion of two rings one on each double bond of benzo[*pqr*]naphtho[8,1,2-*bcd*]perylene generates the PAH dibenzo[*ghi,k*]phenanthro[9,10,1-*cde*]perylene–this case has been already analyzed in Section 3.4.1. According to Figure 5.34., dibenzo[*ghi,k*]phenanthro[9,10,1-*cde*]perylene agrees well with the Annellation Theory expected behavior since the positions of the spectral bands are approximately the same as the positions of the spectral bands in the reference PAH benzo[*pqr*]naphtho[8,1,2-*bcd*]perylene keeping a similar shape on both UV spectra. The second case, the fusion of one ring in either of the two localized double bonds, 4:5 or 11:12, of benzo[*pqr*]naphtho[8,1,2-*bcd*]perylene generates the PAH benzo[*ghi*]phenanthro[9,10,1-*cde*]perylene. Benzo[*ghi*]phenanthro[9,10,1-*cde*]perylene should conform well with the Annellation Theory argument explained previously, i.e., the positions and shape of the spectral bands should be very similar to the positions and shape of the spectral bands of benzo[*pqr*]naphtho[8,1,2-*bcd*]perylene and dibenzo[*ghi,k*]phenanthro[9,10,1-*cde*]perylene. Figure 5.34. shows that compound **V** accomplishes the anticipated spectral behavior of benzo[*ghi*]phenanthro[9,10,1-*cde*]perylene and agrees well with the expected molecular weight of a $C_{32}H_{16}$ isomer, i.e., 400. Thus, it is reasonable to conclude that product **V** is the $C_{32}H_{16}$ PAH benzo[*ghi*]phenanthro[9,10,1-*cde*]perylene.

**Identification of Benz[*a*]anthanthrene:** Out of the nine benzenoid isomers in the $C_{26}H_{14}$ family of PAH only five (naphtho[1,2,3,4-*ghi*]perylene, dibenzo[*b,ghi*]perylene, dibenzo[*e,ghi*]perylene, naphtho[8,1,2-*bcd*]perylene, and dibenzo[*cd,lm*]perylene) have reported UV spectra [Clar 1964, Zander and Franke]. This section discusses about the identification of benz[*a*]anthanthrene, one of the $C_{26}H_{14}$ benzenoid PAH with an unknown UV spectrum detected in the supercritical pyrolysis products of synthetic jet fuel S-8.

For the UV spectral detection of benz[*a*]anthanthrene, the information obtained by application of the solvent program 4.2.-A has been used. The identification of benz[*a*]anthanthrene starts with the designation of the unknown component as **VI** in the HPLC/UV chromatogram of Figure 5.31.

Figure 5.36. shows the mass spectrum of **VI** obtained with the solvent program 4.2.-E. As it has been explained in Section 3.1.3., the first- and second- most abundant ions in the PAH mass spectrum are at M + H and M + 2H, respectively, where M is the molecular weight of the PAH analyte. Therefore, the primary ion at M + H = 327 and the secondary ion at M + 2H = 328, in the mass spectrum of Figure 5.36., reveal that product **VI** is an unsubstituted PAH of molecular weight 326 and molecular formula $C_{26}H_{14}$.

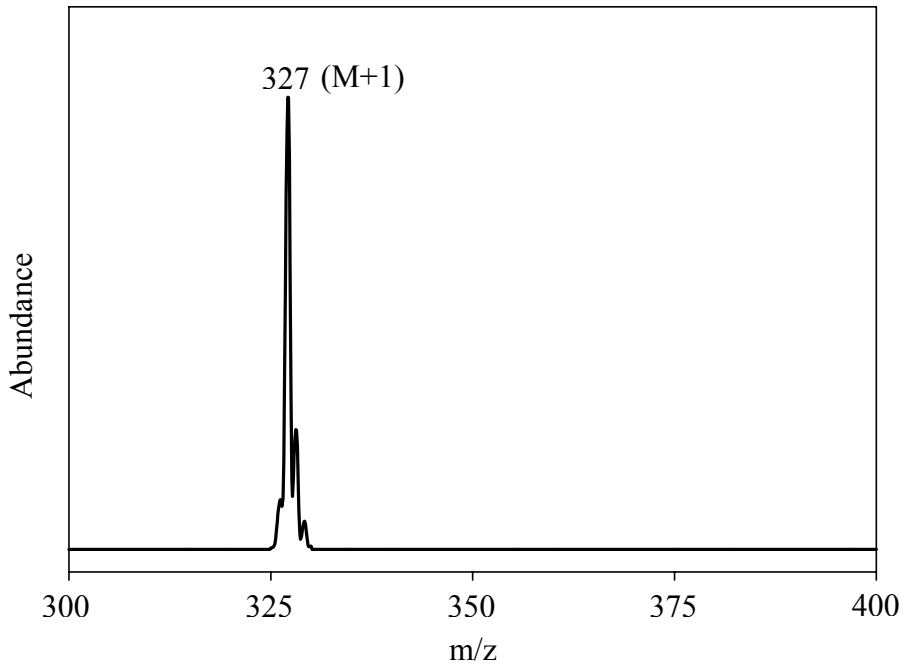


Figure 5.36. The Mass Spectrum of Compound **VI**, the Product Component eluting at 60.5 min in Figure 5.31.

As indicated in Table B.1. (Appendix B), the UV spectra of at least 17 $C_{26}H_{14}$ PAH, both benzenoid [Zander and Franke, Clar et al. 1948, 1956, 1958, 1960] and non-benzenoid [Clar et

al. 1959, 1964, Lang et al., Aitken and Reid, Cho and Harvey, Wilcox and Farley, Jessup and Reiss], have been reported in the literature and none of them match with the UV spectrum of **VI**, reported in Figure 5.37.

Figure 5.37. shows the UV spectra of compound **VI** and anthanthrene, a PAH for which a reference standard is available. Figure 5.37. reveals that the p bands in the UV spectrum of compound **VI** are very similar in terms of shape, position, and intensity to the corresponding features of the p bands in the UV spectrum of anthanthrene. These bands present a stair-step increase in height with increasing wavelength which is characteristic of benzenoid compounds [McClaine et al. 2006]. As it was previously stated, other $C_{26}H_{14}$ PAH with one or more five-membered rings such as acenaphtho[1,2-*k*]-fluoranthene and acenaphtho[1,2-*j*]fluoranthene [Clar 1964], fluoreno[1,9-*ab*]fluoranthene and benzo[*a*]indeno[1,2,3-*cd*]fluoranthene [Clar and Willicks 1958], and fluoreno[9,1-*ab*]fluoranthene [Lang et al.], seldom present distinct peaks that show this type of stair-step increase within the p band of the UV spectrum. Therefore, it is logical to suppose that the structure of compound **VI** should be very closely related to that of anthanthrene.

The argument presented in Section 3.4.2., named the second rule of the Annellation Theory, has been applied for the identification of benz[*a*]anthanthrene. The relation between the UV spectra of compound **VI** and anthanthrene is similar to the relation explained in Section 3.4.2. Figure 5.38. indicates that anthanthrene, the reference PAH used in this identification, has two moving sextets located in rings 1 and 2, and in rings 4 and 5 (determined using the Y-Rule of Gutman and Ruiz Morales). Compound **VI** has spectral characteristics that indicate a possible addition of a benzenoid ring in an angular position of one of these moving sextets of anthanthrene in such a way to generate a new sextet. The addition of a new ring in an angular

position to one of the rings located either in position 1 or position 4 of anthanthrene produces the same PAH, benz[*a*]anthanthrene. This ring addition should cause the same spectral effect as the effect generated by the presence of compound **VI** already described in the previous paragraph.

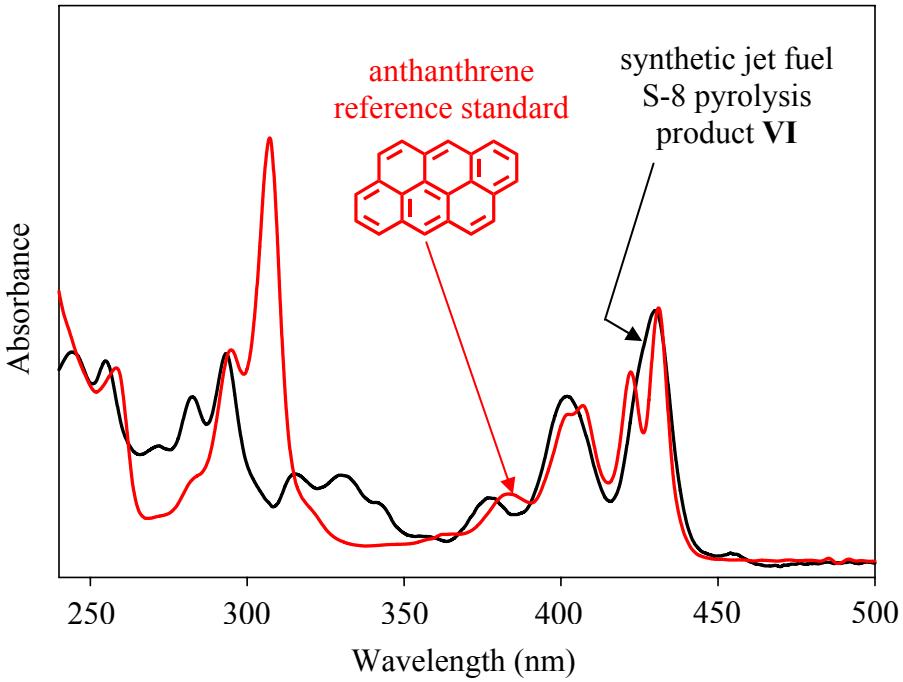


Figure 5.37. UV Absorbance Spectrum for Compound **VI** (black line), the Product Component eluting at 60.5 min in Figure 5.31., in $CH_3CN/CH_2Cl_2$, and UV Absorbance Spectrum for the Reference Standard of Anthanthrene (red line).

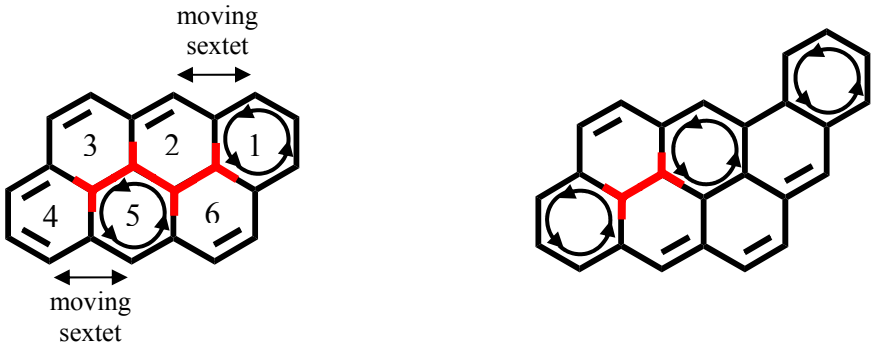


Figure 5.38. Sextets Locations in the Molecules of Anthanthrene and Benz[*a*]anthanthrene by Application of the Y-Rule [Gutman and Ruiz-Morales].

In addition to the preceding analysis, the spectral comparison between the UV spectra of compound **VI**, dibenzo[*a,i*]pyrene, and tribenzo[*cd,ghi,lm*]perylene have provided additional insights about the identity of compound **VI**. Figure 5.39. shows the UV spectrum of compound **VI**, the UV reference spectrum of dibenzo[*a,i*]pyrene, and the postulated UV spectrum of tribenzo[*cd,ghi,lm*]perylene [McClaine et al. 2007b]. Figure 5.39. indicates a sequential spectral pattern for the p bands that starts with dibenzo[*a,i*]pyrene, continues with compound **VI**, and ends with tribenzo[*cd,ghi,lm*]perylene. A shift of 38 nanometers is detected in the last p bands when the UV spectra of dibenzo[*a,i*]pyrene and **VI** are compared. Similarly, a shift of 46 nanometers is measured when the UV spectra of compound **VI** and tribenzo[*cd,ghi,lm*]perylene are compared. In both cases the shapes and intensities of the p bands are perceptible maintained. An equivalent behavior has been seen by McClaine et al. [McClaine et al. 2007b] when they contrasted the spectra of dibenzo[*cd,lm*]perylene, tribenzo[*cd,ghi,lm*]perylene, and tetrabenzo[*cd,ghi,lm,pqr*]perylene during the identification of tribenzo[*cd,ghi,lm*]perylene. In that study, Mc Claine et al. found changes of approximately 40 nanometers in the position of the p bands. The shapes and intensities of the p bands, in that study, did not change noticeable either.

The evidences presented so far, i.e., the molecular weight of 326, the similar characteristics of the UV spectrum of **VI** to the UV spectrum of anthanthrene, the fulfillment of the second rule of the Annellation Theory, and the parallel spectral behavior of the series dibenzo[*a,i*]pyrene, **VI**, and tribenzo[*cd,ghi,lm*]perylene to the spectral behavior of the series of McClaine et al. [McClaine et al. 2007b], lead us to the conclusion that compound **VI** is indeed benz[*a*]anthanthrene.

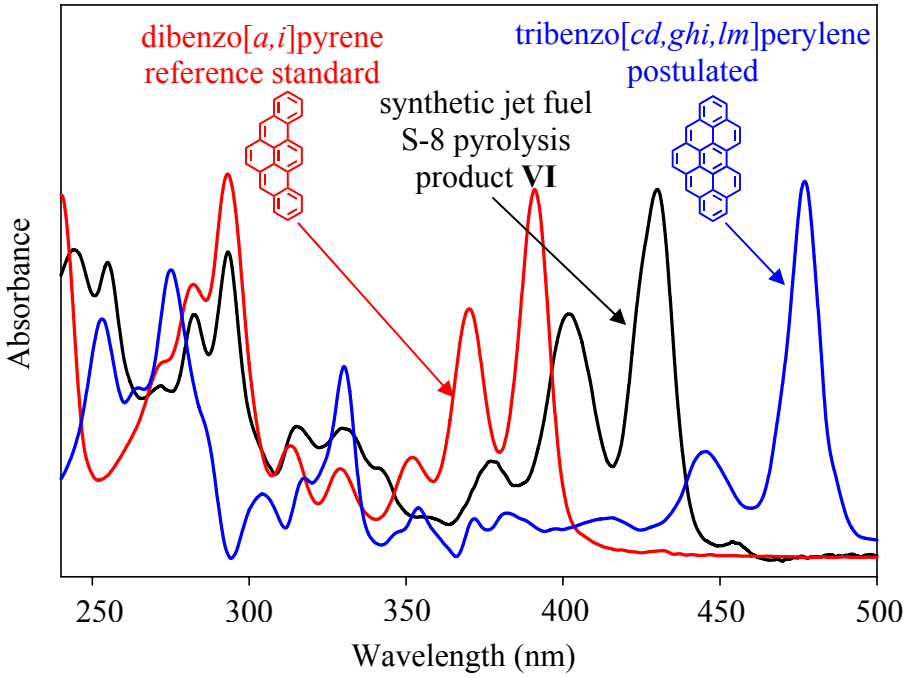


Figure 5.39. UV Absorbance Spectrum for Compound **VI** (black line), the Product Component eluting at 60.5 min in Figure 5.31., in $CH_3CN/CH_2Cl_2$, UV Absorbance Spectrum for the Reference Standard of Dibenzo[*a,i*]pyrene (red line) and Postulated UV Absorbance Spectrum of Tribenzo[*cd,ghi,lm*]perylene [McClaine et al. 2007b] (blue line).

To complement this identification, the elution position of compound **VI**, now identified as benz[*a*]anthanthrene, matches the expected elution order predicted with the L/B ratio for the $C_{26}H_{14}$ benzenoid PAH isomers [Sander], i.e., 1. dibenzo[*b,ghi*]perylene, 2. dibenzo[*e,ghi*]-perylene, 3. naphtho[8,1,2-*bcd*]perylene, 4. benz[*a*]*a*nthanthrene, and 5. dibenzo[*cd,lm*]perylene, as it is observed in Figure 5.31.

**Identification of Other PAH Using the Annellation Theory:** The Annellation Theory has been successful not only for the identification of compounds **V** and **VI** as benzo[*ghi*]phenanthro[9,10,1-*cde*]perylene and benz[*a*]anthanthrene, respectively, but also in the identification of other compounds of the synthetic jet fuel S-8 pyrolysis product mixture. These compounds include benz[*e*]anthanthrene [Oña and Wornat 2008b], benzo[*ghi*]naphtho[8,1,2-*bcd*]perylene (identified also in the pyrolysis products of toluene [McClaine et al. 2006] and

methylcyclohexane (Section 5.2.2.) [Oña and Wornat 2008a]), and tribenzo[*cd,ghi,lm*]perylene (identified also in the pyrolysis products of toluene [McClaine et al. 2007b]). The UV spectral identifications of these PAH products has been accomplished by application of the Annellation Theory rules.

Figure 5.40. shows the fourth and last version of the HPLC/UV chromatogram of the synthetic jet fuel S-8 products using the solvent program of Figure 4.2.-A. The total number of products detected is eighty-five (eighty-four from Figure 5.40. and one more from Figure 5.32.). The techniques applied for the identification of the products in Figures 5.40. and 5.32. are: UV spectral comparison with standards, analysis of the effect of an alkyl substituent on the UV spectra, application of the UV solvent-based adjustment, and application of the Annellation Theory. MS information has been used in all cases to verify the identity of each PAH.

Twenty-nine unsubstituted PAH with six or more rings have never before been identified in the pyrolysis of a long-chain alkane fuel, e.g. synthetic jet fuel S-8. Following the order of elution given in Figure 5.40., these compounds are: naphtho[2,3-*e*]pyrene, naphtho[1,2-*a*]pyrene, naphtho[1,2-*k*]fluoranthene, benzo[*b*]perylene, benz[*e*]anthanthrene, dibenzo-[*b,k*]fluoranthene, naphtho[2,3-*b*]fluoranthene, 8H-dibenzo[*a,jk*]pyrene, naphtho[2,1-*a*]pyrene, dibenzo[*b,ghi*]perylene, phenanthro[2,3-*a*]pyrene, naphtho[2,3-*a*]pyrene, dibenzo[*e,ghi*]perylene, naphtho[8,1,2-*bcd*]perylene, 2,2'-bianthryl, benz[*a*]anthanthrene, benzo[*a*]coronene, dibenzo-[*cd,lm*]perylene, phenanthro[5,4,3,2-*efghi*]perylene, benzo[*cd*]naphtho[3,2,1,8-*pqra*]perylene, benzo[*ghi*]naphtho[8,1,2-*bcd*]perylene, benzo[*pqr*]naphtho[8,1,2-*bcd*]perylene, benzo[*b*]picene, tribenzo[*cd,ghi,lm*]perylene, naphtho[8,1,2-*abc*]coronene, ovalene, benzo[*ghi*]phenanthro-[9,10,1-*cde*]perylene, benzo[*cd*]naptho[1,2,3-*lmn*]perylene, and benzo[*pqr*]dinaphtho[8,1,2-*bcd*:2',1',8'-*lmn*]perylene.

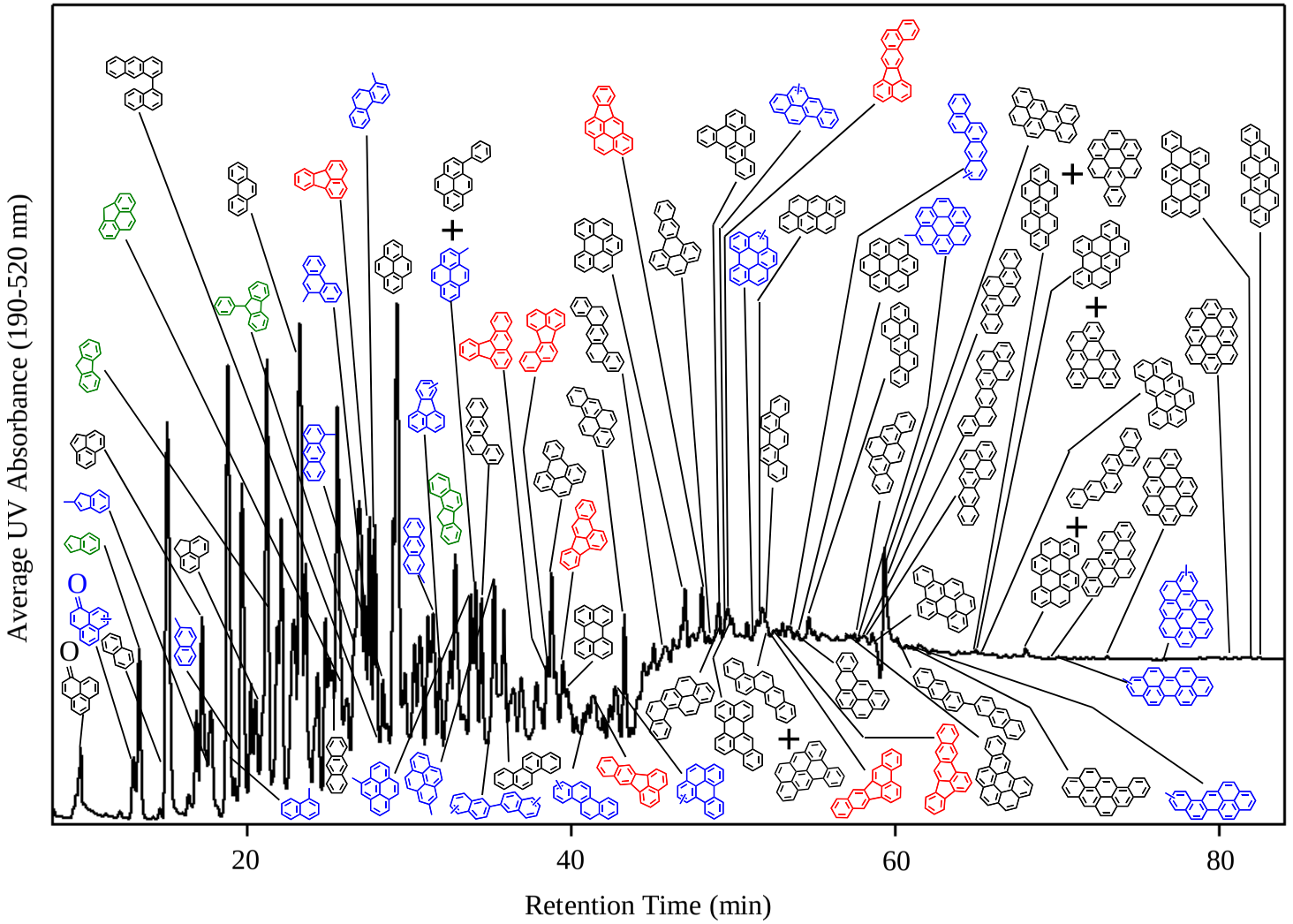


Figure 5.40. HPLC/UV Chromatogram (Fourth Version) of the Synthetic Jet Fuel S-8 Supercritical Pyrolysis Products at 710 ºC and 42 atm.

### 5.1.3. Influence of the Temperature

This investigation has been performed in order to gain understanding of the influence of the temperature in the formation of PAH products from the pyrolysis of synthetic jet fuel S-8 at supercritical conditions. To accomplish this objective, an analysis similar to the analysis presented in section 5.1.2. based on the usage of HPLC chromatography with UV detection has been applied to the products of the synthetic jet fuel S-8 supercritical pyrolysis generated at 666 $^{o}$C and 42 atm [Huang et al. 2002, 2004]. The solvent program used during this analysis comes from Figure 4.2.A.

After this HPLC/UV analysis, the PAH products reported at this new condition have been contrasted with the PAH products reported in section 5.1.2. at 710 $^{o}$C and 42 atm. The HPLC/UV chromatogram of the supercritical pyrolysis products of synthetic jet fuel S-8 at 666 $^{o}$C and 42 atm is shown in Figure 5.41. The HPLC/UV chromatogram of the supercritical pyrolysis products of synthetic jet fuel S-8 at 710 $^{o}$C and 42 atm has already been presented in Figure 5.40. Figures 5.41. and 5.40. demonstrate that a 44 $^{o}$C increase of temperature, from 666 $^{o}$C to 710 $^{o}$C in the supercritical state, brings about a transition from a regime in which PAH with up to seven rings are detected to a new regime in which PAH with up to ten rings are identified. The complexity of the product mixture at 666 $^{o}$C generates a chromatogram with poor resolution in the elution time range between thirty and fifty minutes.

## 5.2. Supercritical Pyrolysis of Methylcyclohexane

The effectiveness of the GC/MS and HPLC/UV techniques evidenced during the identification of the PAH products from the supercritical pyrolysis of synthetic jet fuel S-8 (Sections 5.1.1. and 5.1.2.), has been a motivation to apply the same methodology for the identification of the PAH products from the supercritical pyrolysis of methylcyclohexane.

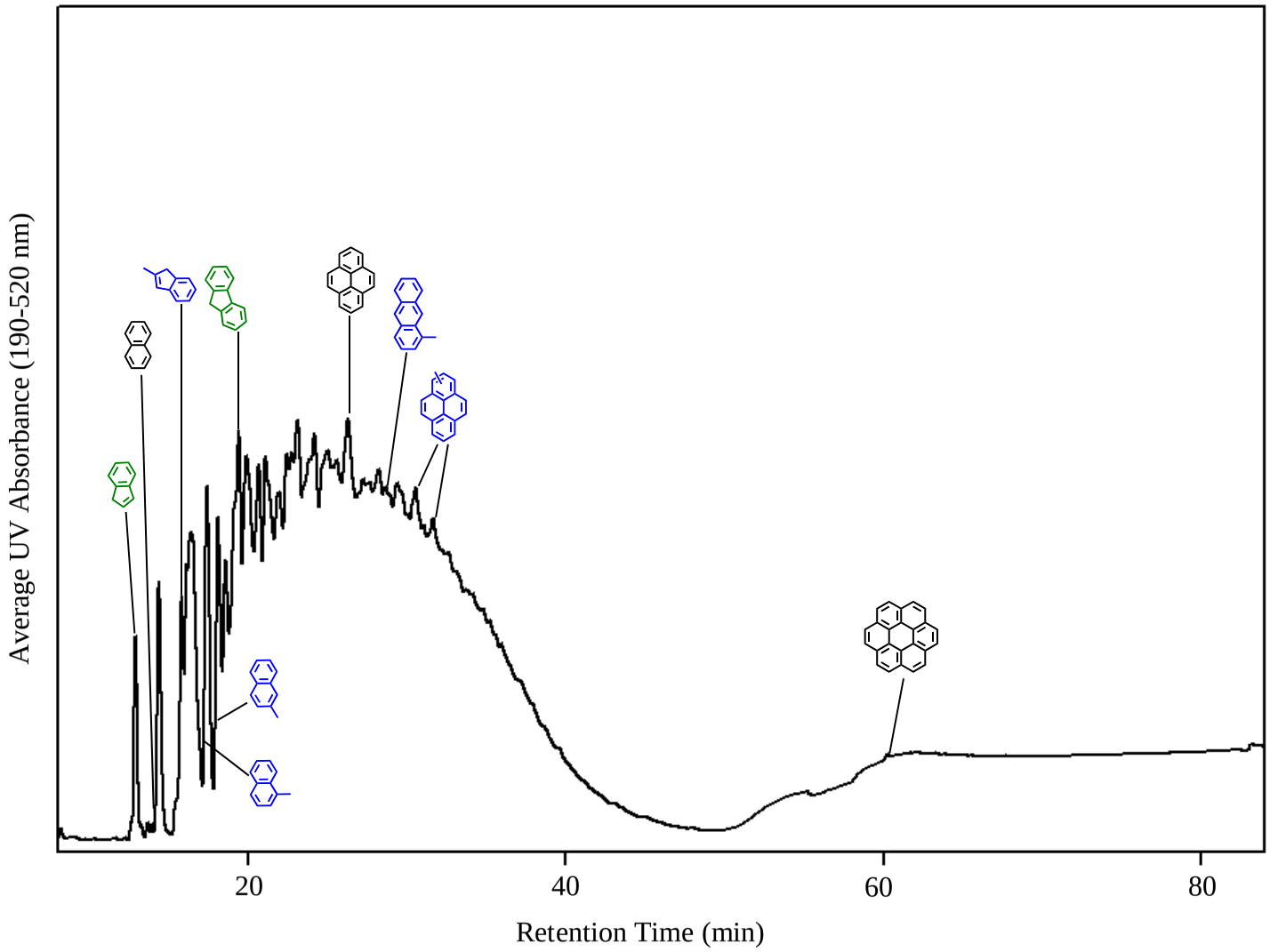


Figure 5.41. HPLC/UV Chromatogram of the Synthetic Jet Fuel S-8 Supercritical Pyrolysis Products at 666 °C and 42 atm.

### 5.2.1. Identification of Polycyclic Aromatic Hydrocarbons Using Gas Chromatography with Mass Spectrometry

Figure 5.42. shows the GC/MS chromatogram of the supercritical pyrolysis products of methylcyclohexane subjected at 570 $^{o}$C, 100 atm, and 140 sec (the most severe condition). A total of 29 different peaks have been identified based on the elution time comparison with the respective elution time of authentic standards. The following compounds have been fully identified: toluene, ethylcyclohexane, ethylbenzene, meta-xylene, para-xylene, ortho-xylene, propylcyclohexane, propylbenzene, butylcyclohexane, 2,3-dihydroindene, indene, and butylbenzene. The full identification of several of these molecules, e.g., methylethylcyclohexenes, methylethylcyclohexanes, methylethylbenzenes, methylpropylbenzene, methylbutylbenzene, trimethylbenzenes, and methylpropylcyclohexanes has not been possible due to the lack of standards to recognize the correct retention time of each compound and due to the presence of isomeric molecules with similar mass spectra.

### 5.2.2. Identification of Polycyclic Aromatic Hydrocarbons Using High-Performance Liquid Chromatography with Ultraviolet-Visible Spectroscopy

Figure 5.43. shows the HPLC/UV chromatogram of the supercritical pyrolysis products of methylcyclohexane subjected at 570 $^{o}$C, 100 atm, and 140 sec (the most severe condition). The solvent program used during this analysis comes from Figure 4.2.A. Theoretically, Figure 4.2.A. shows a change of solvent at 40 minutes from $CH_3CN$ to $CH_2Cl_2$, experimentally, however, this change is evidenced by a hump in the chromatogram of Figure 5.43. at approximately 42 minutes. This difference of about 2 minutes is due to the delay time between the preset solvent program in the computer and the actual chromatographic signal. Fifty-five peaks have been identified based on the UV spectral comparison with the spectral information of authentic standards commercially available and with the spectral information from the literature

[Fetzer and Biggs 1994, Lang and Buffleb, Ojakaar, Friedel and Orchin, Zander and Franke, Clar 1964].

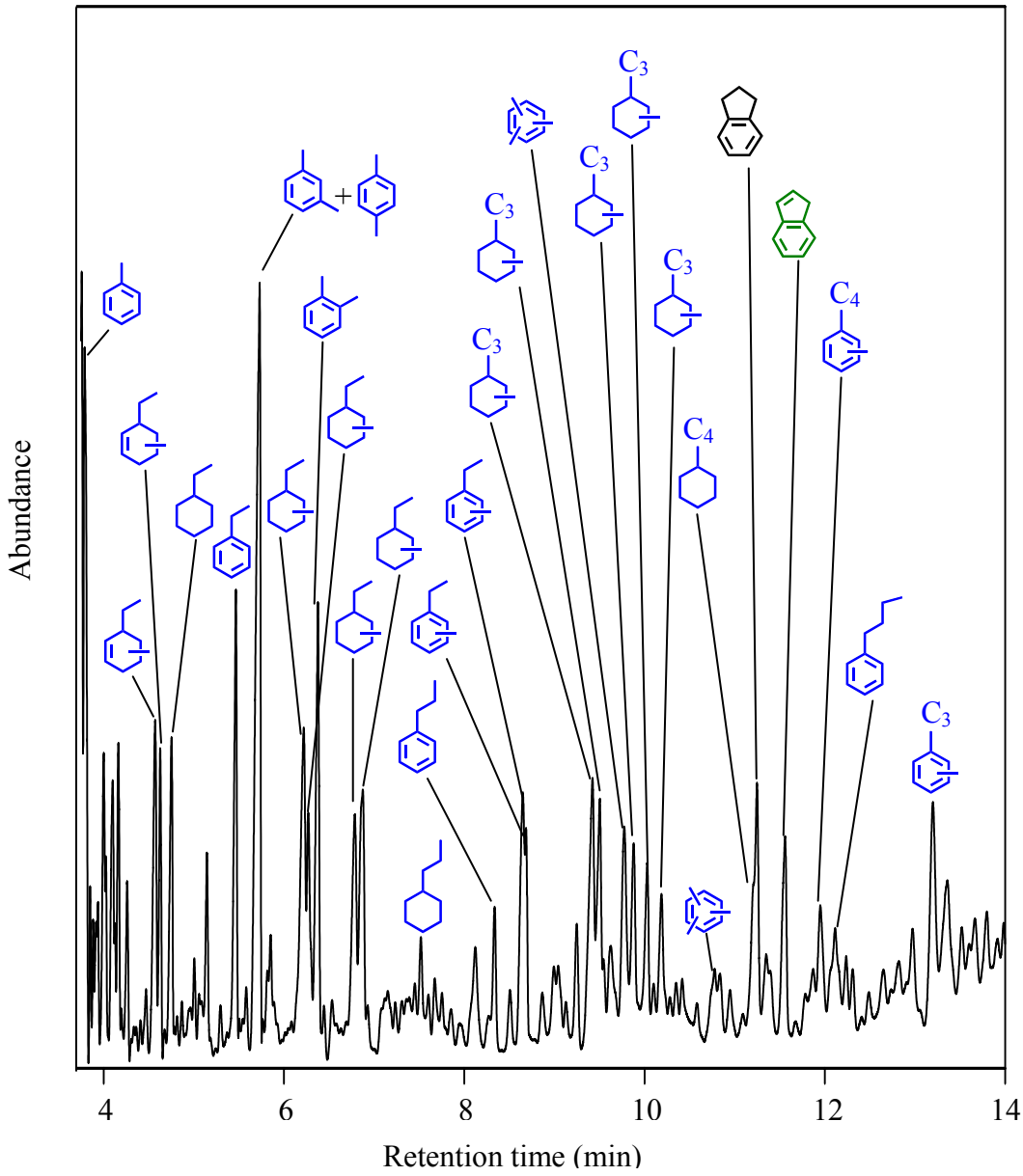


Figure 5.42. GC/MS Chromatogram of the Methylcyclohexane Supercritical Pyrolysis Products at 570 $^{o}$C, 100 atm, and 140 sec.

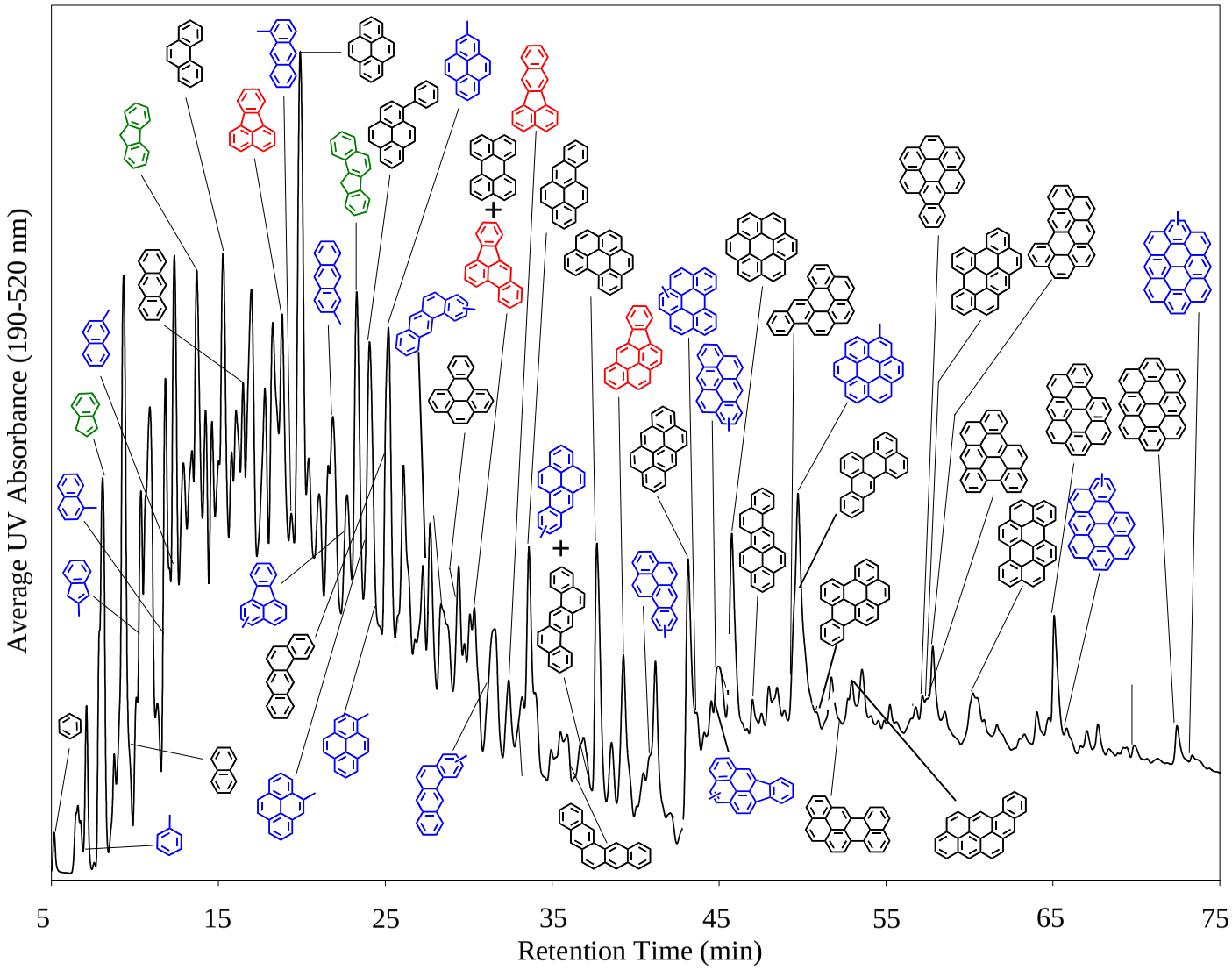


Figure 5.43. HPLC/UV Chromatogram of the Methylcyclohexane Supercritical Pyrolysis Products at 570 °C, 100 atm, and 140 sec.

Some of these compunds, e.g., methylfluoranthene, methylbenz[*a*]anthracene, methylbenzo[*a*]pyrene, methylanthanthrene, methylindeno[1,2,3-*cd*]pyrene, methylbenzo[*ghi*]-perylene, 1-methylcoronene, methylnaphtho[8,1,2-*abc*]coronene, methylovalene, naphtho[8,1,2-*bcd*]perylene, benz[*a*]anthanthrene, dibenzo[*b,ghi*]perylene, dibenzo[*e,ghi*]perylene, and benzo[*ghi*]naptho[8,1,2-*bcd*]perylene, have been identified by further interpretation of the UV spectra by means of the alkyl substitution effect, the UV solvent-based adjustment, and the Annellation Theory, already described in Chapter 3 and applied in section 5.1.2. Therefore, their detailed identification will not be explained here.

The PAH identified can be grouped into: methylated PAH (blue), indene benzologues (green), fluoranthene benzologues (red), and benzenoid PAH (black). The following is the list of the identified PAH in their respective elution order: benzene, toluene, indene, naphthalene, 2-methylindene, 1-methylnaphthalene, 2-methylnaphthalene, fluorene, phenanthrene, anthracene, fluoranthene, 1-methylanthracene, pyrene, 2-methylanthracene, methylfluoranthene, benzo[*a*]-fluorene, 4-methylpyrene, 1-phenylpyrene, 1-methylpyrene, benz[*a*]anthracene, 2-methylpyrene, methylbenz[*a*]anthracene, benzo[*e*]pyrene, perylene co-eluting with benzo[*b*]fluoranthene, methylbenz[*a*]anthracene, benzo[*k*]fluoranthene, benzo[*a*]pyrene, pentaphene, dibenz[*a,h*]-anthracene co-eluting with methylbenzo[*a*]pyrene, benzo[*ghi*]perylene, indeno[1,2,3-*cd*]pyrene, methylbenzo[*a*]pyrene, anthanthrene, methylbenzo[*ghi*]perylene, methylindeno[1,2,3-*cd*]pyrene, methylanthanthrene, coronene, naphtho[2,1-*a*]pyrene, dibenzo[*b,ghi*]perylene, 1-methyl-coronene, benzo[*b*]perylene, dibenzo[*e,ghi*]perylene, naphtho[8,1,2-*bcd*]perylene, benz[*a*]-anthanthrene, benzo[*a*]coronene, phenanthro[5,4,3,2-*efghi*]perylene, benzo[*cd*]naphtho[3,2,1,8-*pqra*]perylene, benzo[*ghi*]naphtho[8,1,2-*bcd*]perylene, benzo[*pqr*]naphtho[8,1,2-*bcd*]perylene, naphtho[8,1,2-*abc*]coronene, methylnaptho[8,1,2-*abc*]coronene, ovalene, and methylovalene.

Representative identifications are presented in Figures 5.44. through 5.47. Figures 5.44., 5.45., 5.46., and 5.47. show the UV spectral matches between the spectra of the reference standards of anthanthrene, coronene, naphtho[2,1-*a*]pyrene, and ovalene (in red) and their respective spectra from the supercritical pyrolysis products of methylcyclohexane (in black). A similar procedure has been followed to identify the rest of the products from the supercritical pyrolysis of methylcyclohexane. The unsubstituted PAH anthanthrene, coronene, naphtho[2,1-*a*]pyrene, dibenzo[*b,ghi*]perylene, benzo[*b*]perylene, dibenzo[*e,ghi*]perylene, naphtho[8,1,2-*bcd*]perylene, benz[*a*]anthanthrene, benzo[*a*]coronene, phenanthro[5,4,3,2-*efghi*]perylene, benzo[*cd*]naphtho[3,2,1,8-*pqra*]perylene, benzo[*ghi*]naphtho[8,1,2-*bcd*]perylene, benzo[*pqr*]-naphtho[8,1,2-*bcd*]perylene, naphtho[8,1,2-*abc*]coronene, and ovalene have never before been detected as products from the pyrolysis or combustion of methylcyclohexane in any context.

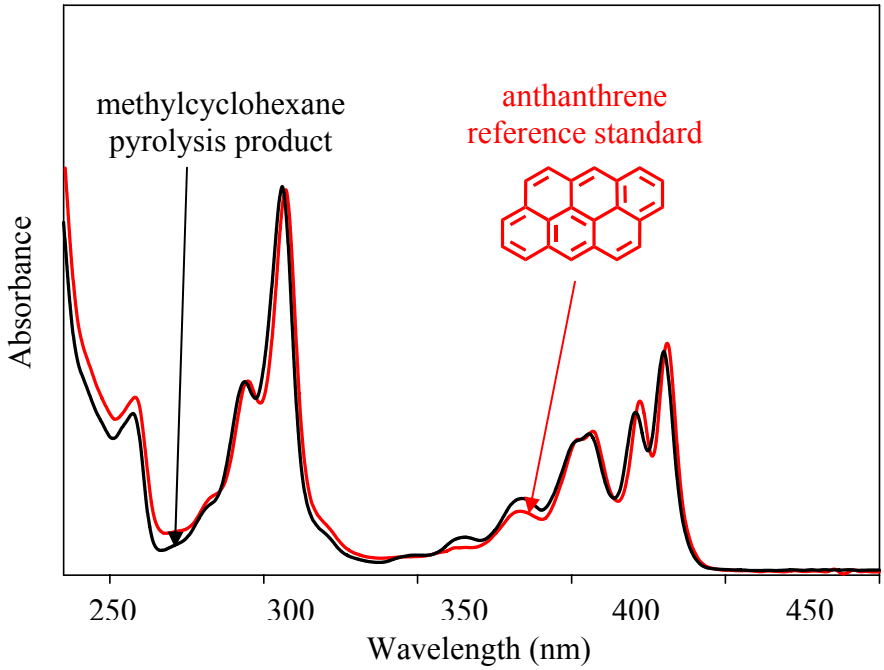


Figure 5.44. UV Absorbance Spectra for the Reference Standard of Anthanthrene and for a Methylcyclohexane Supercritical Pyrolysis Product having the same HPLC Retention Time.

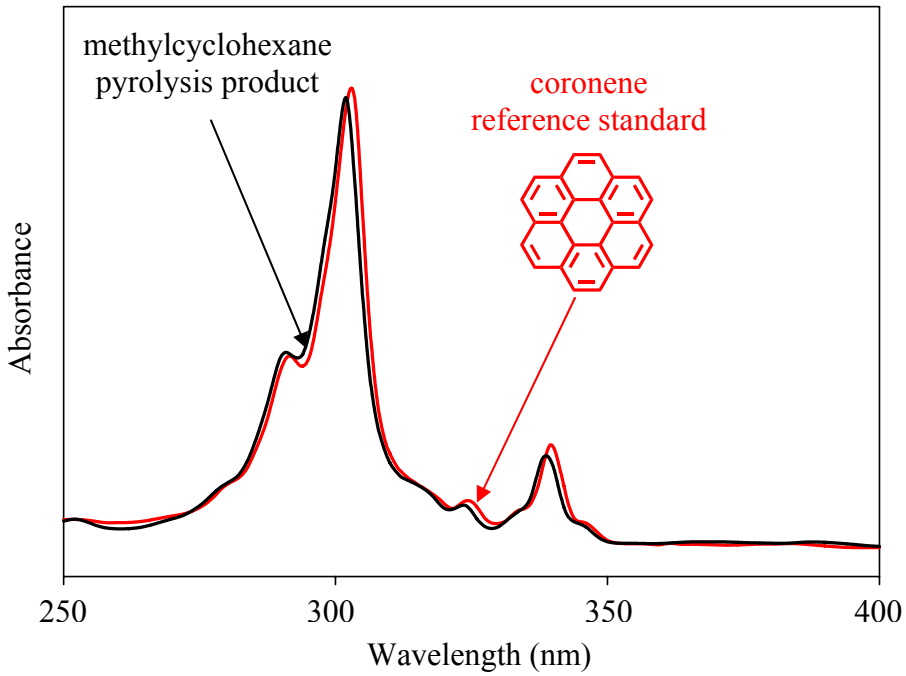


Figure 5.45. UV Absorbance Spectra for the Reference Standard of Coronene and for a Methylcyclohexane Supercritical Pyrolysis Product having the same HPLC Retention Time.

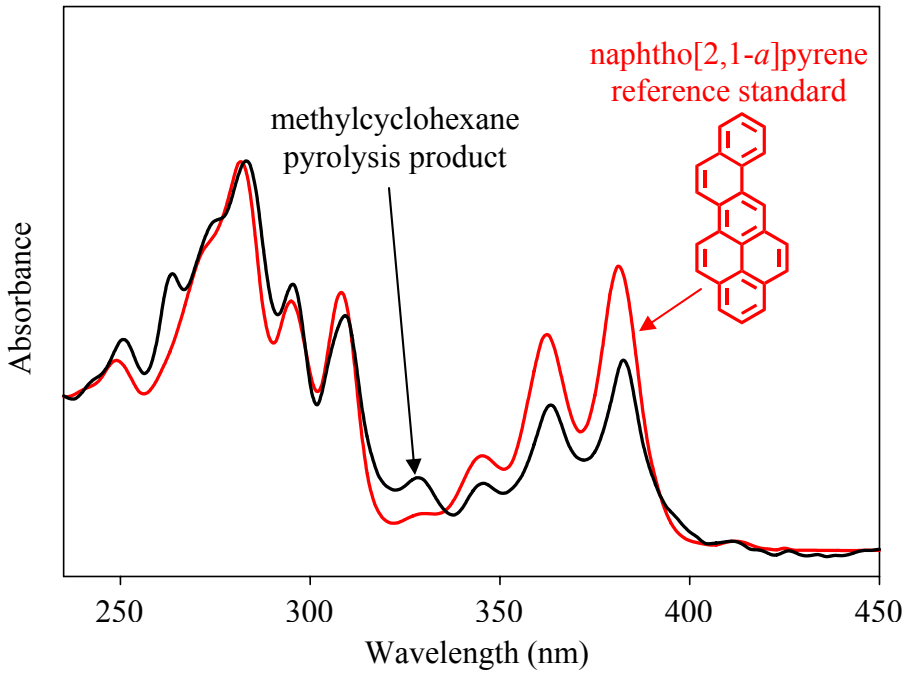


Figure 5.46. UV Absorbance Spectra for the Reference Standard of Naphtho[2,1-*a*]pyrene and for a Methylcyclohexane Supercritical Pyrolysis Product having the same HPLC Retention Time.

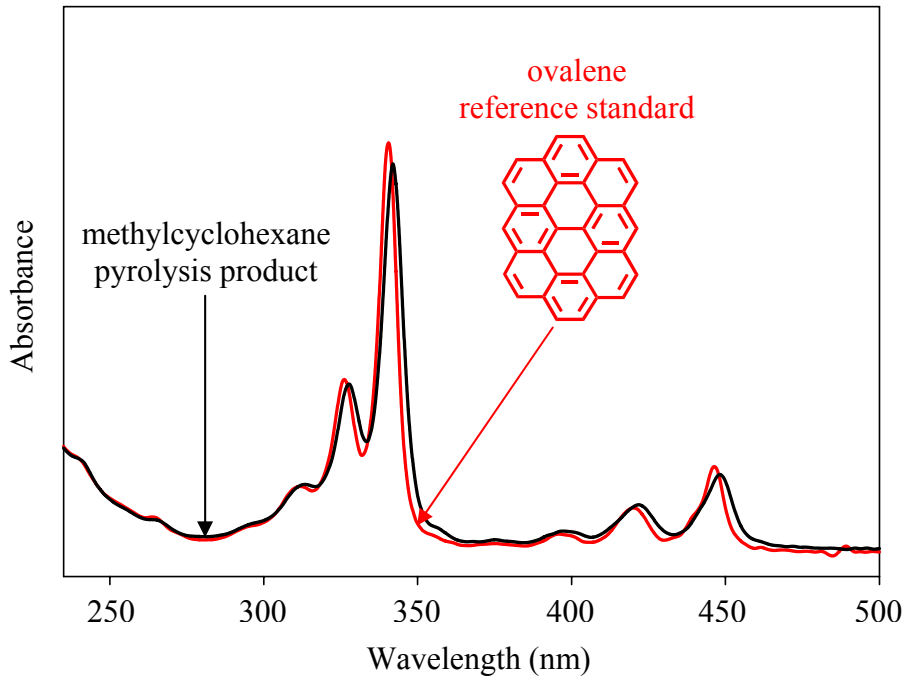


Figure 5.47. UV Absorbance Spectra for the Reference Standard of Ovalene and for a Methylcyclohexane Supercritical Pyrolysis Product having the same HPLC Retention Time.

### 5.2.3. Analogy of PAH Products from Methylcyclohexane Supercritical Pyrolysis and Toluene Supercritical Pyrolysis

In Section 2.3.4. it was stated (and verified later in Figures 5.42. and 5.43.) that toluene is one of the main products from the supercritical pyrolysis of methylcyclohexane. Therefore, it is reasonable to establish an analogy between the PAH products identified from the supercritical pyrolysis of toluene shown in Figure 2.5. and the PAH products from the supercritical pyrolysis of methylcyclohexane shown in Figure 5.43., both of them generated in the same equipment. Moreover, with the exception of the temperature, the experimental conditions applied for the experiment with toluene, i.e., pressure and residence time, are the same as the conditions applied for the experiment with methylcyclohexane.

Table 5.1. presents a list of the PAH detected using HPLC/UV in the products of toluene and methylcyclohexane at supercritical conditions. The analogy between these two sets of PAH

products is evident. Out of the sixty PAH present both in toluene and in methylcyclohexane supercritical pyrolysis products, forty-two compounds have been found in both fuels. In addition, similar small products (up to 4 rings) are detected in both the GC/MS analyses with toluene [McClaine et al. 2007a] and with methylcyclohexane (as it is shown in Figure 5.42.). This product formation parallelism strongly suggests that the generation of these two series of products follows the same mechanism. Therefore, it is logical to conclude that the formation of PAH products from the supercritical pyrolysis of methylcyclohexane follows also the pathway mentioned in Figure 2.6.

Table 5.1. PAH Products detected from the Supercritical Pyrolysis of Toluene (535 $^{o}$C, 100 atm, and 140 sec) and from the Supercritical Pyrolysis of Methylcyclohexane (570 $^{o}$C, 100 atm, and 140 sec) Using HPLC/UV

| PAH | In Toluene Products* | In Methylcyclohexane Products |
|---|---|---|
|  | ✓** | ✓ |
|  | ✓ | ✓ |
|  | ✓ | ✓ |
|  | ✓** | ✓ |
|  | ✓ | ✓ |
|  | ✓ | ✓ |
|  | ✓ | ✗*** |
|  | ✓ | ✓ |
|  | ✓ | ✓ |
| 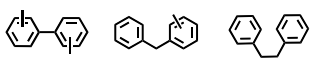 | ✓ | ✗*** |
|  | ✓ | ✓ |
| 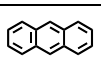 | ✓ | ✓ |

* McClaine et al. 2006, 2007a, 2007b

** Identified by GC/MS

*** Below the detection limit of 187 ng/g methylcyclohexane

(Table 5.1. continued)

| PAH | In Toluene Products | In Methylcyclohexane Products |
|---|---|---|
|  | ✓ | ✓ |
|  | ✗ | ✓ |
|  | ✓ | ✓ |
| 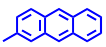 | ✓ | ✓ |
|  | ✗ | ✓ |
| 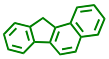 | ✓ | ✓ |
|  | ✗ | ✓ |
| 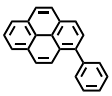 | ✓ | ✓ |
|  | ✓ | ✓ |
| 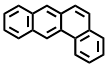 | ✓ | ✓ |
|  | ✗*** | ✓ |
|  | ✗ | ✓ |
| 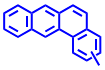 | ✗ | ✓ |
| 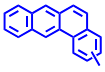 | ✗ | ✓ |
|  | ✓ | ✗*** |
|  | ✓ | ✓ |

*** Below the detection limit of 187 ng/g methylcyclohexane

(Table 5.1. continued)

| PAH | In Toluene Products | In Methylcyclohexane Products |
|---|---|---|
|  | ✓ | ✓ |
| 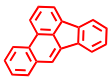 | ✓ | ✓ |
| 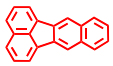 | ✓ | ✓ |
| 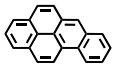 | ✓ | ✓ |
| 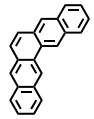 | ✓ | ✓ |
| 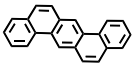 | ✗ | ✓ |
| 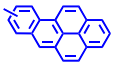 | ✗ | ✓ |
| 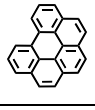 | ✓ | ✓ |
| 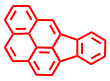 | ✓ | ✓ |
| 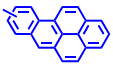 | ✗ | ✓ |
| 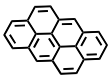 | ✓ | ✓ |
| 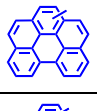 | ✓ | ✗*** |
|  | ✓ | ✓ |
| 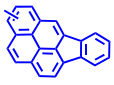 | ✗ | ✓ |
| 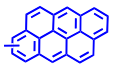 | ✓ | ✓ |

*** Below the detection limit of 187 ng/g methylcyclohexane

(Table 5.1. continued)

| PAH | In Toluene Products | In Methylcyclohexane Products |
|---|---|---|
|  | ✓ | ✓ |
| 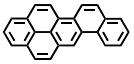 | ✓ | ✓ |
| 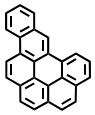 | ✓ | ✓ |
| 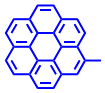 | ✓ | ✓ |
| 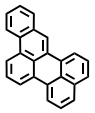 | ✗ | ✓ |
| 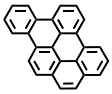 | ✓ | ✓ |
| 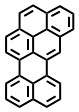 | ✗ | ✓ |
| 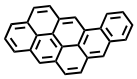 | ✗ | ✓ |
| 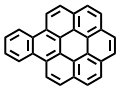 | ✓ | ✓ |
| 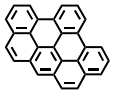 | ✓ | ✓ |
| 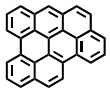 | ✓ | ✓ |
| 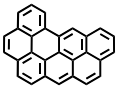 | ✓ | ✓ |
| 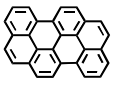 | ✓ | ✓ |

(Table 5.1. continued)

| PAH | In Toluene Products | In Methylcyclohexane Products |
|---|---|---|
| 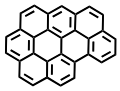 | ✓ | ✓ |
|  | ✓ | ✓ |
| 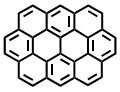 | ✓ | ✓ |
| 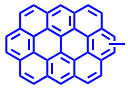 | ✓ | ✓ |

### 5.2.4. Yields of PAH Products from Methylcyclohexane Supercritical Pyrolysis

Figure 5.48. shows the yields of selected PAH products of the supercritical pyrolysis products of methylcyclohexane at 570 $^{o}$C, 100 atm, and 140 sec that have been computed using the information obtained from the HPLC analysis in terms of nanograms per gram of methylcyclohexane fed. These results show that the highest-yield products are 1-methylcoronene, anthanthrene, benzo[*a*]pyrene, indeno[1,2,3-*cd*]pyrene, benzo[*ghi*]perylene, and coronene. Figure 5.48. also shows that the lowest-yield aromatic products are methylovalene, benzo[*cd*]naphtho[3,2,1,8-*pqra*]perylene, and methylnaphtho[8,1,2-*abc*]coronene. For two PAH, 1-methylcoronene and coronene, these results are not surprising since they are characterized by a well-known property called superaromaticity [Clar 1972]. This property provides them more reactive stability than the stability observed in other PAH causing that 1-methylcoronene and coronene increase their concentration over time remaining essentially unaltered as soon as they are formed. On the other hand, for the other highest-yield PAH products, the story is still not clear. It is interesting to mention, however, that the longest p-bands (which behavior is

associated with the stability of a PAH [Oña and Wornat 2008d]) of benzo[*a*]pyrene, benzo[*ghi*]perylene, and indeno[1,2,3-*cd*]pyrene are located at approximately the same wavelength, i.e., 380 nm, which is well-before the longest p-band position for some lowest-yield PAH products such as ovalene, benzo[*cd*]naphtho[3,2,1,8-*pqra*]perylene, and benzo[*pqr*]naphtho[8,1,2-*bcd*]perylene.

**5.2.5. Influence of the Pressure**

Pyrolysis studies have been carried out at constant temperature (570 °C), constant residence time (140 sec), and for a range of pressures (20-100 atm with intervals of 20 atm) to show the influence of the pressure in the formation of PAH products from the supercritical pyrolysis of methylcyclohexane. Consistent with the analyses followed in the previous sections, HPLC chromatography with UV detection has been selected as the analytical technique for PAH identification. The solvent program of Figure 4.2.A. has been used for these analyses.

The HPLC/UV chromatograms illustrated in Figures 5.49., 5.50., 5.51., and 5.52. show the PAH products identified from the supercritical pyrolysis of methylcyclohexane at four experimental conditions: first, 570 $^{o}$C, 20 atm, and 140 sec; second, 570 $^{o}$C, 40 atm, and 140 sec; third, 570 $^{o}$C, 60 atm, and 140 sec; and fourth, 570 $^{o}$C, 80 atm, and 140 sec. The HPLC/UV chromatogram of the supercritical pyrolysis products of methylcyclohexane at 570 $^{o}$C, 100 atm, and 140 sec has already been presented in Figure 5.43.

Figures 5.49., 5.50., 5.51., and 5.52., demonstrate that the formation of PAH in near-critical and super-critical conditions is very sensitive to pressure. As Figures 5.49., 5.50., 5.51., and 5.52. reveal, the increase of pressure brings about an increase in number and in complexity of the molecules detected. To explain this behavior, the points already discussed in Chapter 2 are recalled. According to that analysis, the elevated pressures (≥ 60 atm) create a high-density

environment (known also as cage effect) over the molecules with the higher concentration, e.g., benzene, toluene, and xylenes, that promotes the formation of heavy and compact PAH structures following the scheme of Figure 2.6.

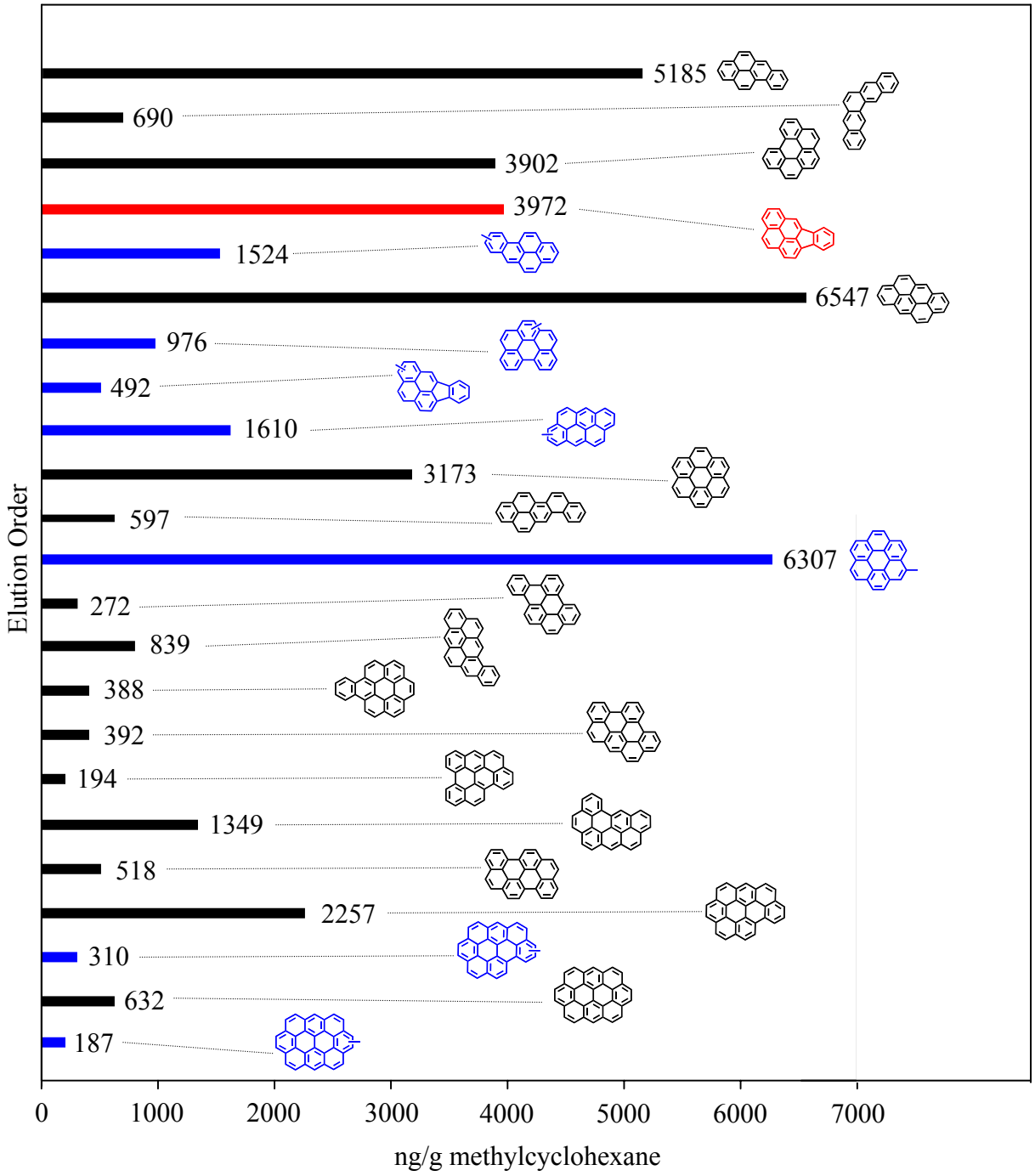


Figure 5.48. Yields of selected PAH Products from the Supercritical Pyrolysis of Methylcyclohexane at 570 $^{o}$C, 100 atm, and 140 sec.

At 570 $^{o}$C, 20 atm, and 140 sec., five PAH have been identified. Structures with up to two rings, e.g., indene, naphthalene, 2-methylindene, 1-methylnaphthalene, and 2-methylnaphthtalene, have been detected. Since methylcyclohexane is still in the gas phase at this pressure, the associated way to form large structures, i.e., the supercritical cage-effect analyzed earlier in this study, is absent. Therefore, large PAH structures are not present in this chromatogram. Unresolved material from 15 to 42 minutes can not be identified due to insufficient UV signal produced by low concentration PAH products eluting at this time range.

At 570 $^{o}$C, 40 atm, and 140 sec, six PAH have been identified. Since methylcyclohexane has exceeded its critical pressure, i.e., 34 atm, new alkylated and non-alkylated structures have started to appear from 15 to 42 minutes. Most of these novel structures can not be identified due to the lack of standards to allow their conclusive recognition and/or due to the low concentration of the reaction products that generates a low UV signal. The compounds observed at this pressure include the majority of the products identified at 20 atm, e.g., indene, naphthalene and their methylated homologues.

At 570 $^{o}$C, 60 atm, and 140 sec, i.e., well beyond the critical point of methylcyclohexane, the HPLC chromatogram reveals that the high pressure favors the formation of large PAH molecules. Thirty-two PAH have been identified at this condition. Some of the identified molecules, e.g., indene, naphthalene, anthracene, pyrene, benzo[*ghi*]perylene, coronene, and 1-methylcoronene, are clearly favored by the reaction. PAH with up to seven rings have been identified at 60 atm.

At 570 $^{o}$C, 80 atm, and 140 sec, forty-six PAH have been identified. Benzenoid PAH, indene benzologues, fluoranthene benzologues, and methylated PAH are the most prominent classes represented in the methylcyclohexane products at 80 atm. PAH with high stabilities, e.g.,

benz[*a*]anthanthrene, benzo[*ghi*]naphtho[8,1,2-*bcd*]perylene, and naphtho[8,1,2-*abc*]coronene, have a significant presence in the large PAH zone. PAH with up to ten rings have been identified at this condition.

The result at 570 $^{o}$C, 100 atm, and 140 sec, has already been discussed in Section 5.2.2. and Figure 5.43. Consistent with the findings at 60 and 80 atm, at 100 atm the high pressure is influencing the formation of the most stable molecules, e.g., benzo[*ghi*]perylene, anthanthrene, coronene, and 1-methylcoronene. Other molecules such as benzo[*pqr*]naphtho[8,1,2-*bcd*]perylene, naphtho[8,1,2-*abc*]coronene, and ovalene are more prominent in this case. Fifty-five PAH with up to ten rings have been identified at this condition.

**5.2.6. Influence of the Temperature**

Pyrolysis studies have been carried out at constant pressure (100 atm), constant residence time (140 sec), and for three temperatures (560 $^{o}$C, 570 $^{o}$C, and 580 $^{o}$C) to show the influence of the temperature in the formation of PAH products from the supercritical pyrolysis of methylcyclohexane. One more time, HPLC chromatography with UV detection has been selected as the analytical technique for PAH identification. The solvent program of Figure 4.2.A. has been used for these analyses.

The HPLC/UV chromatogram of Figure 5.53. shows the PAH products identified from the supercritical pyrolysis of methylcyclohexane at 560 $^{o}$C, 100 atm, and 140 sec. The HPLC/UV chromatogram of the supercritical pyrolysis products of methylcyclohexane at 570 $^{o}$C, 100 atm, and 140 sec has already been presented in Figure 5.43.

Figures 5.53. and 5.43. demonstrate that a 10 $^{o}$C increase of temperature, from 560 $^{o}$C to 570 $^{o}$C, brings about a transition from a regime in which PAH with up to five rings are detected to a new regime in which PAH with up to ten rings are identified.

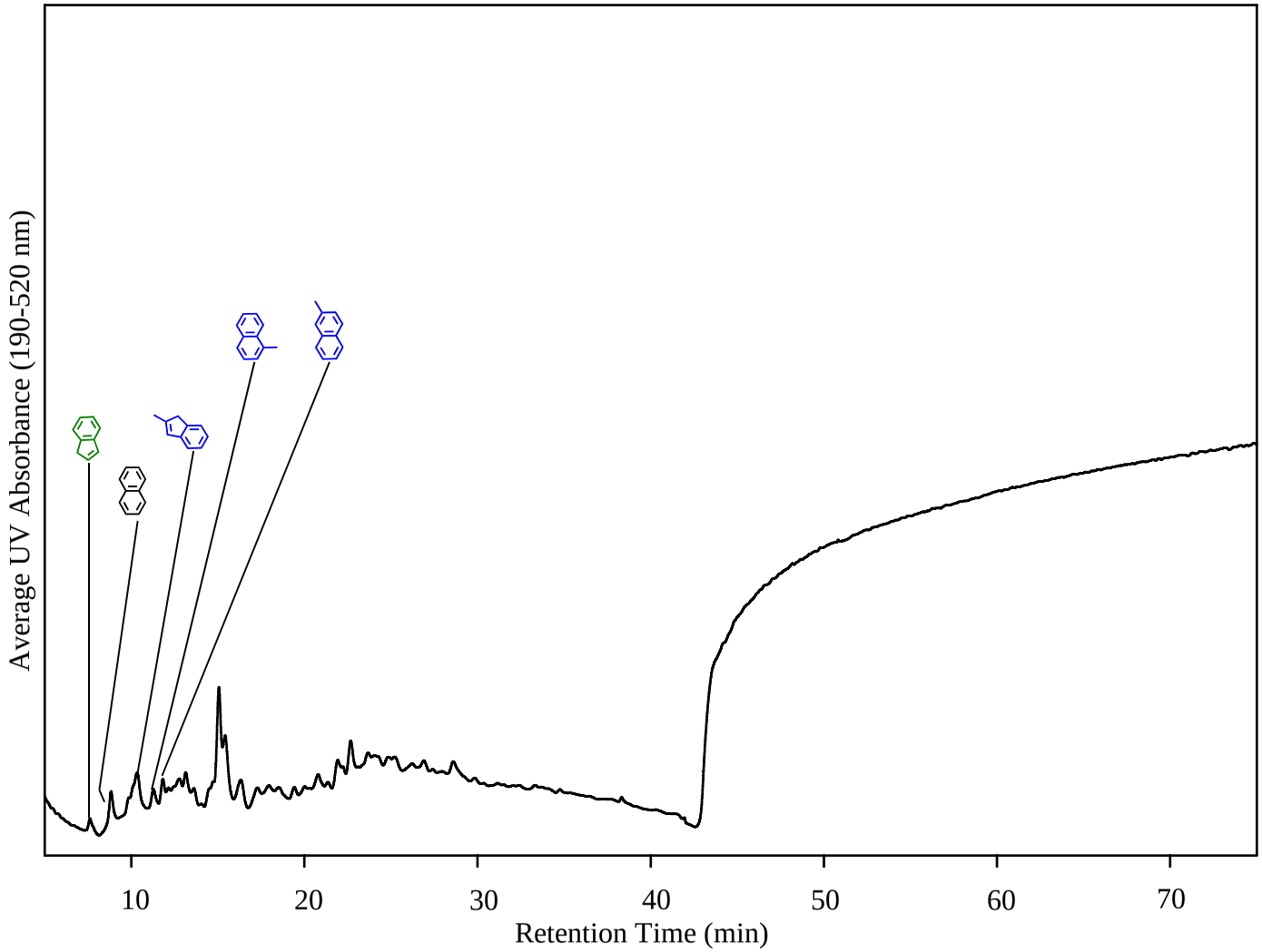


Figure 5.49. HPLC/UV Chromatogram of the Methylcyclohexane Pyrolysis Products at 570 °C, 20 atm, and 140 sec.

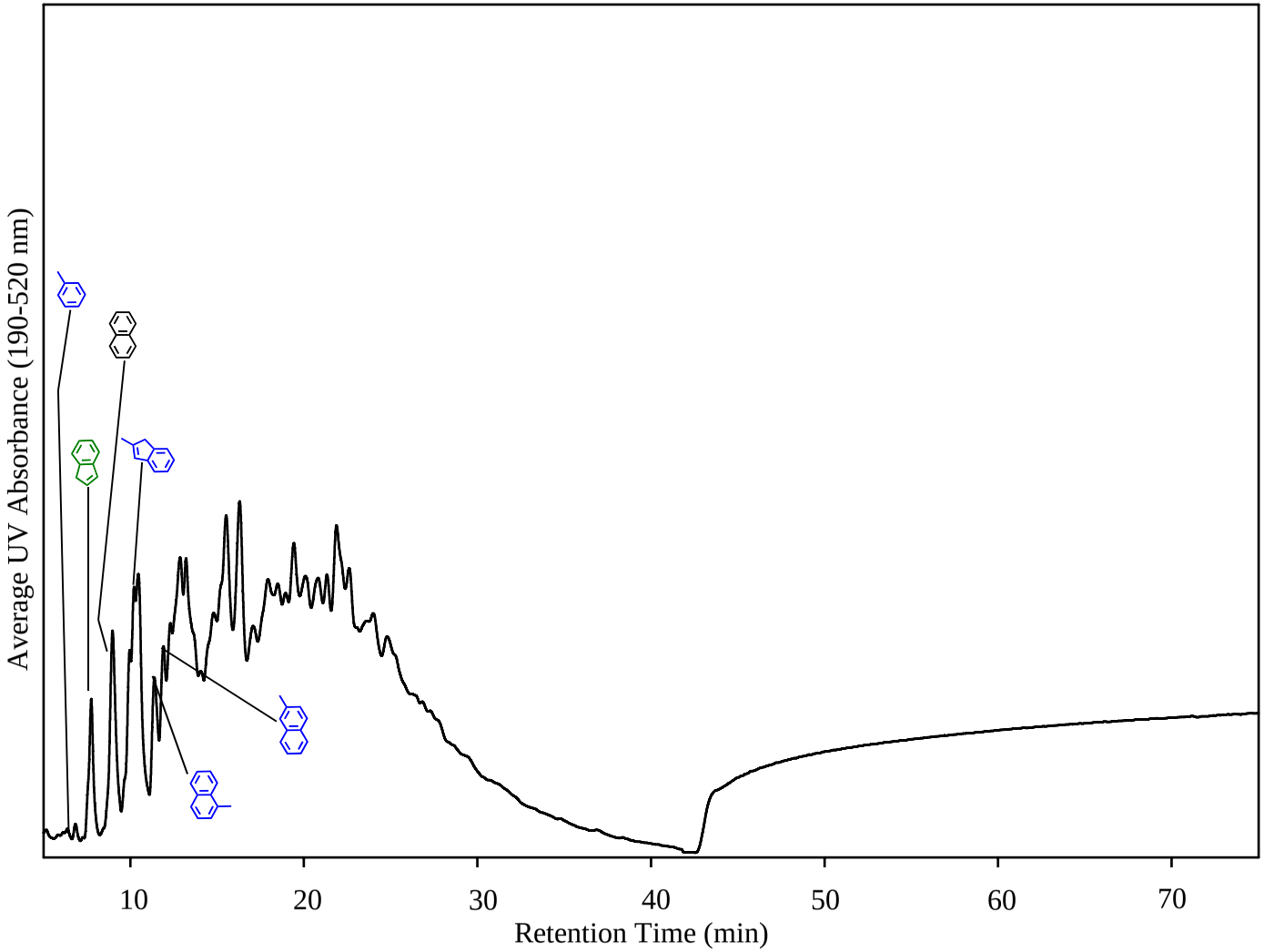


Figure 5.50. HPLC/UV Chromatogram of the Methylcyclohexane Supercritical Pyrolysis Products at 570 °C, 40 atm, and 140 sec.

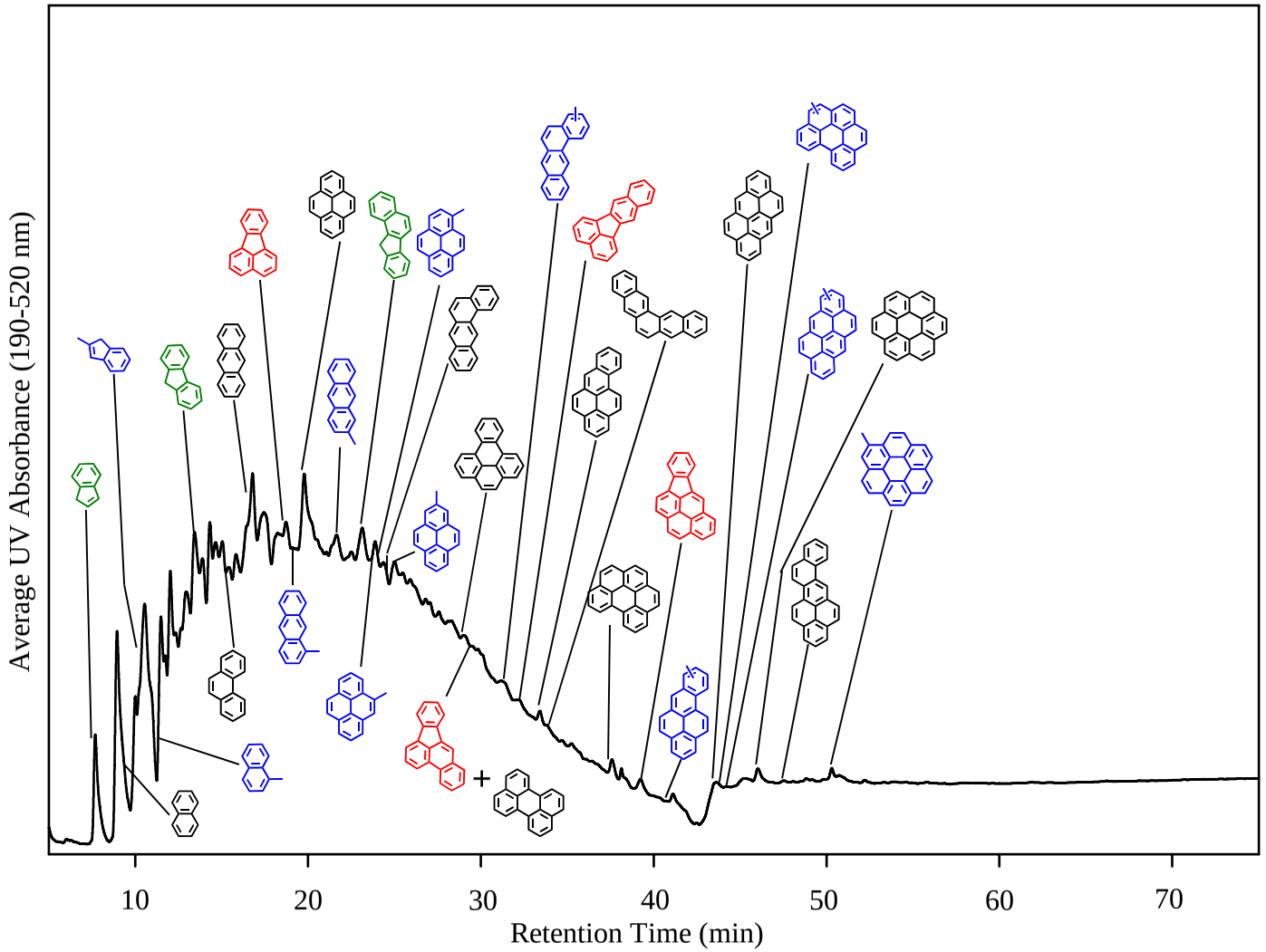


Figure 5.51. HPLC/UV Chromatogram of the Methylcyclohexane Supercritical Pyrolysis Products at 570 °C, 60 atm, and 140 sec.

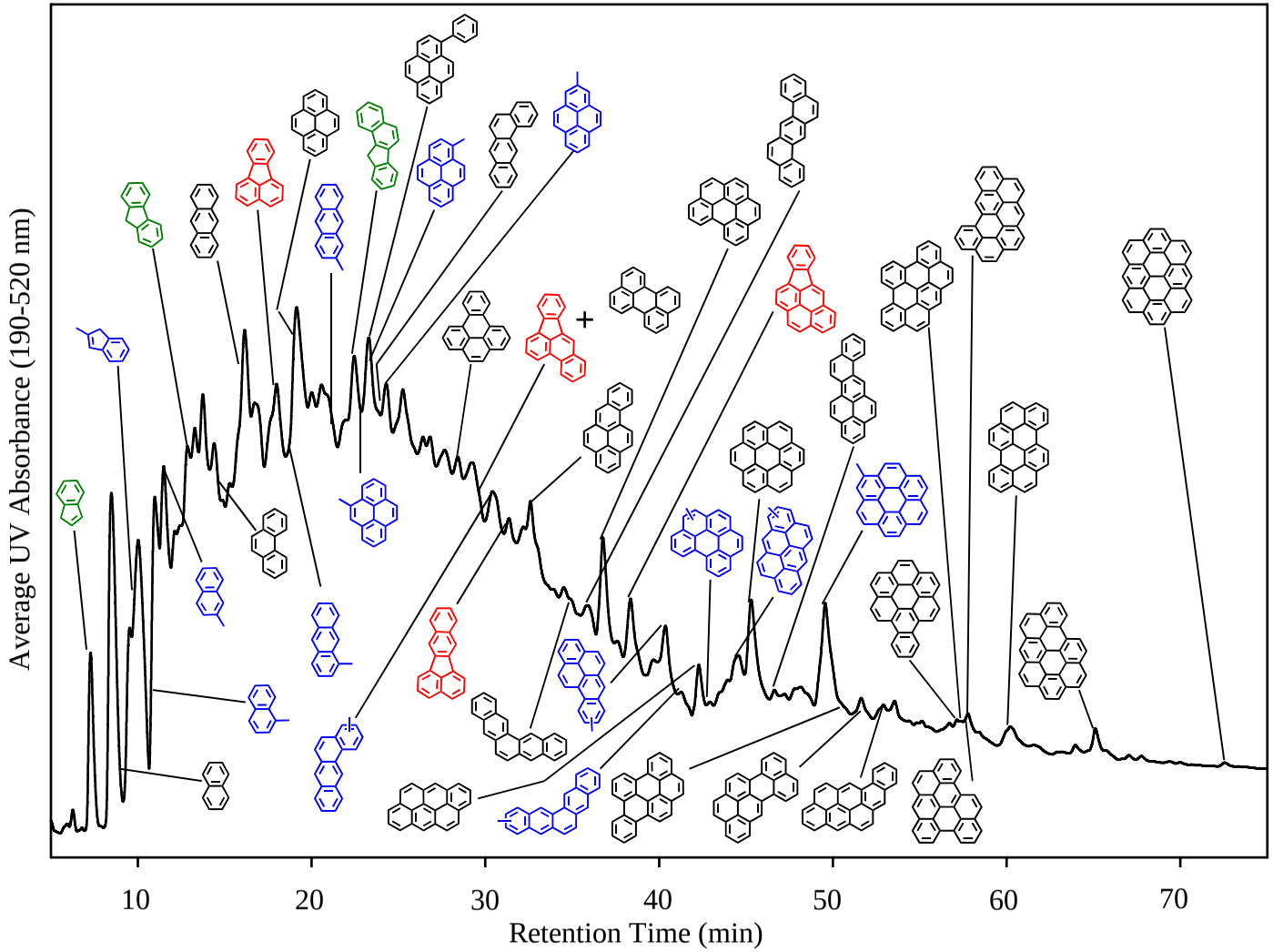


Figure 5.52. HPLC/UV Chromatogram of the Methylcyclohexane Supercritical Pyrolysis Products at 570 °C, 80 atm, and 140 sec.

In contrast with the result at 570 $^{o}$C, where the PAH products identified reach a number of fifty-five, at 560 $^{o}$C the number of PAH identified reaches only a number of sixteen. This extreme sensitivity to temperature is corroborated by the fact that the experiment at 580 $^{o}$C (just 10 $^{o}$C above the condition at 570 $^{o}$C) resulted in plugging of the reactor, due to solid deposit formation.

**5.2.7. Influence of the Residence Time**

To examine the influence of the residence time in the formation of PAH products from the supercritical pyrolysis of methylcyclohexane, studies have been performed at constant pressure (100 atm), constant temperature (570 $^{o}$C), and for two residence times (70 and 140 sec). The products obtained have been analyzed using HPLC/UV with the solvent program 4.2.-A.

The HPLC/UV chromatogram of Figure 5.54. shows the PAH products identified from the supercritical pyrolysis of methylcyclohexane at 570 $^{o}$C, 100 atm, and 70 sec. The HPLC/UV chromatogram of the supercritical pyrolysis products of methylcyclohexane at 570 $^{o}$C, 100 atm, and 140 sec has already been presented in Figure 5.43.

Figure 5.54. demonstrates that a fifty percent decrease of the residence time, i.e., from 140 sec to 70 sec, causes the disappearance of a significant number of PAH. Therefore, the effect in the formation of PAH from the supercritical pyrolysis of methylcyclohexane due to the decrease of the residence time has comparable consequences as the consequences already analyzed for the pressure and for the temperature. On one hand, thirty-one PAH have been detected at 570 $^{o}$C, 100 atm, and 70 sec; on the other, fifty-five PAH have been detected at 570 $^{o}$C, 100 atm, and 140 sec.

Also, after a comparison between the results presented in Figures 5.43. and 5.54., it can be established that the reactions leading to the formation of large PAH need longer residence

times to take place. Thus, there is a reason to observe the residence time effect as one of the factors that control the formation of solids in this supercritical environment.

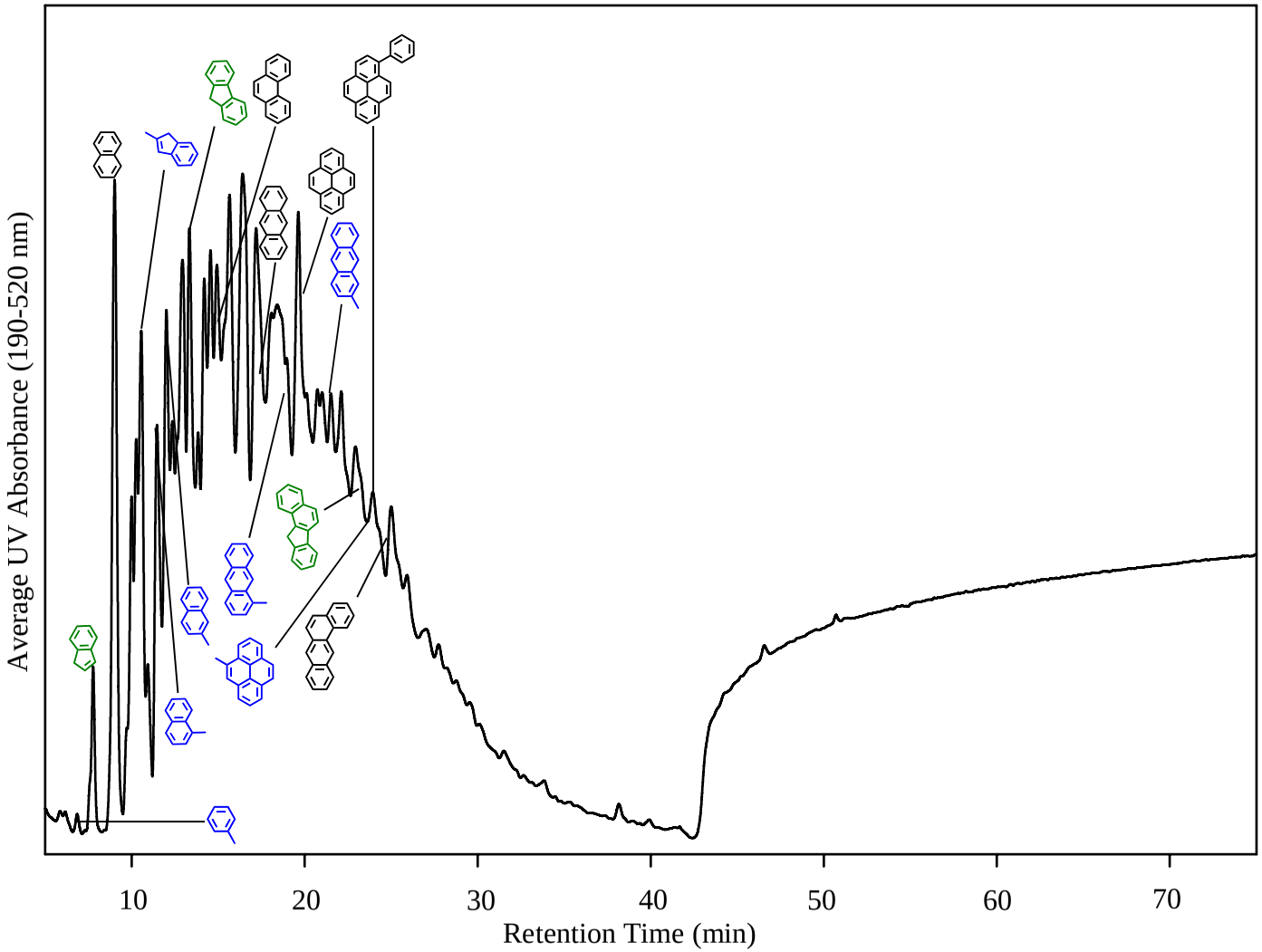


Figure 5.53. HPLC/UV Chromatogram of the Methylcyclohexane Supercritical Pyrolysis Products at 560 °C, 100 atm, and 140 sec.

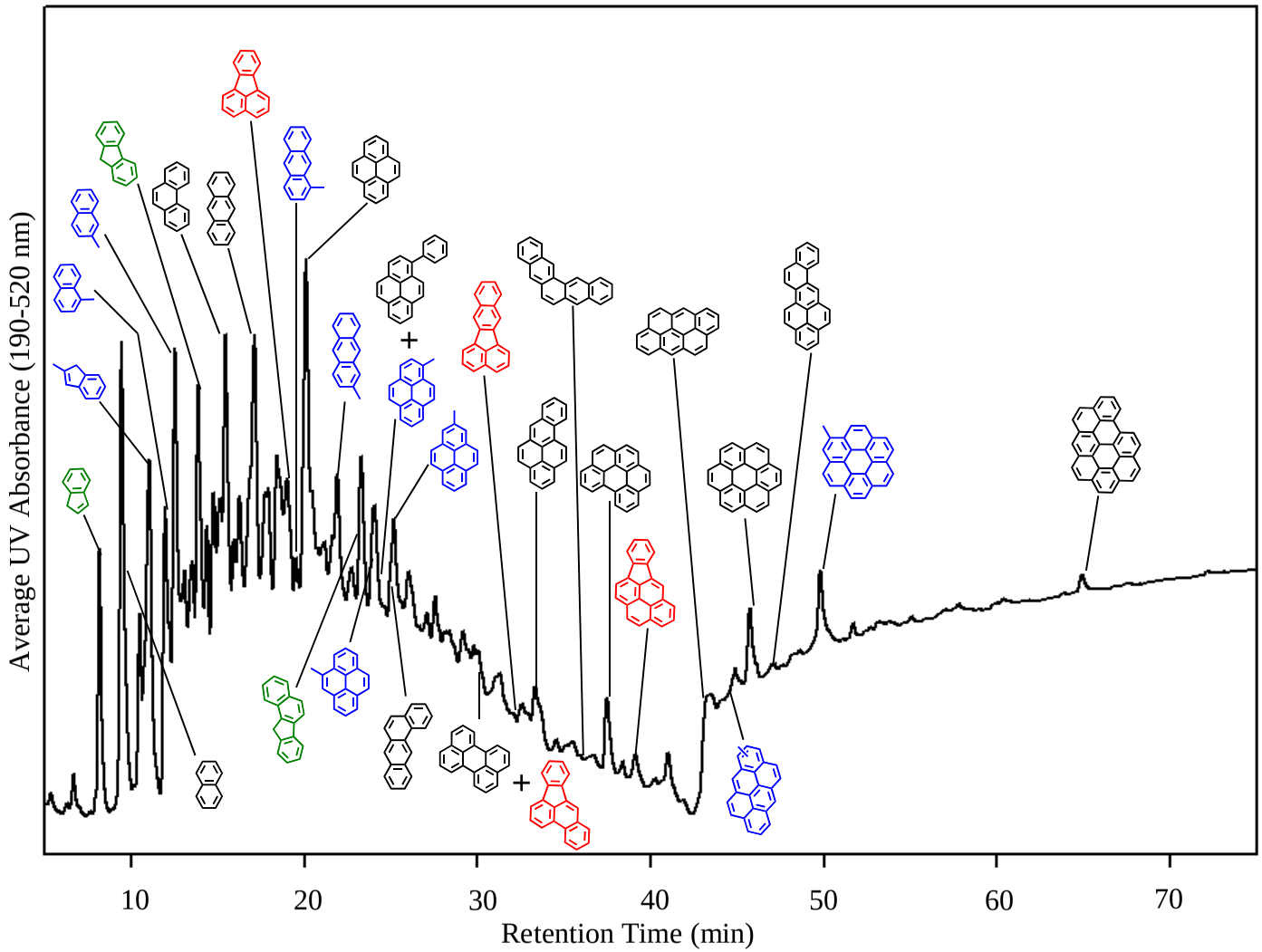


Figure 5.54. HPLC/UV Chromatogram of the Methylcyclohexane Supercritical Pyrolysis Products at 570 °C, 100 atm, and 70 sec.

# CHAPTER 6. SUMMARY AND CONCLUSIONS

Inside the pre-combustor fuel lines of high-speed aircraft, at supercritical conditions, hydrocarbon fuels react to form PAH and eventually solid deposits. These depositis can block fuel lines, foul fuel nozzles, and lead to undesirable effects for the aircraft operation. In order to achieve a clear elucidation of the pathways that lead to the formation of PAH (and ultimately, solids formation), the identification of the PAH products generated by the reactions is critical. In this context, two fuels have been analyzed: synthetic jet fuel S-8 and methylcyclohexane. Synthetic jet fuel S-8 is important due to its non-petroleum origin (uncommon for the majority of hydrocarbon fuels). Methylcyclohexane is important due to its endothermic behavior. Therefore, the goal of this study is the identification of the PAH products from the supercritical pyrolysis of synthetic jet fuel S-8 and from the supercritical pyrolysis of methylcyclohexane.

The products of the synthetic jet fuel S-8 supercritical pyrolysis analyzed here have been obtained at two conditions: First, 710 $^{o}$C and 42 atm; and second, 666 $^{o}$C and 42 atm. The products of the supercritical pyrolysis of methylcyclohexane, in contrast, come from experiments that have been carried out at three different set of conditions: First, constant temperature (570 $^{o}$C), variable pressure (20 atm, 40 atm, 60 atm, 80 atm, and 100 atm), and constant residence time (140 sec); second, constant pressure (100 atm), variable temperature (560 $^{o}$C, 570 $^{o}$C, and 580 $^{o}$C), and constant residence time (140 sec); and third, constant temperature (570 $^{o}$C), constant pressure (100 atm), and variable residence time (70 sec and 140 sec).

GC/MS, HPLC/UV, and HPLC/UV/MS have been used to analyze the supercritical pyrolysis products of synthetic jet fuel S-8 and the pyrolysis products of methylcyclohexane. The synthetic jet fuel S-8 and methylcyclohexane product mixtures have each been subjected to a time sequence of solvents for HPLC/UV analysis. Additionally, the synthetic jet fuel S-8

product mixtures have been subjected to four separate analyses (two HPLC/UV and two HPLC/UV/MS), each using a different time sequence and series of solvents.

Table 6.1. shows the number of PAH products detected from the supercritical pyrolysis of synthetic jet fuel S-8 and from the supercritical pyrolysis of methylcyclohexane by application of the techniques: UV spectral comparison with standards, analysis of the effect of an alkyl substituent on the UV spectra, application of the UV solvent-based adjustment, and analysis of the UV spectra combined with the application of Annellation Theory.

Table 6.1. Number of PAH Products identified from the Supercritical Pyrolysis of Methylcyclohexane (MCH) and from the Supercritical Pyrolysis of Synthetic Jet Fuel S-8 (SJF S-8)

| | Methylcyclohexane | | | | | | | SJF S-8 | |
|---|---|---|---|---|---|---|---|---|---|
| | 570 °C 140 sec 20 atm | 570 °C 140 sec 40 atm | 570 °C 140 sec 60 atm | 570 °C 140 sec 80 atm | 570 °C 140 sec 100 atm | 560 °C 140 sec 100 atm | 570 °C 70 sec 100 atm | 666 °C 42 atm | 710 °C 42 atm |
| UV spectral comparison | 5 | 6 | 27 | 36 | 39 | 16 | 29 | 10 | 61 |
| Alkyl substitution effect | 0 | 0 | 5 | 6 | 11 | 0 | 2 | 0 | 12 |
| UV solvent-based adjustment | 0 | 0 | 0 | 2 | 3 | 0 | 0 | 0 | 7 |
| Annellation Theory | 0 | 0 | 0 | 2 | 2 | 0 | 0 | 0 | 5 |
| Total | 5 | 6 | 32 | 46 | 55 | 16 | 31 | 10 | 85 |

Based on the findings presented in Chapter 5 about the influence of the temperature, of the pressure, and of the residence time in the formation of PAH, three important observations can be established. First, the isobaric increase of the temperature in the synthetic jet fuel S-8 supercritical pyrolysis and in the methylcyclohexane supercritical pyrolysis has the same effect. This effect consists in the increase of the number of products and the appearance of heavier PAH

structures. Second, the isothermal increase of the pressure in the methylcyclohexane supercritical pyrolysis has a similar effect as the previous one reported for the temperature. The increase of the pressure favors the formation of heavier PAH with higher stabilities. This trend is more pronounced above the critical point of methylcyclohexane. Third, the isothermal and isobaric increase of the residence time in the methylcyclohexane supercritical pyrolysis has a similar behavior as the ones analyzed for the increase of the temperature and for the increase of the pressure, i.e., an increase in the formation of complex, heavier, and stable PAH structures.

Twenty-nine unsubstituted PAH with six or more rings have never before been identified as products from the pyrolysis of a long-chain alkane fuel, e.g. synthetic jet fuel S-8. These compounds are: naphtho[2,3-*e*]pyrene, naphtho[1,2-*a*]pyrene, naphtho[1,2-*k*]fluoranthene, benzo[*b*]perylene, benz[*e*]anthanthrene, dibenzo[*b,k*]fluoranthene, naphtho[2,3-*b*]fluoranthene, 8H-dibenzo[*a,jk*]pyrene, naphtho[2,1-*a*]pyrene, dibenzo[*b,ghi*]perylene, phenanthro[2,3-*a*]-pyrene, naphtho[2,3-*a*]pyrene, dibenzo[*e,ghi*]perylene, naphtho[8,1,2-*bcd*]perylene, 2,2'-bianthryl, benz[*a*]anthanthrene, benzo[*a*]coronene, dibenzo[*cd,lm*]perylene, phenanthro[5,4,3,2-*efghi*]perylene, benzo[*cd*]naphtho[3,2,1,8-*pqra*]perylene, benzo[*ghi*]naphtho[8,1,2-*bcd*]perylene, benzo[*pqr*]naphtho[8,1,2-*bcd*]perylene, benzo[*b*]picene, tribenzo[*cd,ghi,lm*]perylene, naphtho-[8,1,2-*abc*]coronene, ovalene, benzo[*ghi*]phenanthro[9,10,1-*cde*]perylene, benzo[*cd*]naptho-[1,2,3-*lmn*]perylene, and benzo[*pqr*]dinaphtho[8,1,2-*bcd*:2',1',8'-*lmn*]perylene.

Fifteen unsubstituted compounds with six or more rings have never before been detected as products from the pyrolysis or combustion of methylcyclohexane in any context. These compounds are: anthanthrene, coronene, naphtho[2,1-*a*]pyrene, dibenzo[*b,ghi*]perylene, benzo[*b*]perylene, dibenzo[*e,ghi*]perylene, naphtho[8,1,2-*bcd*]perylene, benz[*a*]anthanthrene, benzo[*a*]coronene, phenanthro[5,4,3,2-*efghi*]perylene, benzo[*cd*]naphtho[3,2,1,8-*pqra*]perylene,

benzo[*ghi*]naphtho-[8,1,2-*bcd*]perylene, benzo[*pqr*]naphtho[8,1,2-*bcd*]perylene, naphtho[8,1,2-*abc*]coronene, and ovalene.

These results confirm the applicability of model fuel studies to the understanding of actual jet fuels and emphasize the importance of laboratory-scale experiments in elucidating the pyrolysis behavior of fuels under near-critical or supercritical conditions.

The two analysis presented here: One about the identifications of PAH products from the supercritical pyrolysis of synthetic jet fuel S-8 and from the pyrolysis of methylcyclohexane, and the other about the behavior of synthetic jet fuel S-8 and methylcyclohexane at several conditions of temperature, pressure, and residence time, will be helpful so as to achieve the main goal of this research, i.e., the development of reliable fuel systems that will not be subject to carbonaceous solids formation.

# CHAPTER 7. RECOMMENDATIONS

The results reported here about the identifications of the PAH products from the supercritical pyrolysis of synthetic jet fuel S-8 and methylcyclohexane represent two of the largest comprehensive compilations of PAH with six or more rings detected in the pyrolysis or combustion of any fuel in any context. In spite of this major accomplishment, some structures still remain unknown even when their elution time, UV spectra, and MS spectra have been experimentally observed. The reasons of this product indistinctness are: the lack of aunthentic standards for UV spectral comparison, the extreme complexity of the UV absorption spectra (especially for non-benzenoid compounds), the HPLC co-elution of several species, and/or the reduced resolution of the UV absorption spectrum that frequently produces very low intensity spectral bands. Therefore, extra analytical and/or theoretical work is needed so as to discern the identity of the unknown structures present in these samples.

Additionally, a clearer understanding of the pyrolytic behavior of the synthetic jet fuel S-8 in the supercritical state will be obtained with new experiments at different conditions of pressure, temperature, and residence time. Present and future work with model fuels, e.g., n-decane, n-undecane, and others, will give a more comprehensive scenario of the pyrolysis conduct of this synthetic mixture and will alow a more detailed mechanistic understanding of PAH formation.

Besides that, it has been demonstrated the importance of non-traditional analytical techniques, e.g., the influence of the alkyl substituents on the UV spectra, the UV spectral solvent-based adjustment, and the Annellation Theory, to identify PAH never before seen in the pyrolysis or combustion of fuels. The identification of a greater number of compounds provides

better mechanistic clues about the kinetic pathways that the reactants follow during their transformation to products.

In spite of the conclusive proofs presented in this and other studies to demonstrate the usefulness of the Annellation Theory as an analytical resource for the identification of PAH, its application should be cautious and judicious. The enormous number of PAH structures in some isomer families could lead to the misidentification of a compound due to the incorrect application of the Annellation Theory rules. Excellent results have been obtained when the Annellation Theory has been used, in combination with other analytical techniques, to elucidate the identity of a particular PAH in an isomer family composed of fifty or less isomers.

## REFERENCES


Air Force Research Laboratory. 2006. Fischer-Tropsch (F-T) Blend Fuel Flight Demonstration. Wright Patterson AFB, Ohio.

Aitken I.M. and Reid D.H. 1960. Conjugated Cyclic Hydrocarbons and their Heterocyclic Analogues. Part III. The Addition of Benzyne and 1-Bromoacenaphthylene to Indeno[2,1-*a*]perinaphthene. Journal of the Chemical Society, 663-665.

Bagley S. and Wornat M.J. 2008. to be submitted for publication.

Bahl A., Grahn W., Stadler S., Feiner F., Bourhill G., Braüchle C., Reisner A., and Jones P.G. 1995. Angewandte Chemie. International edition in English 34(13/14):1485-1488.

Bayliss N.S. and McCrae E.G. 1954. Solvent Effects in Organic Spectra: Dipole Forces and the Franck-Condon Principle. Journal of Physical Chemistry. 58(11), 1002-1006.

Burland D.M., Miller R.D., and Walsh C.A. 1994. Second-order nonlinearity in poled-polymer systems. Chemical Reviews 94(1), 31-75.

Cho B.P. and Harvey R.H. 1987. Polycyclic Fluoranthene Hydrocarbons. 2. A New General Synthesis. Journal of Organic Chemistry 52(26), 5668-5678.

Clar E. 1948. Höhere Benzologe des Benzanthrens und das 1.12,2.3-Dibenz-perylen (Aromatische Kohlenwasserstoffe, XLVII. Mitteil.). Chemische Berichte 81(6), 520-527.

Clar E. 1952. Aromatische Kohlenwasserstoffe: Polycyclische Systeme. Springer-Verlag, Berlin.

Clar E. and Kühn O. 1956. Aromatische Kohlenwasserstoffe LXXVIII. Höher Kondensierte Pyrene. Justus Liebigs Annalen der Chemie 601(1), 181-192.

Clar E. and Willicks W. 1958. 2:3-Benzorubicene, Rubicene, and their derivatives. Journal of the Chemical Society, 942-946.

Clar E., Ironside C.T., and Zander M. 1959. Asymmetric and Symmetric Annellation Effects—III: Benzocoronenes. Tetrahedron 6, 358-363.

Clar E., Fell G.S., Ironside C.T., and Balsillie A. 1960. Benzologues and other derivatives of Peropyrene. Tetrahedron 10, 26-36.

Clar E. 1964. Polycyclic Hydrocarbons. Academic Press, London.

Clar E. 1972. The Aromatic Sextet. John Wiley & Sons, London.

Cutler A.H., Antal M.J., and Jones M. 1988. A Critical Evaluation of the Plug-Flow Idealization of Tubular-Flow Reactor Data. Industrial and Engineering Chemistry Research 27(4), 691-697.

Dagget D., Hadaller O., Hendricks R., and Walther R. 2006. Alternative Fuels and their Potential Impact on Aviation. ICAS 2006-5.8.2, 25th ICAS Congress.

Dagget D.L., Hendricks R.C., Walther R., and Corporan E. 2007. Alternate Fuels for Use in Commercial Aircraft. The Boeing Company, Seattle.
Davis G. 1994. An Experimental Study of Supercritical Methylcyclohexane Pyrolysis. M.S.E. Thesis, Department of Mechanical and Aerospace Engineering, Princeton University, Princeton.

Debad J.D., Morris J.C., Magnus P., and Bard A.J. Anodic Coupling of Diphenylbenzo[*k*]fluoranthene: Mechanistic and Kinetic Studies Utilizing Cyclic Voltammetry and Electrogenerated Chemiluminescence. Journal of Organic Chemistry 62(3), 530-537.

Dias J.R. 1987. Handbook of Polycyclic Hydrocarbons. In: Physical Sciences Data 30. Elsevier, Amsterdam.

Dinjus E., Fornika R., and Scholz M. 1997. Organic Chemistry in Supercritical Fluids. In: Chemistry Under Extreme or Non-Classical Conditions, Van Eldik R. and Hubbard C.D. (Eds.). John Wiley & Sons, New York, pp. 219-271.

Edelman R.B., Farmer R.C., and Wang T.-S. 1987. Combustion and Emission of Synthetic Fuel Components: Analysis and Modeling. In: Combustion of Synthetic Fuels, Vol 217, Bartok W. (Ed.). American Chemical Society, Division of Petroleum Chemistry, ACS Symposium Series, pp. 29-48.

Edwards T. 2006. Cracking and Deposition Behavior of Supercritical Hydrocarbon Fuels. Combustion Science and Technology 178, 307-334.

Fetzer J.C. 2000. Large (C > = 24) Polycyclic Aromatic Hydrocarbons: Chemistry and Analysis. In: A Series of Monographs on Analytical Chemistry and its Applications, Vol 158, Winefordner J. (Ed.). John Wiley & Sons, New York.

Fetzer J.C. and Biggs W.R. 1984. The High-Performance Liquid Chromatography of Peropyrene-type Polycyclic Aromatic Hydrocarbons. Journal of Chromatography 295, 161-169.

Fetzer J.C. and Biggs W.R. 1985. Solvated Structure-Retention Relationships of Peropyrene type Polycyclic Aromatic Hydrocarbons. Journal of Chromatography 322, 275-286.

Fetzer J.C. and Biggs W.R. 1994. Identification of a New Eight-Ring Condensed Polycyclic Aromatic Hydrocarbon. Polycyclic Aromatic Compounds 5, 193-199.

Fiesel R., Huber J., and Scherf U. 1996. Synthesis of an Optically Active Poly(para-phenylene) Ladder Polymer. Angewandte Chemie. International edition in English 35(18):2111-2113.

Freerks R.L. and Muzell, P.A. 2004. Production and Characterization of Synthetic Jet Fuel Produced from Fischer-Tropsch Hydrocarbons. Preprints of Papers, American Chemical Society, Division of Fuel Chemistry 49, 407-410.

Freudenthal R.I. and Jones P. 1976. Carcinogenesis: A Comprehensive Survey. Volume 1. Polycyclic Aromatic Hydrocarbons: Chemistry, Metabolism, and Carcinogenesis. Raven Press, New York.

Friedel R.A. and Orchin M. 1951. Ultraviolet Spectra of Aromatic Compounds. John Wiley & Sons, New York.

Gallagher R.T., Balogh M.P., Davey P., Jackson M.R., Sinclair I., and Southern L.J. 2003. Combined Electrospray Ionization-Atmospheric Pressure Chemical Ionization Source for use in High- Throughput LC-MS Applications, Analytical Chemsitry 75(4), 973-977.

Gamma V. Henriques R.T., Bonfait G., Almeida M., Meetsma A., Smaalen S. van, and Boer J.L. de. 1992. (Perylene)Co(mnt)$_2$($CH_2Cl_2$)$_{0.5}$: a mixed perylenecobalt complex as molecular and polymeric conductor. Journal of the American Chemical Society 114 (6), 1986-1989.

Glassman I. 1988. Soot Formation in Combustion Processes. Proceedings of the Combustion Institute 22, 295-311.

Graselli J.G. and Ritchey W. 1975. Atlas of Spectral Data and Physical Constants for Organic Compounds. CRC Press, Cleveland.

Gül Ö., Rudnick L.R., and Schobert, H.H. 2006. The Effect of Chemical Composition of Coal-Based Jet Fuels on the Deposit Tendency and Morphology. Energy and Fuels 20(6), 2478-2485.

Gutman I. and Ruiz-Morales Y. 2007. Note on the Y-Rule in Clar Theory. Polycyclic Aromatic Compounds. 27, 41-49.

Heneghan S.P., Zabarnick S., and Harrison W.E. 1996. JP-8+100: The Development of High-Thermal Stability Jet Fuel. Journal of Energy Resources Technology 118, 170-179.

Hiramoto M., Kishigami Y., and Yokoyama M. 1990. Doping Effect on the Two-layer Organic Solar Cell. Chemical Letters 119-122.

Hites R.A. 1997. Gas Chromatography Mass Spectrometry. In: Handbook of Instrumental Techniques for Analytical Chemistry, Settle F.A. (Ed.). Prentice Hall PTR, Upper Saddle River, NJ

Holtrup F.O., Müller G.R.J., Quante H., Feyter S. de, Schryver F.C. de, and Müllen K. 1997. Terrylenimides: New NIR Fluorescent Dyes. Chemistry and European Journal 3, 219-225.

Huang H. Spadaccini L.J., and Sobel D.R. 2002. Fuel-Cooled Thermal Management for Advanced Aero Engines. Paper No. GT-2002-30070, Proceedings of the ASME Turbo Expo, Amsterdam.

Huang H., Spadaccini L.J., and Sobel D.R. 2004. Fuel-Cooled Thermal Management for Advanced Aero Engines. Journal of Engineering for Gas Turbines and Power, 284-293.

Hudgins D.M. and Sandford S.A. 1998. Infrared Spectroscopy of Matrix Isolated Polycyclic Aromatic Hydrocarbons. 3. Fluoranthene and the Benzofluoranthenes. Journal of Physical Chemistry A 102 (2), 353-360.

Jaffé H.H. and Orchin M. 1962. Theory and Applications of Ultraviolet Spectroscopy. John Wiley & Sons, New York.

Jessup P.J. and Reiss J.A. 1976. Cyclophanes. V. Biphenylnaphthalenophanes and the Synthesis of Hexa[7]circulene. Australian Journal of Chemistry 29, 173-178.

Jinno K.T. 1996. Polycyclic Aromatic Hydrocarbons Data Base in Alphabetical Order. Available from http://chrom.tutms.tut.ac.jp/JINNO/DATABASE/00alphabet.html#HEAD.

Jones R.N. 1945. Some Factors Influencing the Ultraviolet Absorption Spectra of Polynuclear Aromatic Compounds. I. A General Survey. Journal of the American Chemical Society 67(12), 2127-2150.

Katrizky A.R., Fara D.C., Yang H., Tamm K., Tamm T., and Karelson M. 2004. Quantitative Measures of Solvent Polarity. Chemical Reviews 104(1), 175-198.

Klempier N. and Binder H. 1983. Determination of Polycyclic Aromatic Hydrocarbons in Soot by Mass Spectrometry with Direct Sample Insertion. Analytical Chemistry 55(13), 2104-2106.

Kundt A. 1878. Über den Einfluss von Lösungsmitteln auf die Absorptionsspektren Gelöster Absorbierender Medien (On the Influence of Solvents on the Absorption Spectra of Dissolved Absorbing Media). Poggendorfs Annalen der Physik und Chemie 4, 34–54.

Lai W.-C. and Song C. 1996. Pyrolysis of Alkylcyclohexanes in or near the supercritical phase. Product Distribution and Reaction Pathways. Fuel Processing Technology 48, 1-27.

Laidler K.J. 1987. Chemical Kinetics, 3rd Ed., Harper Collins, New York.

Lander H.R. and Nixon A.C. 1987. Endothermic Fuels for High Mach Vehicles. Symposium on Structure of Future Jet Fuels, American Chemical Society, Denver.

Lang K.F. and Buffleb H. 1957. Die Pyrolyse Eines Gemisches von Benzol und Pyren. Chemische Berichte 90(12), 2894-2898.

Lang K.F., Buffleb H., and Zander M. 1960. Die Pyrolyse des Fluorens. Chemische Berichte 94(2), 523-526.

Ledesma E.B., Wornat M.J., Felton P.G., and Sivo J.A. 2005. The Effects of Pressure on the Yields of Polycyclic Aromatic Hydrocarbons Produced During the Supercritical Pyrolysis of Toluene. Proceedings of the Combustion Institute 30, 1371-1379.

Lee J.C.Y. 1996. Simulations of Two-Dimensional Chemically Reactive Flows. Ph.D. Dissertation, Department of Mechanical and Aerospace Engineering, Princeton University, Princeton.

Lee M.L. and Hites R.A. 1976. Characterization of Sulfur-Containing Polycyclic Aromatic Compounds in Carbon Blacks. Analytical Chemistry 48(13), 1890-1893.

LeRosen A.L. and Reid C.E. 1952. An Investigation of Certain Solvent Effect in Absorption Spectra. The Journal of Chemical Physics 20(2), 233-236.

Marks T.J. and Ratner M.A. 1995. Design, Synthesis, and Properties of Molecule-Based Assemblies with Large Second-Order Optical Nonlinearities. Angewandte Chemie. International edition in English 34(2):155-173.

McClaine J.W., Zhang X., Wornat M.J. 2006. First Identification of Benzo[*ghi*]naphtho[8,1,2-*bcd*]perylene as a Product of Fuel Pyrolysis, Using High-Performance Liquid Chromatography with Diode-Array Ultraviolet-Visible Absorbance Detection and Mass Spectrometry. Journal of Chromatography A 1127, 137-146.

McClaine J.W. and Wornat M.J. 2007a. Reaction Mechanisms Governing the Formation of Polycyclic Aromatic Hydrocarbons in the Supercritical Pyrolysis of Toluene: $C_{28}H_{14}$ Isomers. Journal of Physical Chemistry C 111, 86-95.

McClaine J.W., Oña J.O., and Wornat M.J. 2007b. Identification of a New $C_{28}H_{14}$ Polycyclic Aromatic Hydrocarbon as a Product of Supercritical Fuel Pyrolysis: Tribenzo[*cd,ghi,lm*]-perylene. Journal of Chromatography A 1138, 175–183.

McKay J.F. and Latham D.R. 1973. Polyaromatic Hydrocarbons in High-Boiling Petroleum Distillates: Isolation by Gel Permeation Chromatography and Identification by Fluorescence Spectrometry. Analytical Chemistry 45(7), 1050-1055.

Metzger J.O., Hartmanns J., Malwitz D., Koll P. 1983. Thermal Organic Reactions in Supercritical Fluids. In: Chemical Engineering at Supercritical Fluid Conditions, Paulatis M.E., Penninger J.M.L., Gray R.D.Jr., Davidson P. (Eds.). Ann Arbor Science, pp. 515-533.

Moriwaki H., Ishitake M., Yoshikawa S., Miyakoda H., and Alary J.F. 2004. Determination of Polycyclic Aromatic Hydrocarbons in Sediment by Liquid Chromatography Atmospheric Pressure Photoionization-Mass Spectrometry, Analytical Sciences 20, 375–377.

Neue U.D. 1997. HPLC Columns: Theory, Technology, and Practice. Wiley VCH, New York.

Oh C.H., Park I.D., Ryu J.H., Cho J.H., and Han J.S. 2007. Syntheses and Characterization of Cyclopropane-fused Hydrocarbons as New High Energetic Materials. Bulletin Korean Chemical Society 28(2), 322-324.

Ojakaar L. 1964. The Synthesis of Some New Aromatic Polycyclic Hydrocarbons. Ph.D. Thesis, Department of Chemistry, Virginia Polythecnic Institute, Blacksburg.

Oña J.O. and Wornat M.J. 2007. Identification of the $C_{30}H_{16}$ Polycyclic Aromatic Hydrocarbon Benzo[*cd*]naphtho[1,2,3-*lm*]perylene as a product of the supercritical pyrolysis of a synthetic jet fuel. Polycyclic Aromatic Compounds 27, 165-183.

Oña J.O. and Wornat M.J. 2008a. To be submitted to Polycyclic Aromatic Compounds.

Oña J.O. and Wornat M.J. 2008b. To be submitted to Analytical and Bioanalytical Chemistry.

Oña J.O. and Wornat M.J. 2008c. The Influence of Solvents on the Ultraviolet-Visible Absorption Spectra of Polycyclic Hydrocarbons: Applications in the Identification of Fuel Products by HPLC/UV/MS. Polycyclic Aromatic Compounds 28, 15-38.

Oña J.O. and Wornat M.J. 2008d. To be submitted to Environmental, Science, and Technology.

Orme J.P., Curran H.J., and Simmie J.M. 2006. Experimental and Modeling Study of Methyl Cyclohexane Pyrolysis and Oxidation. Journal of Physical Chemistry A 110(1), 114-131.

Pant, K.K. and Kunzru D. 1997. Pyrolysis of methylcyclohexane: Kinetics and modeling. Chemical Engineering Journal 67, 123-129.

Peaden P.A., Lee M.L., Hirata Y., and Novotny M. 1980. High-Performance Liquid Chromatographic Separation of High-Molecular-Weight Polycyclic Aromatic Compounds in Carbon Black. Analytical Chemistry 52(14), 2268-2271.

Raffaelli A. and Saba A. 2003. Atmospheric Pressure Photoionization Mass Spectrometry. Mass Spectrometry Reviews 22(5), 318–331.

Sander L.C. and Wise S. 1997. NIST Special Publication 922: Polycyclic Aromatic Hydrocarbons Structure Index. Chemical Science and Technology Laboratory, National Institute of Standards and Technology, Gaithersburg.

Savage P.E., Gopalan S., Mizan T.I., Martino C., and Brock E.E. 1995. Reactions at Supercritical Conditions: Applications and Fundamentals. AICHE Journal 41(7), 1723-1778

Schlichting P., Rohr U., Müllen k. 1997. New Synthetic Routes to Alkyl-Substituted and Functionalized Perylenes. Liebigs Annalen/Recueil, 395-407.

Sobel D.R. and Spadaccini L.J. 1997. Hydrocarbon Fuel Cooling Technologies for Advanced Propulsion. ASME Journal of Engineering for Gas Turbines and Power 119, 344-351.

Somers M.L. and Wornat M.J. 2007. To be submitted to Journal of Chromatography A.

Stewart J.F. 1999. Supercritical Pyrolysis of Endothermic Fuels. Ph.D. Thesis, Department of Mechanical and Aerospace Engineering, Princeton University, Princeton.

Syage J.A. 2004. Mechanism of $[M+H]^+$ Formation in Photoionization Mass Spectrometry, Journal of the American Society of Mass Spectrometry 15, 1521-1533.

Syntroleum Inc. 2004. Syntroleum: Material Safety Data Sheet, Product Name: S-8 Synthetic Jet Fuel. Revision Date: November 2004.

Tiltscher H. and Hofmann H. 1987. Trends in High Pressure Chemical Reaction Engineering. Chemical Engineering Science 42(5), 959-977.

Timmermans J. 1950. Physico-Chemical Constants of Pure Organic Compounds. Elsevier Publishing Company Inc., New York.

Umemoto T., Kawashima T., Sakata Y., and Misumi S. 1975. Layered Compounds. XXV. Peropyrene and Teropyrene–A New Synthetic Route of Pyrene-like Polynuclear Aromatic Hydrocarbons–. Tetrahedron letters 12, 1005-1006.

Venables D. S. and Schmuttenmaer C.A. 1998. Far-Infrared Spectra and associated Dynamics in Acetonitrile–Water Mixtures measured with Femtosecond THz Pulse Spectroscopy. Journal of Chemical Physics 108, 4935-4943.

Vingiello F.A. and Ojakaar L. 1966. New Polycyclic Aromatic Hydrocarbons with Seven Fused Rings. Tetrahedron 22, 847-860.

Washburn E.W., West C.J., and Dorsey N.E. 2003. International Critical Tables of Numerical Data, Physics, Chemistry and Technology. Knovel, New York.

Wilcox C.F. and Farley E.N. 1985. Cyclooctannelated Biphenylenes. Diagnosis of an Anomalous Bond Length by Analysis of Ring Current Geometric Factors. Journal of Organic Chemistry 50(3), 351-356.

Wise S.A., Bonnett W.J., Guenther F.R., and May W.E. 1981. A Relationship Between Reversed-Phase $C_{18}$ Liquid Chromatographic Retention and the Shape of Polycyclic Aromatic Hydrocarbons. Journal of Chromatographic Science 19, 457-465.

Wornat M.J., Ledesma E.B., Sandrowitz A.K., Roth M.J., and Dawsey S.M. 2001. Polycyclic Aromatic Hydrocarbons identified in Soot Extracts from Domestic Coal-burning Stoves of Henan Province, China. Environmental Science and Technology 35(10), 1943-1952.

Wornat M.J., McClaine J.W., Ledesma E.B., and Oña J.O. 2008. To be submitted to Polycyclic Aromatic Compounds.

Wu B.C., Klein M.T., and Sandler S.I. 1991. Solvent Effects on Reactions in Supercritical Fluids. Industrial and Engineering Chemistry Research 30(5), 822-828.

Zander M. and Franke W.H. 1966. 1.12;4.5-dibenzo-perylen und 1.12-benzo-[naphtho-2.3:4.5-perylen], Chemische Berichte 99(4), 1275-1278.

Zhang X., Somers M.L., Robles J.A., and Wornat M.J. 2006. Detection of Polycyclic Aromatic Hydrocarbons by Liquid Chromatography Atmospheric-Pressure-Photoionization Mass Spectrometry. Poster presented at the Fifty-Fourth ASMS Conference on Mass Spectrometry and Allied Topics, Seattle.

## APPENDIX A – INFORMATION UTILIZED FOR THE IDENTIFICATION OF BENZO[*cd*]NAPHTHO[1,2,3-*lm*]PERYLENE

Table A.1. Refractive Indices (*n*) of Organic Solvents at 15 $^{o}$C, Variation with Temperature, and Computed *n* at 30 $^{o}$C

| Solvent | n at 15 $^{o}$C[a] | dn/dT (1/$^{o}$C)[a] | Computed n at 30 $^{o}$C |
|---|---|---|---|
| Methanol, $CH_3OH$ | 1.32897 | -0.00040 | 1.32297 |
| Dichloromethane, $CH_2Cl_2$ | 1.42466 | -0.00054 | 1.41656 |
| Benzene, $C_6H_6$ | 1.49952 | -0.00063 | 1.49007 |
| Acetonitrile, $CH_3CN$ | 1.34464 | -0.00046 | 1.33774 |

[a]Timmermans

Table A.2. Calculated Refractive Indices (*n*) of Solvent Mixtures at 30 $^{o}$C

| Solvent Program (from Figure 4.2.) | Elution Time of Compound **I** (ETI) (min) | Approx Mobile Phase Composition at ETI[a] | Computed n (at 30 $^{o}$C) of Mobile Phase at ETI |
|---|---|---|---|
| A | 82.0 | 4.6/95.4 $CH_3CN/CH_2Cl_2$ | 1.413 |
| C | 96.7 | 18.0/82.0 $CH_3CN/C_6H_6$ | 1.463 |
| D | 149.1 | 12.1/87.9 $CH_3OH/CH_2Cl_2$ | 1.405 |

[a]Delay times of 3.84, 3.90, and 5.20 min have been taken into account in order to correct for the elution time differences between the theoretical solvent programs A, C, and D with their respective counterparts observed in the HPLC chromatograms.

## APPENDIX B – INFORMATION UTILIZED FOR THE IDENTIFICATION OF DIBENZO[*b,ghi*]PERYLENE, 8H-DIBENZO[*a,jk*]PYRENE, AND BENZO[*pqr*]DINAPHTHO[8,1,2-*bcd*:2',1',8'-*lmn*]PERYLENE

Table B.1. Literature References of UV Spectra for $C_{26}H_{14}$ PAH

| Name | Structure | Ref | Name | Structure | Ref |
|---|---|---|---|---|---|
| Naphtho[1,2,3,4-*ghi*]-perylene |  | [Clar et al.1959] | Benz[*a*]indeno-[1,2,3-*cd*]fluoranthene[d] | 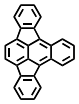 | [Clar and Willicks 1958] |
| Dibenzo[*e,ghi*]-perylene[a] |  | [Clar 1948] | Fluoreno[3,2,1,9-*defg*]-chrysene |  | [Aitken and Reid] |
| Naphtho[8,1,2-*bcd*]-perylene |  | [Clar and Kühn 1956] | Benz[*def*]indeno-[1,2,3-*hi*]chrysene |  | [Cho and Harvey] |
| Dibenzo[*cd,lm*]-perylene | 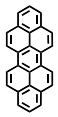 | [Clar et al. 1960] | Benz[*def*]indeno-[1,2,3-*qr*]chrysene |  | [Cho and Harvey] |
| Dibenzo[*b,ghi*]-perylene |  | [Zander and Franke] | Fluoreno[9,1,2,3-*cdef*]-chrysene | 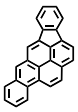 | [Cho and Harvey] |
| Acenaphtho[1,2-*k*]-fluoranthene | 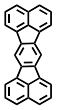 | [Clar 1964] | Naphtho[2",3":3',4']-cyclobuta[1',2':6,7]-cycloocta[1,2,3,4-*def*]-biphenylene | 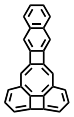 | [Wilcox and Farley] |
| Acenaphtho[1,2-*j*]-fluoranthene | 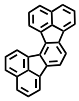 | [Clar 1964] | | | |
| Fluoreno[1,9-*ab*]-fluoranthene[b] | 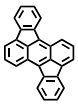 | [Clar and Willicks 1958] | Benzo[3',4']cyclobuta-[1',2':6,7]dicycloocta-[1,2,3,4-*def*:1',2',3',4'-*jkl*]biphenylene[e] | 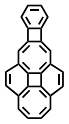 | [Wilcox and Farley] |
| Fluoreno[9,1-*ab*]-fluoranthene[c] |  | [Lang et al.] | Hexa[7]circulene[f] |  | [Jessup and Reiss] |

[a] IUPAC name Dibenzo[*b,pqr*]perylene
[b] IUPAC name rubicene; NIST (National Institute of Standards and Technology) name Diindeno[1,2,3-*de* ,1',2',3'-*kl*]anthracene
[c] Lang et al. expressed some doubt about the identification of this compound.
[c] IUPAC name Benz[*e*]indeno[1,2,3-*hi*]acephenanthrylene
[d] IUPAC name Benz[*a*]indeno[1,2,3-*fg*]aceanthrylene
[e] IUPAC name Benzo[3',4']cyclobuta[1',2':6,7]cycloocta[1,2,3,4-*def*]cycloocta[*jkl*]biphenylene
[f] IUPAC name Benzo[*no*]naphtho[2,1,8,7-*ghij*]pleiadene

Table B.2. Position of the UV Spectral p Band of Several PAH in Solvents Benzene and Methanol

| Name | Structure | Wavelength of maximum absorbance (nm) | | Δλ (nm) |
|---|---|---|---|---|
| | | λ in $C_6H_6$[a] | λ in $CH_3OH$[b] | |
| Anthanthrene |  | 433 | 428 | 5 |
| Coronene |  | 341.5 | 338 | 3.5 |
| Benzo[*ghi*]-perylene |  | 387.5 | 383 | 4.5 |
| Benzo[*a*]-coronene | 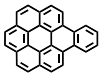 | 376 | 371 | 5 |
| Benzo[*a*]-naphthacene | 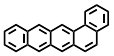 | 452.5 | 449 | 3.5 |
| Picene | 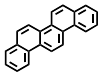 | 329 | 326 | 3 |
| Benzo[*ghi*]-fluoranthene |  | 350 | 347 | 3 |

[a] Clar 1964
[b] Jinno

Table B.3. Refractive Indices (*n*) of Organic Solvents at 15 °C and 20 °C, Variation with Temperature, and Computed *n* at 25 °C and 30 °C

| Solvent | *n* | | d*n*/dT (1/°C)[a] | Computed *n* |
|---|---|---|---|---|
| | 15 °C[a] | 20 °C[b] | | 30 °C[c] |
| Methanol, $CH_3OH$ | 1.32897 | — | -0.00040 | 1.32297 |
| Ethanol, $C_2H_5OH$ | 1.36330 | — | -0.00038 | 1.35760 |
| Dichloromethane, $CH_2Cl_2$ | 1.42466 | — | -0.00054 | 1.41656 |
| Benzene, $C_6H_6$ | 1.49952 | — | -0.00063 | 1.49007 |
| Acetonitrile, $CH_3CN$ | 1.34464 | — | -0.00046 | 1.33774 |
| 1,2,4-Trichlorobenzene | — | 1.56710 | -0.00048[d] | 1.56230 |
| 37:63 $CH_3CN$:$CH_2Cl_2$ | — | — | — | 1.38740[e] |
| 30:70 $CH_3CN$:$CH_2Cl_2$ | — | — | — | 1.39291[e] |

[a] Timmermans
[b] Washburn
[c] temperature used for analysis on the Agilent 1100 HPLC/UV/MS instrument
[d] d*n*/dt taken from 1,2-dichlorobenzene
[e] Calculated according to the procedure described during the identification of Benzo[*cd*]naptho[1,2,3-*lm*]perylene

Table B.4. Calculated Refractive Indices (*n*) of HPLC Mobile Phase Solvent Mixtures

| Compound | Compound observed in products of | Solvent Program (from Figure 4.2.) | Elution time of compound (ET) (min) | Approx mobile phase composition at ET[a] | Computed *n* of mobile phase at ET |
|---|---|---|---|---|---|
| **II** | Synthetic jet fuel S-8 | A | 57.0 | 67.1/32.9 $CH_3CN/CH_2Cl_2$ | 1.36367 (30 $^oC$) |
| **III** | Synthetic jet fuel S-8 | A | 53.0 | 77.1/22.9 $CH_3CN/CH_2Cl_2$ | 1.35579 (30 $^oC$) |
| **IV** | Synthetic jet fuel S-8 | E | 159.0 | 100 $CH_2Cl_2$ | 1.41656 (30 $^oC$) |

[a]A delay time of 3.84 min have been taken into account in order to correct for the elution time differences, in the identifications of compounds **I** and **II**, between the theoretical solvent programs and the actual solvent chromatographic signal.

Table B.5. Position of the UV Spectral p Band of Several PAH in Solvents 1,2,4-Trichlorobenzene and two Acetonitrile/Dichloromethane HPLC Solvent Mixtures

| Name | Structure | Wavelength of maximum absorbance (nm) | | Δλ (nm) |
|---|---|---|---|---|
| | | λ in 1,2,4-$C_6H_3Cl_3$ | λ in ($CH_3CN/CH_2Cl_2$) | |
| Tribenzo[*e,ghi,k*]-perylene | 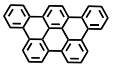 | 374 | 367[a] | 7 |
| Dibenzo[*a,g*]-coronene | 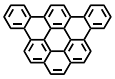 | 379.5 | 374[b] | 5.5 |

[a] solvent composition 37:63 $CH_3CN$:$CH_2Cl_2$
[b] solvent composition 30:70 $CH_3CN$:$CH_2Cl_2$

# APPENDIX C – PERMISSION TO REPRINT


**Title:** THE INFLUENCE OF SOLVENTS ON THE ULTRAVIOLET-VISIBLE ABSORPTION SPECTRA OF POLYCYCLIC HYDROCARBONS: APPLICATIONS IN THE IDENTIFICATION OF FUEL PRODUCTS BY HPLC/UV/MS

**Author:** Jorge O. Oña, Mary J. Wornat

**Publication:** Polycyclic Aromatic Compounds

**Publisher:** Taylor & Francis

**Date:** Jan 1, 2008



## Thesis / Dissertation Reuse Request

Taylor & Francis is pleased to offer reuses of its content for a thesis or dissertation free of charge contingent on resubmission of permission request if work is published.


**Title:** IDENTIFICATION OF THE $C_{30}H_{16}$ POLYCYCLIC AROMATIC HYDROCARBON BENZO[*cd*]NAPHTHO[1,2,3-*lm*]PERYLENE AS A PRODUCT OF THE SUPERCRITICAL PYROLYSIS OF A SYNTHETIC JET FUEL

**Author:** Jorge O. Oña, Mary J. Wornat

**Publication:** Polycyclic Aromatic Compounds

**Publisher:** Taylor & Francis

**Date:** Jan 6, 2007



## Thesis / Dissertation Reuse Request

Taylor & Francis is pleased to offer reuses of its content for a thesis or dissertation free of charge contingent on resubmission of permission request if work is published.

## Thesis / Dissertation

A thesis/dissertation license authorizes an advanced degree candidate to republish the requested material in his/her doctoral thesis or dissertation free of charge. No license is required although resubmission of permission request, for a fee, is required if the work is published.

## VITA

The author was born in Ecuador. He achieved his undergraduate degree in chemical engineering from the Universidad Central of Ecuador in Quito. After this stage, he started his doctoral studies in chemical engineering in the United States. Since then, he has traveled around the United States and Canada presenting his research in conferences about analytical chemistry, polycyclic aromatic compounds, and combustion. Between his classes, his conferences, and his polycyclic aromatic hydrocarbons identification research; the author spends his time playing guitar, doing exercise in the gym, and walking around the university lakes with his wife Diana.